DEVELOPMENT AND APPLICATIONS OF A LASER MICROMACHINED INTER-DIGITATED CAPACITIVE STRAIN SENSOR

by

SHREYAS KIRAN THAKAR

Presented to the Faculty of the Graduate School of

The University of Texas at Arlington in Partial Fulfillment

of the Requirements

for the Degree of

MASTER OF SCIENCE IN ELECTRICAL ENGINEERING

THE UNIVERSITY OF TEXAS AT ARLINGTON

AUGUST 2011

ACKNOWLEDGEMENTS

I want to thank my supervising professor, Dr. Chiao for giving me the opportunity to be part of his excellent research group. He has supported me throughout my thesis with his patience, knowledge and practical insights. He was always eager to listen and to give advice regarding my research and career. I feel honored to have worked with him on a great project.

My special thanks to Dr. Davis and Dr. Dillon for their interest in my research and for taking their valuable time to be on my thesis defense committee.

I want like to give a special thanks to Mr. Hung Cao and Mr. Uday Tata for mentoring and guiding me throughout my research work.

I want to thank my father Kiran Thakar, my mother Aparna Thakar, my brother Shantanu Thakar and Ms. Manasi Sahasrabudhe for their unconditional support and encouragement to pursue my interests and for providing the highest level of motivation.

I also want to offer my thanks and regards to all iMEMS group members, roommates and friends who supported me during the completion of the thesis.

July 15, 2011

ABSTRACT

DEVELOPMENT AND APPLICATIONS OF LASER MICROMACHINED INTER-DIGITATED CAPACITIVE STRAIN SENSORS

Shreyas Thakar, M.S.

The University of Texas at Arlington, 2011

Supervising Professor: Jung-Chih Chiao

Reliable strain measurement plays a very important role in the damage detection of the mechanical and civil structures. It can also have a significant contribution in assisting the proper functioning of human body and organs. The current strain sensors and measurement systems have significant drawbacks in terms of high sensitivity to temperature, low gauge factor, low biocompatibility and bulky data acquisition/conditioning circuitry. These factors make the strain measurement unreliable and expensive. In this work, a laser micro-machined inter-digitated capacitive strain sensor was developed which overcame the limitations of existing strain sensing technologies. The structural health monitoring along with bladder volume sensing applications were targeted and the suitability of the sensor to these applications was verified. The capacitive strain sensor was made up of a low cost metal sheet which was micro-machined with a laser to form an inter-digitated structure. This structure was then encapsulated in a flexible, bio-compatible material which also acted as the dielectric. The connections were made on the metal with the help of a conductive paste to acquire the data. Design of the Inter-digitated capacitors with the highest possible capacitance value, precision and repeatability was

chosen for the desired applications. The inter-digitated structure was sensitive to stretching and bending resulting in capacitance changes. Modifications and amendments were made in the initial device to enhance its suitability and performance for structural health monitoring applications. The sensor was attached to load bearing structures such as cantilevers and the variation in initial capacitance value was checked experimentally for different strains. A simple circuit was implemented to convert the capacitance changes into frequency changes for ease of remote data transmission. Devices with flexible inter-digitated fingers were fabricated through laser micro-machining in order to improve their performance for *in-vivo* applications. The suitability of the new devices was shown experimentally for monitoring strain changes of structures such as the urinary bladder. The testing of these devices is done with a wireless, batteryless circuit to verify the working of the strain sensors for inside body applications. In this work, the design, fabrication, observations and results for the desired applications have been discussed.

TABLE OF CONTENTS

LIST OF ILLUSTRATIONS

Figure Page

LIST OF TABLES

CHAPTER 1

INTRODUCTION

1.1 Significance of strain measurements

Strain is the change of shape of any object produced by stress applied on that object [1]. If the stress is a longitudinal pull on a metallic rod, strain is the lengthening of the rod in the direction of the pull. A material is called elastic if the strain on it disappears when the stress is removed. If the material fails to return to its original state on application of stress or load, the strain generated on it is permanent. Every material is perfectly elastic for small stresses and plastic for large stresses. Each and every mechanical, civil or biological structure or organ has a limit on the amount of elastic strain which can be generated. Beyond a certain level, the generated strain will not remain elastic and will result in permanent deformations [1] [2]. It is important to detect the strain levels for important structures and prevent them from exceeding the levels of permanent strains. To achieve this, strain sensing is essential. Also, strain can be used as a feedback to understand the current state of different structures. In this work, strain sensors were developed and implemented with strain sensing systems for two crucial applications- structural health monitoring and urinary bladder volume monitoring. For structural health monitoring, measurement of strain allowed understanding of the physical well being of the structures while in bladder volume monitoring, strain measurements give information of the volume of liquid content in the bladder. The importance of strain sensing for both these applications is elaborated below.

1.2 Importance of strain measurements in structural health monitoring

Timely damage detection plays a significant role in preventing catastrophic failures in structures such as dams, bridges, huge mechanical structures such as boilers, turbines and so on. The external factors such as heavy live loads, earthquakes, high winds, ocean waves and flood water can cause onset of deformation or degradation of such crucial structures [3]. Aging of structures, as a result of long periods of service, can also deteriorate the load bearing ability of the structures and reduce its immunity to hazardous external conditions [4][5]. This makes it all the more important to measure the onset of deformations or degradations on the structures and prevent disasters. With the ability to detect deformations at initial stages, repairing costs and time can be substantially reduced [6]. For systems implemented for structural health monitoring, it is important that they possess the ability to measure very high loads and the reaction of the structures to these high loads [7]. Such measurements are possible with the help of strain sensors and sensing systems allow measurement of minute deformation in beams, columns and other load bearing regions in a structure [8]. Hence, strain sensors and sensing systems can play a vital role in maintaining safer operation of structures and equipments with substantially reduced repair expenditures and efforts. In this work, a capacitive strain sensor capable of measuring deformations in the mechanical or civil structures is developed and tested.

1.3 Importance of strain measurements in malfunctioning urinary bladder

Urinary incontinence (UI) is the involuntary loss of urine due to bladder dysfunction. About 25 million Americans suffer from UI, out of which about 9-13 million have severe symptoms according to The National Association of Continence. Severe symptoms can also give rise to kidney failure. Sensory feedback to the central nervous system is cut off in UI leaving the patient incapable of knowing when to void the bladder. Over a long period of time, this incapability can lead to reverse flow of the urine resulting in extensive kidney damage and

the need for the patient to undergo haemodialysis [9][10]. This calls for a need of measuring the bladder volume and artificially stimulating the bladder when the volume is close to the full capacity [11]. Three types of techniques are used to measure the bladder pressure or volume. Some of the non-invasive techniques measure the amount of urine flow which is then correlated with the pressure in the urinary bladder while some measure the pressure at a penile cuff which is needed to interrupt the urine flow [12][13]. Such methods are often inconvenient to patients and restrict patient movement. Highly invasive devices try to measure the bladder pressure with the entire system inside the bladder. Such systems require insertion of catheters in to the bladder through an extensive surgical procedure [11]. Apart from the above mentioned techniques, the slightly invasive bladder pressure sensing systems requiring sensor or device attachment to the bladder walls. These are a lot less invasive as compared to the highly invasive devices and are way more accurate as compared to the non-invasive techniques [14][15].

1.4 Conventional strain sensors

The desirable features of the strain sensing elements include linear working in the elastic range, low hysteresis, high sensitivity and low temperature effects [1]. Conventional strain sensors for structural health monitoring include resistive strain gauges, piezoelectric strain sensors and fiber optic strain sensors. The resistive strain gauges show a change in resistance as their dimensions change with applied strain and can be either metallic or semiconductor based. The performance of the resistive strain gauges is judged by their gauge factor which is given as ratio of change in resistance over original resistance for a particular strain. The metallic strain gauges show stable performances at different temperatures but have a small gauge factor of about 2-5. This limits the resolution of the metallic resistive strain gauges. On the other hand, the semiconductor based resistive strain gauges offer very high gauge factors of about 130 allowing measurements of very small strains. But these types of

strain sensors show non-linear behavior for high strains and are more expensive to fabricate as compared to metallic strain gauges. The most important drawback of the semiconductor based strain gauges is their high sensitivity to temperatures resulting in unpredictable performances at different temperatures [16] [17]. Also, all the resistive strain gauges require a complicated circuitry to enable remote monitoring consisting of whetstone's bridge and signal conditioning units to interface with microcontrollers. This in turn requires higher number of components and hence high power requirements [18]. Piezoelectric sensors work on the principle of change in electric dipole moment per unit volume changes on straining. These types of sensors are also very sensitive to temperature changes [19]. Optical fiber strain sensors show a change in their light throughput with deformation due to strain. Both the piezoelectric and fiber optic strain sensors however, have poor durability, unfavorable compatibility with concrete structures and high cost [20].

Thick film resistive strain sensors along with polymer based resistive strain gauges have been proposed for bladder volume monitoring. These have simple fabrication technique and are robust with low manufacturing costs [10] [21]. Since they are resistance based, they need complex circuitry for data processing and signal conditioning including current amplifiers and Schmitt triggers [10] resulting in increased power consumption. This will in turn give rise to frequent battery changes leading to inconvenience to the patients.

Capacitive strain sensors offer several advantages over the resistive, piezoelectric and fiber optic strain sensors. They offer better sensitivity with high gauge factors up to 20-30, better immunity to noise and reduced sensitivity to temperatures. This makes capacitive strain sensors suitable for structural health monitoring applications where large temperature variations may be observed. Also, simple circuits such as inductive-capacitive resonant circuits can be implemented for low power wireless operations making them suitable for *in-vivo* applications [17][22][23]. Keeping the above advantages in mind, capacitive strain sensors have been developed.

1.5 Proposed strain sensing system

In this work, a laser micro-machined inter-digitated capacitive strain sensor was developed which could be used for structural health monitoring as well as bladder volume monitoring applications. For any parallel plate capacitor, the fundamental formula for the capacitance is given as

$$C(parallel) \propto \varepsilon lb/d \tag{1.1}$$

$$C(parallel) \propto \varepsilon A/d$$

where ε is the permittivity of the dielectric medium, l and b are the length and breadth of the parallel plates with surface area A, and d is the gap between them occupied by the dielectric. Inter-digitated capacitors (IDCs) are parallel plate capacitors modified to increase the surface area of the metallic conductor plates. They consist of well grooved finger-like projections on the surface of each of the conductors with dielectric present in between the two sets of fingers. This gives a larger capacitance compared with simple parallel plate capacitors of the same size since they offer increased conductor surface area. For the IDCs, the surface area of the capacitor increases with increase in the number of finger pairs on the conductor surface. Hence, the modified equation for capacitance of the IDC is given as

$$C(theoretical) \propto \varepsilon NLt/d \tag{1.2}$$

where N is the number of finger pairs, L is the finer length and t is the thickness/height of the finger. The area of each finger is given by A which is the product of finger length L and thickness t. Hence, for the same gap (d) and same device height ($b = t$) and same device size, the capacitance of the Inter-digitated capacitor (IDC) is much higher than the capacitance offered by the simple parallel plate capacitors. The higher initial capacitance makes the sensor less sensitive to parasitic capacitances and gives a higher resolution. These IDCs were encapsulated in flexible substrate which also formed the dielectric between the fingers. The flexible encapsulation permitted stretching and bending of the device resulting in relative

displacement of the IDC fingers causing changes in the capacitance values. The working principle of the designed IDC can be schematically explained from Figure 1.1 below.

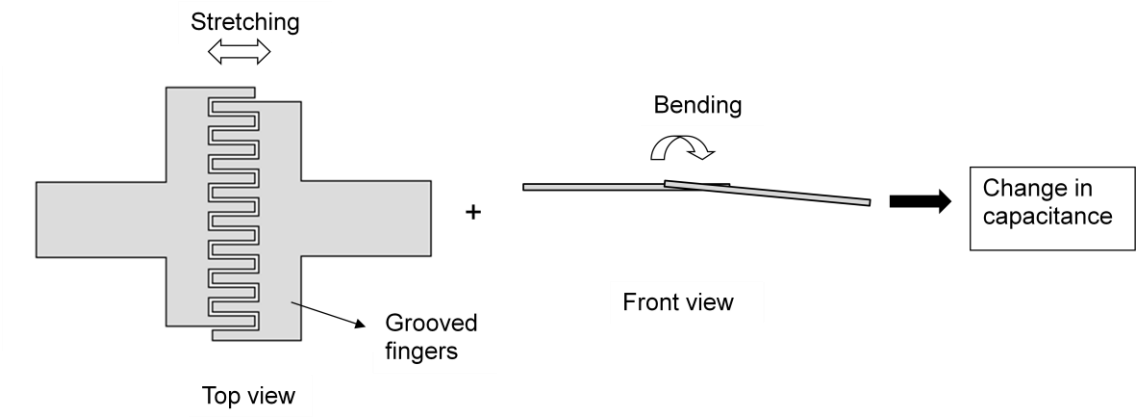

Figure 1.1: The working principle of IDC strain sensor.

The IDCs were formed by a novel laser micro-machining technique in which a 120 μm thick metal sheet was cut to give the desired shape to the metal sheet. 120 μm thick, purely metallic fingers directly enhanced the capacitance obtained as evident from Equation (1.2). This offers a major advantage over the other conventional IDCs which are formed by MEMS techniques yielding IDCs with thin metallic films [24] [25]. Larger feature sizes of the order of 35 μm have been achieved through printable inter-digitated capacitors on paper board [26] [27] but they are three times smaller than the feature sizes developed in this work. As the fingers were completely metallic, no extra metal deposition step was required and the high aspect ratio of about 120 improved the resolution substantially with a high gauge factor of 80. The capacitance output of the strain sensor was converted into a square wave with frequency inversely proportional to the capacitance using a simple circuitry having minimum number of components. Low-power remote data acquisition was achieved. The above system can also be implemented for multi-sensing applications with numerous sensors connected together to form a network.

The advantages of the developed metallic capacitive strain sensors over some of the conventional strain sensors can be summarized:

- Sensitivity: Substantially higher gauge factor as compared to metallic resistive strain gauges and other capacitive strain gauges.
- Linearity: Good operating linearity for elastic strains.
- Temperature performance: Sensitivity remains unaffected for a wide range of temperatures.
- Applications: A single fabrication method can be implemented for a wide variety of applications including structural health monitoring to *in-vivo* bladder volume monitoring.
- Circuitry: Simple circuitry for data acquisition and wireless data transfer. High power and excess signal conditioning not required.
- Multiplexing capabilities: The capacitive strain sensors can be multiplexed to form wireless networks for strain sensing of large areas.

1.6 Thesis Indexing

Chapter 1 deals with the importance of strain measurements in structural health monitoring and bladder volume monitoring applications. It gives an overview of the strain sensing principle implemented with the help of inter-digitated capacitive strain IDCs. Chapter 2 discusses the design considerations while selecting the final design for the metallic IDCs. Complete fabrication process for all the different generations developed and tested is elaborately explained in Chapter 3. The advantages and limitations of each of the generations for different applications are also highlighted in this chapter. Experiments carried out to prove the concept of the flexible capacitive strain sensors are explained in Chapter 4. With these experiments as the background, extensive testing of the strain sensor for structural health monitoring and bladder volume monitoring applications using essential setups is carried out in Chapter 5. Elaborate experiments with wireless setups are also included in this chapter.

Chapter 6 gives the conclusion followed by the possible future work in Chapter 7. It also includes experiments to prove the suitability of the new generation of strain sensors for bladder volume monitoring.

CHAPTER 2

DESIGN OF INTER DIGITATED CAPACITOR

In this chapter, the discussion is focused on the various parameters which affect the design of the IDC. Taking in to account the design constraints and fabrication issues for various physical parameters of the IDC, the final design is chosen.

2.1 Principles of operation of IDCs as strain sensing elements

Before the optimal design of the IDC was selected, it was important to understand how the IDCs could be used for strain detection. The IDCs have been used for strain measurements in two ways depending upon the orientation of the IDC with respect to the object on which it was placed [28]. Depending upon the strain direction relative to the finger orientation, IDCs can be categorized as lateral IDCs and transverse IDCs.

2.1.1. Lateral IDCs

In lateral IDCs, the direction of strain is parallel to the finger length and strain results in changes in the overlap length of the fingers. This in turn reduces the capacitance of the IDC. Hence, for lateral IDC strain sensors, the change in capacitance due to strain is a function of finger length. If the finger length was kept large as compared with the finger gaps, lateral orientation allowed for a greater range of strain measurements. At the same time, the risk of shorting of fingers was reduced if the IDCs were oriented exactly in parallel with the direction of strain. With smaller gaps and larger finger lengths, lateral IDCs allowed for higher initial capacitance values as compared with transverse IDCs. Figure 2.1 shows the working principle of lateral IDCs.

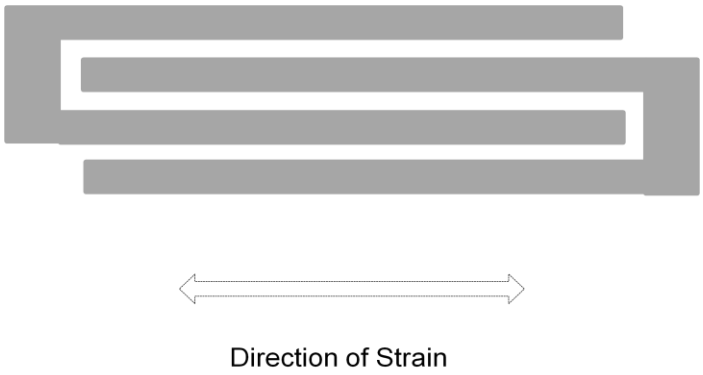

Figure 2.1: The direction of strain relative to fingers for lateral IDCs.

2.1.2. Transverse IDCs

The direction of strain for transverse IDCs iss normal to the finger length and changes in strain result in changes in the gap between the fingers. This in turn results in a change in the capacitance. As a result, the capacitance change due to strain was directly proportional to the finger gap [28] [29]. For such IDCs, it is necessary that the finger gap be large as compared with the lateral IDCs in order to avoid shorting. Also, since larger gaps reduced the capacitance, initial capacitance values were low when compared with fingers of same length for the lateral IDCs. Figure 2.2 shows the working principle of a transverse IDC.

Lateral IDCs allow a larger range of operation as compared to transverse IDCs. For transverse IDCs, the possibility of fingers shorting is higher allowing only a small range of stretching for strain measurements. Also, lateral IDCs provide for higher initial capacitance values when compared with transverse IDCs of the same finger length and finger number since they have much smaller finger gaps which are not permitted in transverse IDCs to avoid shorting. Hence, lateral IDCs of the same initial capacitance will be smaller in size when compared with transverse IDCs. Due to the advantages of lateral IDCs over transverse IDCs, the former have been designed and developed for strain sensing applications.

Figure 2.2: The direction of strain relative to fingers for transverse IDCs.

2.2 Design factor considerations

The main requirements for good IDC performance include high initial capacitance and high sensitivity. High initial capacitance allows detection of smaller relative change along with reduced parasitic capacitance effects [28]. In order to obtain the highest possible initial capacitance, according to Equation (1.2), it is essential to have the longest possible finger length, highest number of fingers, highest possible finger height/device thickness and smallest possible finger gap. Also, a dielectric with a high dielectric constant allows for a high initial capacitance. But the above design considerations are limited by the size of the device for the targeted application. Most of the applications require the smallest possible device size. Issues such as bending, sagging may arise during fabrication of larger devices. Hence, there is a trade-off between obtaining high initial capacitance and the device size. Therefore, the IDC needs to be designed in such a way that it is small enough to be used in the desired applications and, at the same time, have a high enough initial capacitance value. Keeping in

mind the targeted applications and the fabrication technique to be implemented, the most important criteria to determine the best possible design were:

1) Precise and repeatable fabrication
2) Small device size
3) Highest possible capacitance
4) Low fringe effects

All the above criteria depend on the physical parameters of the IDC such as the:

1) number of fingers
2) finger gaps
3) finger lengths.

In order to find out the best possible design from the point of view of the above mentioned points, 27 designs with different physical parameters were fabricated. It was important to find out which design best met the above criteria. A design was called precise when it was free of any sort of misalignment and repeatable when the desired precision was observed every time it was fabricated. Repeatablity for larger devices was found to be very low since longer finger lengths and larger finger pairs led to misaligned fingers. A range of values of different parameters was decided by keeping in mind the size limitations of the devices. Various designs were made with the parameters varied in the following manner:

1) Finger lengths of 400, 500 and 600 μm.
2) Finger gaps of 5, 10 and 15 μm.
3) Number of finger pairs varied as 20, 30 and 40.

The table below shows the 27 different designs.

Table 2.1: IDC designs made with different physical parameters.

Finger Gaps → / Finger Lengths ↓	5 (μm)	10 (μm)	15 (μm)
400 (μm)	20 fingers 30 fingers 40 fingers	20 fingers 30 fingers 40 fingers	20 fingers 30 fingers 40 fingers
500 (μm)	20 fingers 30 fingers 40 fingers	20 fingers 30 fingers 40 fingers	20 fingers 30 fingers 40 fingers
600 (μm)	20 fingers 30 fingers 40 fingers	20 fingers 30 fingers 40 fingers	20 fingers 30 fingers 40 fingers

2.2.1 Considerations for finger lengths

It was expected that finger lengths smaller than 400 μm would give a very low capacitance while fingers lengths of 600 μm would show the highest capacitance out of the three chosen lengths. Though this was observed to be true, precison and repeatability in the fabrication were not observed for fingers of 600 μm length. 400 μm and 500 μm finger lengths showed high device precison and repeatability but 600 μm fingers were often observed to slack by few microns. This was because, even though the fingers were designed for a thickness of 50 μm for any particular finger gap, in reality the average finger thickness was observed to be about 30 μm because the average finger gap after fabrication was always 5-10 μm more than the designed gap. The reason for this lies in the way laser performs the mico-machining and is explained in Chapter 3 on fabrication. This resulted in a reduced thickness to length ratio for the fingers. It was evident that even though IDCs with 600 μm fingers did offer a higher capacitance

than smaller lengths, they did not show repeatable fabrication compared with the devices having smaller finger lengths. Hence, there was always a trade off observed between the finger size and the precision and repeatabilty of fabrication.

From the SEM images shown below, the misalignments of the 600 µm finger length IDCs were clearly evident. It was an obvious indication that adjacent fingers were not in the same plane and these misalignments could lead to random capacitance values. Hence was essential to avoid the misalignments.

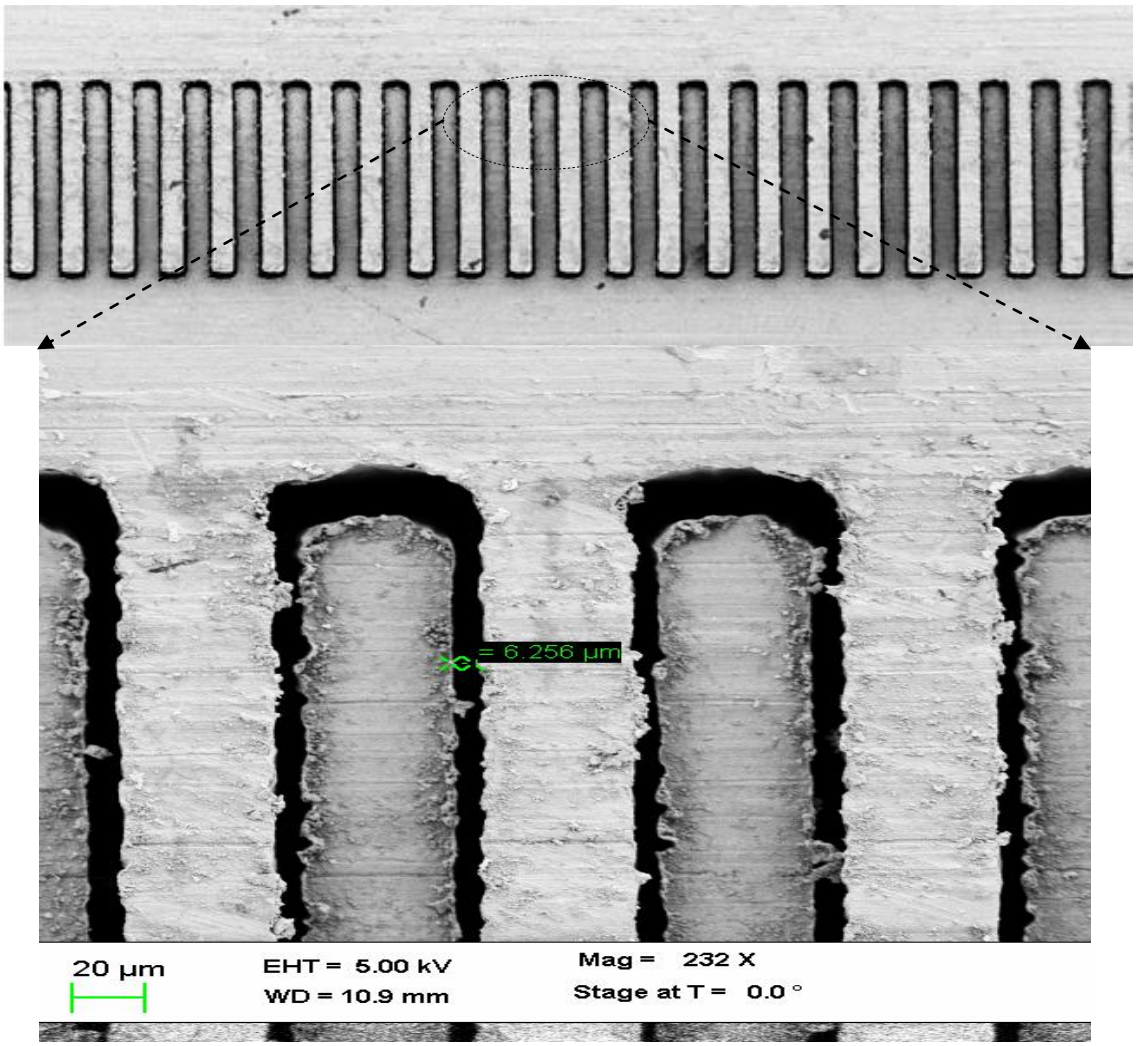

Figure 2.3: SEM image showing plane mismatching of 600 µm finger lengths.

2.2.2 Considerations for finger gaps

For the finger gaps, it was required that the gap be as small as possible so as to have the highest capacitance value. This was limited by the minimum feature size possible through laser micro-machining. The micromachining technique for device fabrication allowed for a minimum gap of 5 μm between objects. This was because the laser beam thickness was about 5-6 μm. Hence, the minimum finger gap possible in between the fingers was limited to about 5 μm. This was the first choice for the devices though a gap much higher than this was observed. The reasons for this are explanied in Chapter 3.

2.2.3 Considerations for finger numbers

The number of finger pairs were chosen as 20, 30 and 40 because these three numbers allowed for high initial capacitance along with small sizes. Devices with greater than 40 fingers resulted in very wide devices which showed problems during fabrication due to large width. If the number of finger pairs were less than 20, an initial capacitance in the range of 1-2 pF would be obtained, which would require a very sensitive and accurate measuring system to measure the capacitance changes. Of the three chosen lengths, 20 fingers showed the least capacitance while 40 fingers showed highest capacitance as expected. Although 40 fingers had the maximum capacitance, the fabrication was not always repeatable. Precise fabrication was sometimes observed but the same settings did not always yield a precise outcome. The reason for this non-repeatable fabrication was because 40 finger devices covered a much larger area on the metal sheet while laser micro-machining. During fabrication, the metal sheet was placed on the platform and the point of attachment of the sheet on the platform was at Jig-position 1 as shown in the Appendix. This location was perfect in size to allow parallel fabrication and always yielded repeatable devices. It was essential that, the metal sheet was perfectly clamped on to this jig 1 position and that it remained in the same plane. Slacking or bumps on the laser sheet reduced the device precision. Hence, if a design had a large area, it was essential that the

sheet remain in the same plane for the complete device area. The 40 finger devices had a larger area as compared with devices of smaller finger number and the metal sheet, even on the jig 1 position which yielded the most repeatable devices, could not remain in the same plane because of slight slacking. As a result, 40 finger devices often had misaligned fingers. This can be seen in the Figure 2.4 below.

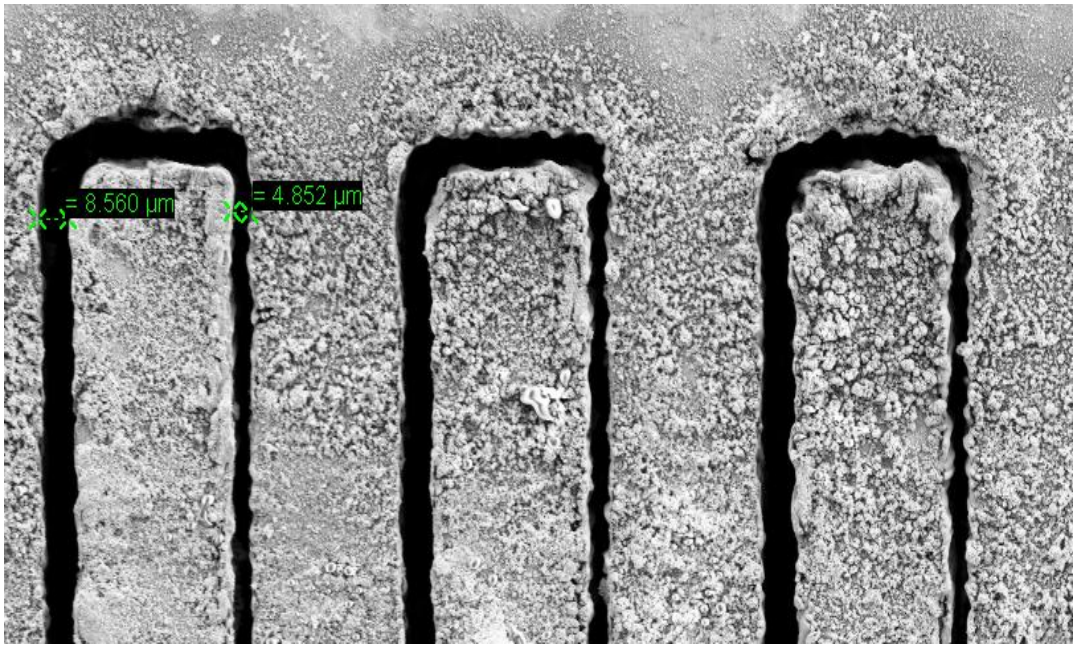

Figure 2.4: SEM image showing the back end of an IDC with uneven finger gaps on the two sides of each finger.

It can be seen from the SEM image above that the gap on the two sides of the IDC fingers is not the same. One side shows a gap of about 8.56 µm while the other side shows a gap of 4.852 µm. Even though the 40 finger pair IDCs had higher initial capactance than the 30 finger ones, they were not used for experiments because they often yielded imperfect IDCs. If the jig position was to be changed to prevent sheet slacking, some of the smaller positions were too small to accommodate even one of the devices. Larger jig positions showed even larger slacking of the metal sheet. 20 and 30 finger designs occupied a much smaller size that reduced the chances of finger misalignment.

2.2.4 Considerations for fringe effect

Apart from the size, initial capacitance and reliability issues, another important factor which played a vital role in design selection was the fringe effect. The fringe effect is caused by the electric fields present on the tip of the fingers and the other parasitic capacitances present around the device. In this case, we refer to the fields present at the tip of the fingers as the fringe fields assuming that the other parasitic fields are not contributing. This is shown in Figure 2.5. It was important to know which devices have the highest fringe effect and which devices have the least out of the different designs fabricated. In the case of lateral IDCs, the change in capacitance was a function of the change in overlap length of the fingers due to strain. Small fringe effect contribution meant that the total capacitance value was dependant more on the electric fields present along the finger lengths rather than on the fringe fields at the tips. This was expected to result in a greater change in capacitance on reduction in overlap finger length. Even though the above assumption could be made, it was important to study the behavior of the fringe effect contribution for devices with different physical parameters.

2.2.5 Calculations for fringe effect

The fringe effects were calculated after fabricating IDCs of different designs. Once the IDCs were fabricated, the theoretical values of capacitances of the IDCs were found from Equation (1.2) keeping constant of proportionality as one. These theoretical values were compared with the practically obtained values. It was evident that the practical capacitance values were always 3-5 times greater than the theoretical values. The practically obtained capacitance could be now expressed as

$$C(practical) = \Upsilon C(theoretical) = \Upsilon \varepsilon NLt/d \tag{2.1}$$

where Υ was the constant of proportionality and $3 < \Upsilon < 5$. As discussed previously, the theoretical formula did not give an estimate for the fringe effects arising in the IDC. Equation (1.2) takes into account the capacitance of the IDC only as a function of overlap length L, of the

fingers. The electric fields along the lengths of the fingers were considered, while the fields at the tips contribute to fringe effect. This may have a substantial contribution in the practically observed capacitance. The effect is represented diagrammatically in Figure 2.5 above. Hence, the constant of proportionality 'Y' introduced earlier was modified to a factor called 'The fringe effect factor' F, to take into account the fringe effect. Equation (2.1) can be then re-written as

$$C(practical) = FC(theoretical) = F\varepsilon NLt/d \qquad (2.2)$$

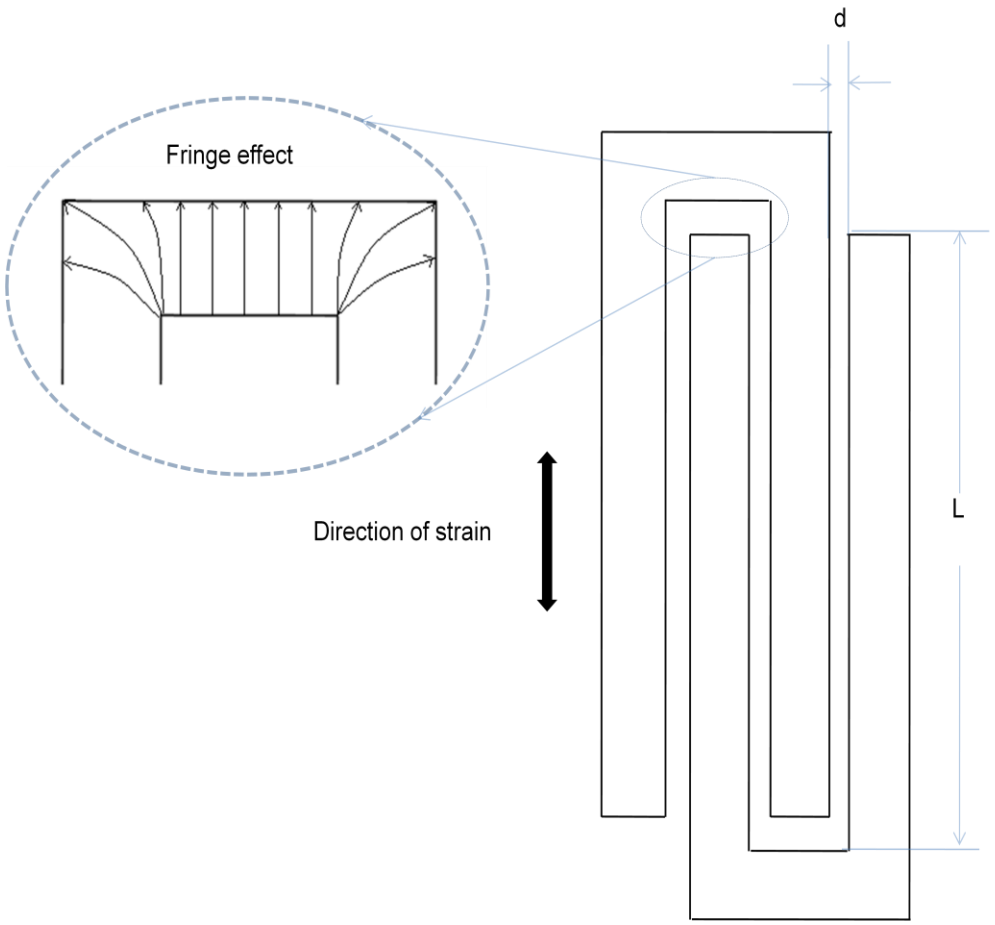

Figure 2.5: Location of fringe fields in inter-digitated capacitors

In order to know the behavior of fringe effect factor F, it was important to know which physical parameters of the IDC affect its value, and how. Its behavior with respect to physical

parameters of the IDC was studied from the 27 different device designs fabricated earlier. All the devices had different finger lengths, finger gaps and finger numbers. The practical capacitance values obtained were then compared with the theoretical values which were calculated using Equation (1.2) with constant of proportionality of unity. Table 2.1 shows the values for fringe effects for various IDC designs.

Table 2.2: Comparison for capacitance values for IDCs with different physical parameters.

Number	Design			Theoretical Capacitance(F)	Practical Capacitance (F)	Fringe effect factor
	Length (μm)	Gap (μm)	Number of fingers			
1	400	5	20	1.92354×10^{-12}	7.58×10^{-12}	3.94064328
2	400	5	30	2.78314×10^{-12}	1.1×10^{-11}	3.95236372
3	400	5	40	3.77778×10^{-12}	1.4825×10^{-11}	3.924261
4	400	10	20	1.00384×10^{-12}	5.12×10^{-12}	5.10043223
5	400	10	30	1.51984×10^{-12}	6.91×10^{-12}	4.5465371
6	400	10	40	2.04556×10^{-12}	9.04×10^{-12}	4.419319
7	400	15	20	9.34816×10^{-13}	4.93×10^{-12}	5.27376268
8	400	15	30	1.42788×10^{-12}	6.67×10^{-12}	4.67125819
9	400	15	40	1.83657×10^{-12}	8.48×10^{-12}	4.61731294
10	500	5	20	2.71543×10^{-12}	1.096×10^{-11}	4.03619896
11	500	5	30	3.42689×10^{-12}	1.371×10^{-11}	4.00071163
12	500	5	40	5.69391×10^{-12}	1.98×10^{-11}	3.47740226
13	500	10	20	1.40165×10^{-12}	6.8×10^{-12}	4.85142227
14	500	10	30	2.13704×10^{-12}	9.3×10^{-12}	4.35182055
15	500	10	40	2.77819×10^{-12}	1.207×10^{-11}	4.34455256
16	500	15	20	1.21306×10^{-12}	6.39×10^{-12}	5.26766882
17	500	15	30	1.92986×10^{-12}	8.19×10^{-12}	4.24382945
18	500	15	40	2.51479×10^{-12}	1.046×10^{-11}	4.15938887
19	600	5	20	2.62862×10^{-12}	1.184×10^{-11}	4.50426032
20	600	5	30	3.69113×10^{-12}	1.643×10^{-11}	4.451216
21	600	5	40	5.38053×10^{-12}	2×10^{-11}	3.71710567
22	600	10	20	1.75644×10^{-12}	8×10^{-12}	4.55465577
23	600	10	30	2.7632×10^{-12}	1.094×10^{-11}	3.95918384
24	600	10	40	3.6058×10^{-12}	1.386×10^{-11}	3.84381249
25	600	15	20	1.4836×10^{-12}	7×10^{-12}	4.71824276
26	600	15	30	2.21962×10^{-12}	9.22×10^{-12}	4.1538631
27	600	15	40	3.05356×10^{-12}	1.164×10^{-11}	3.81195016

With the different designs which were fabricated, following observations were made:

a) The device with 400 µm finger length, 15 µm finger gap and 20 finger pairs (number 7) showed the least initial capacitance and one of the highest fringe effect contributions.

b) The device with 600 µm finger length, 5 µm finger gap and 40 finger pairs (number 21) showed the highest initial capacitance and one of the least fringe effect contributions.

c) The devices with 500 µm finger length showed moderate capacitance values and fringe effect contributions (numbers 10 to 18).

The conclusions which can be derived from Table 2.1 are:

a) As the device finger length increased, the fringe effect factor decreased. From this information, it was infered that as the finger length increases, the contribution of fringe effect in the total observed capacitance value is less. This means, for an IDC with large finger length, the capacitance due to the finger length overlap has larger contribution to the total capacitance than an IDC having a smaller finger length. This can be observed in the Figure 2.6 below.

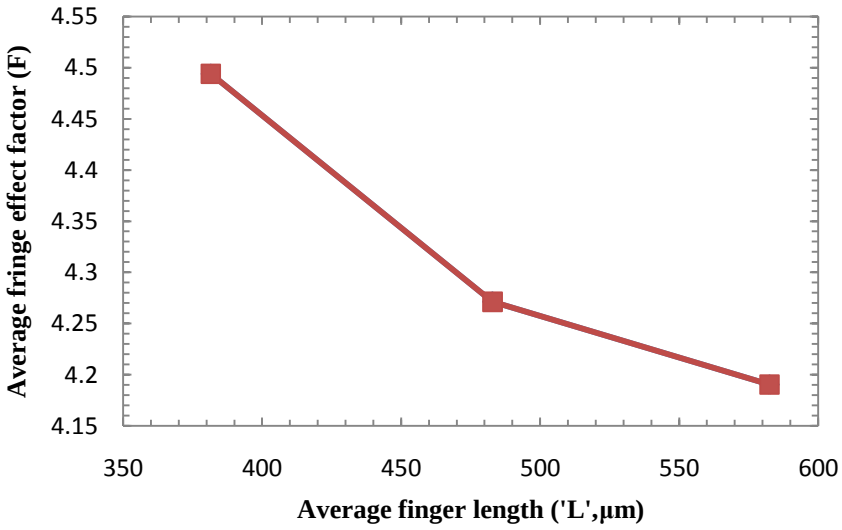

Figure 2.6: Variation of average fringe effect (F) with average finger length (L).

b) The fringe effect contribution to the total capacitance decreases with the increase in finger number. Hence, a 40 finger pair IDC has less contribution of the fringe effect than the 20 finger pair IDC.

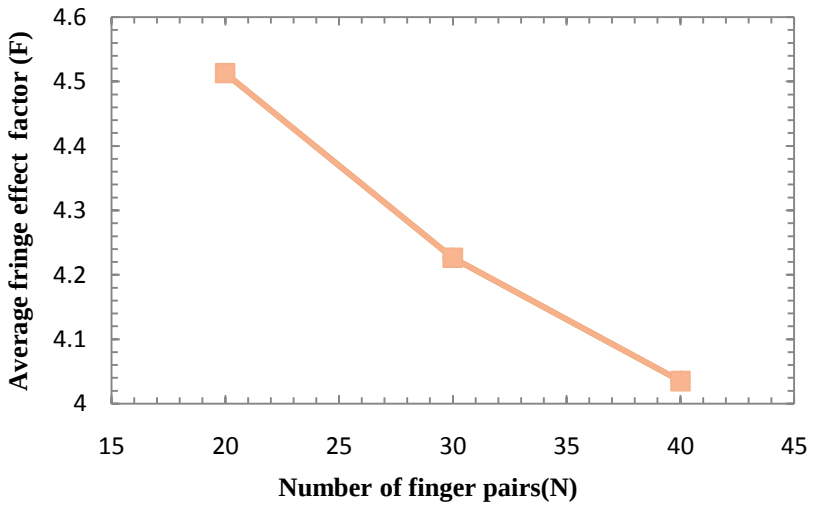

Figure 2.7: Variation of average fringe effect (F) with finger pair number (N).

c) The fringe effect increases linearly with increase in the average finger gap. Hence, an IDC with a 15 μm finger gap will have a higher fringe effect than an IDC with 5 μm finger gap.

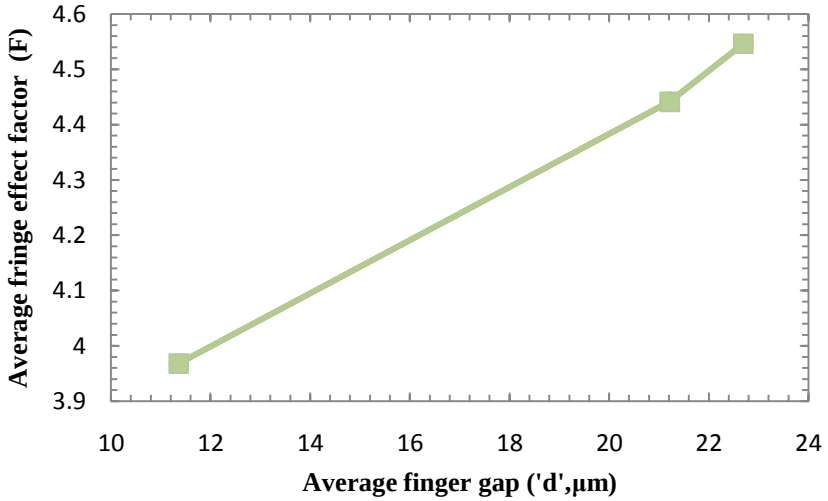

Figure 2.8: Variation of average fringe effect (F) with average finger gap (d).

The variation of capacitanace was observed with respect to the different physical parameters of the IDCs, and the behaviour was as shown below in Figures 2.9, 2.10 and 2.11. The average capacitance values are shown by the dotted lines.

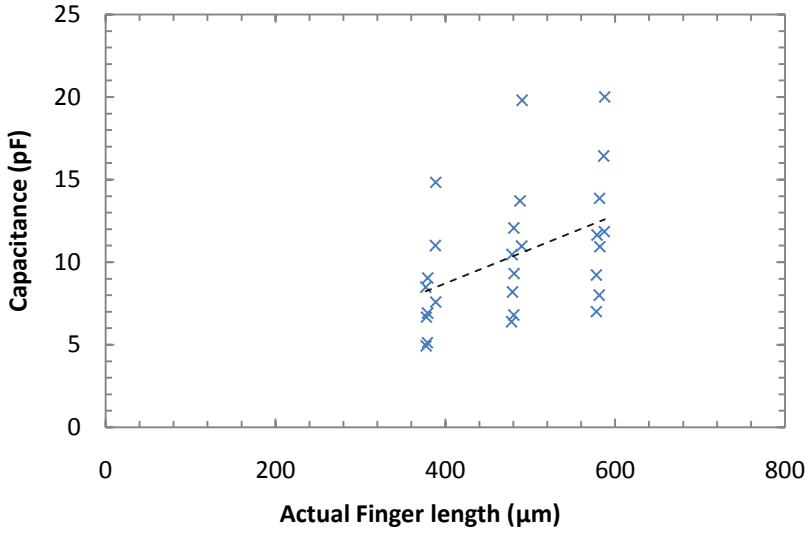

Figure 2.9: Variation of capacitance with actual finger length

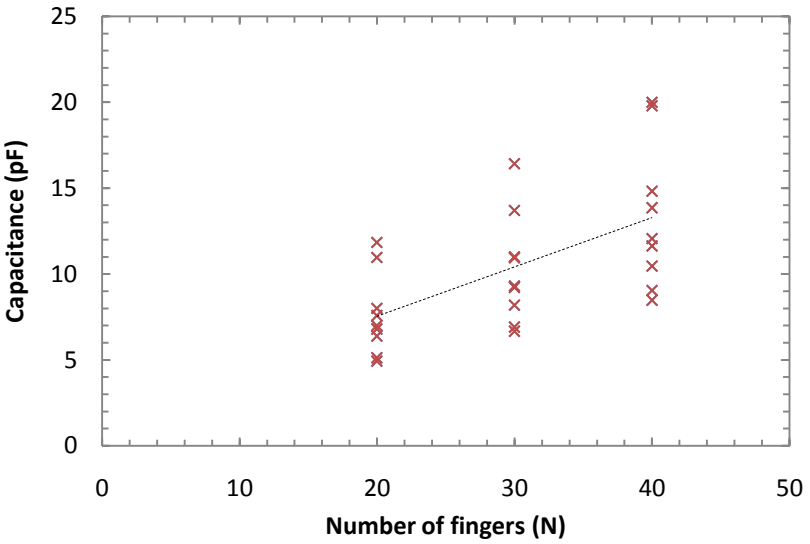

Figure 2.10: Variation of capacitance with number of fingers (N)

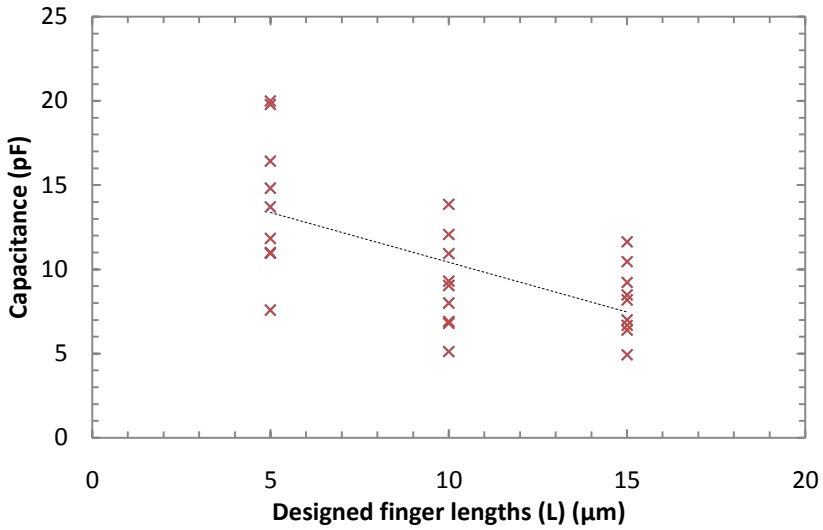

Figure 2.11: Variation of capacitance with designed finger lengths (L).

2.3 Final design selection

The final design was chosen after the following points were taken into consideration.

1) Finger length: Keeping in mind the precision and repeatability issues with 600 µm length fingers, it was seen that IDCs with a finger length of 500 µm offered a substantially high initial capacitance and also did not seem to have the drawbacks seen in the IDCs of the earlier configuration. Hence, 500 µm finger lengths offered a much higher reliability during fabrication. They also had a smaller size compared with the 600 µm finger length devices. At the same time, it was observed that the fringe effects were marginally higher than the 600 µm fingers but substantially less than the 400 µm long fingers. Hence, 500 µm finger lengths were finalized in the design.

2) Finger gaps: It was clearly evident from the formula (2.2), graph and Table 2.1 that 5 µm finger gaps not only give the highest initial capacitance, but also the least fringe effect factor. Hence, a gap of 5 µm was chosen in the design.

3) Finger number: For the number of fingers, it was evident from the previous section that the 40 finger devices often had uneven gaps on the two sides of each finger. Such errors or misalignments reduced the repeatability and precision of the devices with this design. Although the 40 finger devices showed a higher capacitance as compared with the 30 finger ones, it was the precision and repeatability of the design which was given a higher priority. Hence, it was decided to have 30 fingers in the final design.

CHAPTER 3

STRAIN SENSOR FABRICATION

The second chapter contained the main considerations essential to optimize the IDC design. In this chapter, discussion will focus on the fabrication technique which has been implemented in fabricating the sensor. Also, the different generations of devices and the modifications made during fabrication to adapt to the targeted applications are covered in detail.

3.1 Introduction

Most of the MEMS IDCs are fabricated by coating a thin metal film on non-metallic substrates [24][25][30]. It can be seen that this method does not yield very thick metallic fingers, resulting in small initial capacitance. In order to obtain higher capacitance with metal coated inter-digitated fingers, the overall finger dimensions will have to be increased or the finger gaps made as small as possible. To fabricate smaller finger gaps, very precise metal deposition techniques such as e-beam evaporation, thermal evaporation or physical vapor deposition would be needed along with very good masks. But these techniques can be used to obtain metal deposition only up to few microns and cannot be used to have high aspect ratios or higher finger thickness. Aspect ratio is the ratio of the feature thickness to the smallest feature size for a particular device. To make the metal coating thicker, high aspect ratio fabrication techniques such as LIGA [Lithographie, Galvanoformung, Abformung (Lithography, Electroplating, and Molding)] would be needed. Using LIGA thicknesses as high as 200 μm can be achieved but this technique is costly and time consuming.

In this work, a simple laser micromachining technique was used to achieve thick, purely metallic or non-metallic inter-digitated fingers. The micromachining technique was used along with simple fabrication steps to manufacture the IDC strain sensors. The IDC was encapsulated

in a flexible, bio-compatible polymer which also acted as a dielectric permitting a high degree of stretching.

3.2 Micromachining technique

In the fabrication technique used, a metal sheet, about 127 μm thick was cut out in the desired shape and size by using an *Oxford diode laser,* manufactured by "Industrial Systems". Dedicated software- '*Alphacam Advanced profiling'* was used to sketch the designs and define the cut paths for the laser beam to follow. The software also allowed generation of an output program for the cut path defined in the design. This output program was then loaded and compiled in the laser. The laser had a dedicated computer for interface with the user which allowed compiling the programs generated in the *Alphacam Advanced Profiling* software. Adjustments to the laser beam for various settings could also be made using the interface. Laser settings could be changed as per the sample to be cut and the specifications of the cut out. Figure 3.1 below shows the *Oxford laser* which is used to cut the metallic IDCs.

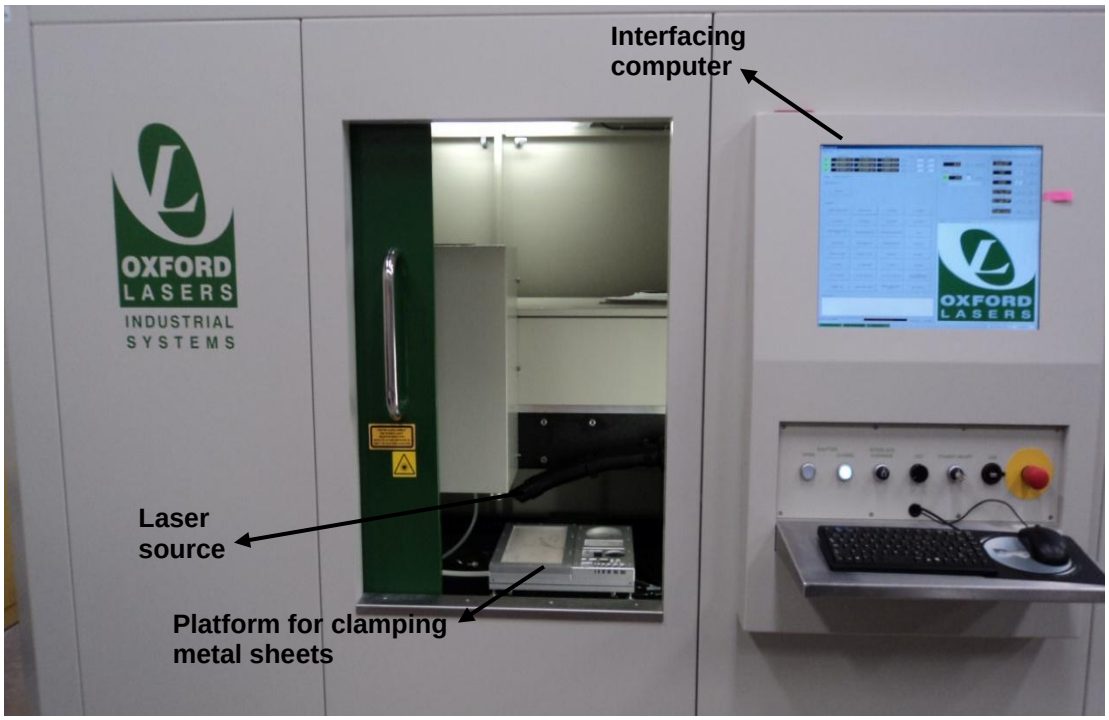

Figure 3.1: Oxford laser.

The entire laser micro-machining technique can be explained from the algorithm below.

Step 1- The design to be cut in the laser was first sketched in the *Alphacam Advanced Profiling* software. Figure 3.2 below shows the screen shot for the software with device tool paths for three 40 fingers IDCs with 15 µm finger gaps and variable finger lengths.

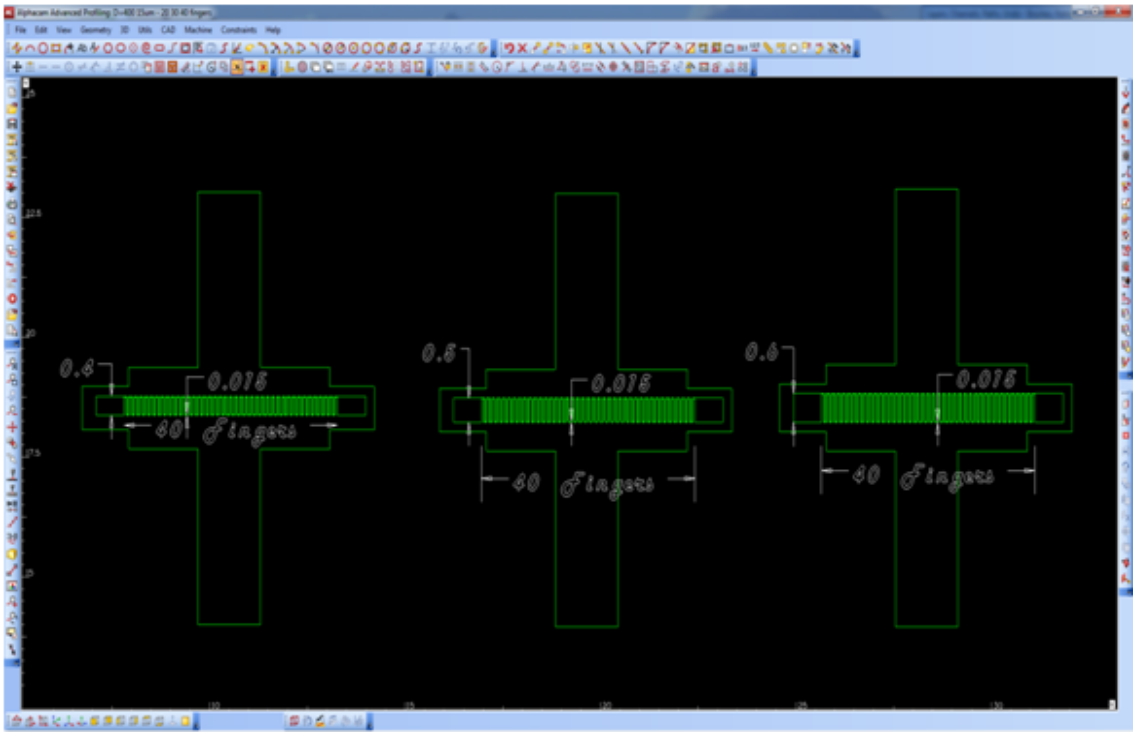

Figure 3.2: Screen shot of *Alphacam Advanced Profiling* software showing different IDC designs.

Step 2- Once the design was made in *Alphacam Advanced Profiling*, the cut paths were assigned to the design. Cut path denoted the path and the direction along which the designs were needed to be cut in the laser. An output program file was generated which contained the co-ordinates for the various designs defined by the cut path. This file was edited for functional optimization and converted in to a text file to be loaded in to the laser user interface. A sample program for an IDC of 500 µm finger lengths, 5 µm finger gaps and 30 finger pairs is provided in Appendix for reference.

Step 3- Once the output files for the design were created, the laser was turned on. The procedure for turning on the laser had to be precisely followed. It was essential to check if the coolant water level was above a certain minimum requirement and that the water level remained well above the minimum mark till the laser completed the cut outs. Once the preliminary work was completed, the *Oxford Laser CNC* software was started on the interfacing computer. Before the laser was started, the metal sheet to be cut was clamped on to the work bench platform with the help of screws. Smaller jig positions on the platform were preferred as they allowed the metal to be clamped with minimum slacking. Once the metal sheet was fixed, the internal laser shutter was opened followed by turning on the laser diode and allowing the current to build up to the working value of 48.08 Ampere. Once the laser emission was turned on, the platform was homed to get to its initial position of x,y,z (0,0,0). Once all the axes are zeroed, the laser was manually moved along x and y axes to point the beam on the perfect position of the metal sheet. With this, the metal sheet was ready for calibration. Images of the platform, interfacing computer are shown in the Appendix.

Step 4- For any design, there were four main parameters needed to accurately set for perfect cut out. These included the laser power, the number of loops for the laser to follow a cut path, laser speed and the vertical distance between the metal sheet and the laser. Calibration was done by cutting a small piece of circle on the metal sheet after adjusting the power and speed at a particular setting and adjusting the number of loops such that the cut out circle fell through completely. The amount of loops or passes required for the cut out depended on the type of substrate or metal sheet to be cut and the sheet thickness. Brittle metals such as nickel or brass required less cut out time compared with more ductile metals such as titanium. Metals with higher ductility also invariably required more laser power to obtain the same cut out. Figure 3.3 below shows the images of perfect cut outs on the titanium and brass sheets placed at jig 1 position on the laser. All the devices were cut at jig position 1 since it allowed parallel cutting of

four IDCs accurately. Other jig positions were too small to allow IDC cut outs or were too big resulting in slacking of the metal piece resulting in loss of laser beam focus.

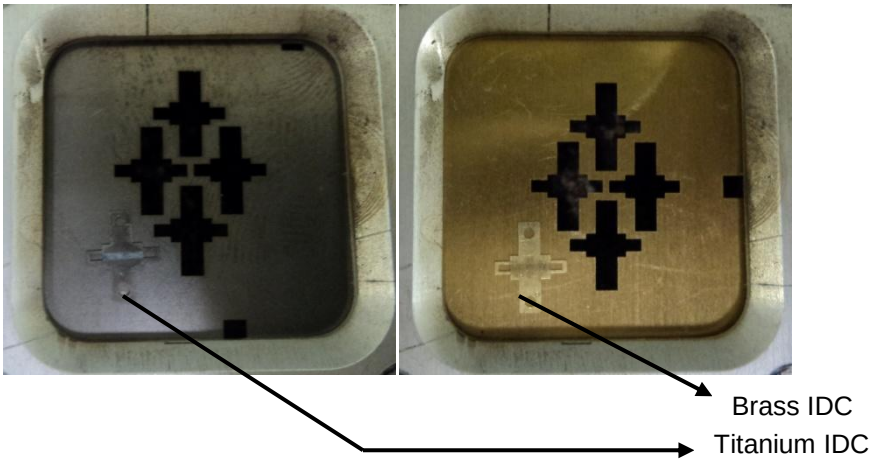

Figure 3.3: Jig 1 position showing (a) Titanium IDC cut out (b) Brass IDC cut out.

Step 5- Once the calibration was done, the text file containing the cut out coordinates (*Output NC file*) for the device design was loaded on to the *Oxford Laser CNC* software on the interfacing computer on the laser. This software allowed us to adjust the various different settings for the cut outs to be obtained and calibrate the Output NC file generated on *Alphacam Advanced Profiling*. Detailed images for the *Oxford Laser CNC software* are provided in the Appendix I. The external shutters on the laser were then opened and the laser was allowed to run on the programmed coordinates.

3.3 Side walls after fabrication

For the chosen finger gaps, it was always observed that there was a difference between the actual finger gap seen in the device and the device design made in the *Alphacam Advanced Profiling.* If the device design was made to have the finger gap of 5 μm, it was expected that the actual finger gap on the front and back of the IDC would be 5 μm. This meant, the side walls of the fingers were expected to be straight. But this was not observed in reality. To understand the

reason for this difference, it was important to see how the laser actually eroded the metal surface. When the metal sheet was fixed at the jig 1 position at the beginning of the micro-machining, the laser beam was focused on the top face of the sheet. As the number of passes made by the laser beam went on increasing, the top layer of the sheet melted, exposing the lower layers of the sheet. This meant that the laser was actually going out of focus as the number of cutting loops increased. The beam actually had maximum power when it was cutting the top surface of the sheet and the power kept on decreasing as the lower layers of the metal sheet were being exposed. This gave rise to slanting side walls of the fingers of the IDC similar to anisotropic etching in silicon. Hence, the designed gap of 5 μm was not seen in the actually fabricated device. Instead, gaps of about 6-8 μm were observed at the back end of the metal sheet while the front face of the metal showed larger gaps of about 12-15 μm as it was exposed to higher laser power. Such slanting finger walls were observed in all the materials used to make IDCs. If the laser power was reduced to achieve gaps of about 5 μm on the top surface as per the design, complete through cuts were not observed. Keeping this in mind, average finger gaps were considered instead of individual front or back face finger gaps. Figure 3.4 below show the resultant finger cross after complete fabrication.

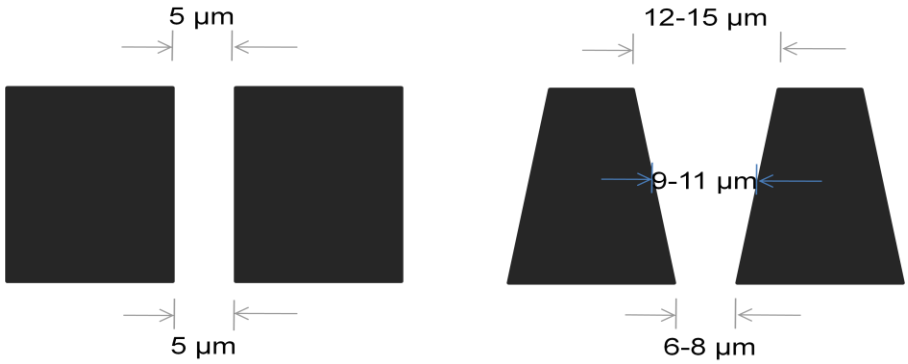

Figure 3.4: Finger cross section (a) Expected cross section (b) Observed cross section.

3.4 Titanium strain sensor fabrication

Laser micro-machining was the most crucial step in the strain sensor fabrication process. The details of this process were explained in the previous section. In this section, the pre and post laser micro-machining processes involved in the complete sensor fabrication are explained. The fabrication was done using three major materials to form IDCs. Also, the fabrication methodology and the materials used were modified according to the targeted applications. Firstly, the fabrication technique involving titanium IDC is explained. This was the first method used to fabricate sensors.

3.4.1 Titanium IDC with PDMS encapsulation (Generation I) strain sensor

The first generation strain sensors were fabricated using titanium sheet to form the Inter-digitated capacitor. Titanium was chosen because it is highly inert inside the human body since it is unaffected by bodily fluids and it offers good biocompatibility. Being strong and tensile, it allowed micro-machining in the desired way and was the first choice for the metallic IDCs. Titanium IDCs were completely encapsulated in the dielectric poly dimethyl siloxane (PDMS). PDMS is a bio-compatible polymer and is widely used in implantable devices [31] [32]. PDMS not only formed the dielectric in between the fingers, it also allowed the entire device, along with the connections, to be completely encapsulated making the entire device implantable for future applications. This polymer itself was the bottom most layer of the device which was used to adhere the strain sensor on the structure.

Generation I strain sensor fabrication consisted of the following steps:

Step 1- Pre micro-machining

As mentioned before, the laser repeatedly melts the metal along the cut path it follows. It is important that the debris formed due to the melting be removed in post micro-machining steps. To make the removal of debris easier, before laser micro-machining, one face of the titanium

sheet was spun coated with a layer of *S1813* photoresist. This photoresist layer protected the region of titanium which was not directly impacted by the laser and aided easy removal of the debris and ash resulting from the melting titanium.

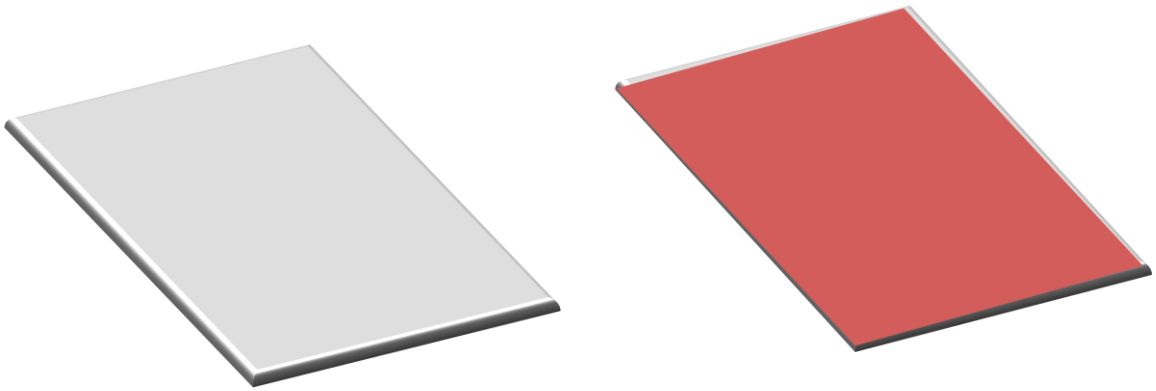

(a) (b)

Figure 3.5: After fabrication step 1 (a) titanium sheet before photoresist and (b) titanium sheet after photoresist coating.

Step 2- Laser Micro-machining

The photoresist coated titanium sheet was placed in the jig position 1 which allowed for uniform metal cut outs. The micro-machining was done as per the steps explained in section 3.2. When the cut out was made, it was important that the two finger pairs were not allowed to separate. Hence, “bridges” were introduced in the design to keep the two sets of fingers together. As shown in the Figure 3.5, the “bridges” were just extension of the main titanium device. These were later cut off from the device so to break the connectivity.

Step 3- Post micro-machining

After the IDCs were cut in the laser, they were kept in a beaker with acetone and cleaned in an ultrasonic machine (*Branson 1510)* for 5-10 minutes. The high frequency vibrations caused the loose debris within the fingers to get washed away. The integrity of the devices was checked

under a microscope and the non-precise devices were discarded. Figure 3.6 shows the schematic of the IDC after steps 2 and 3. Figure 3.7 shows the fingers of titanium IDC after complete cleaning process.

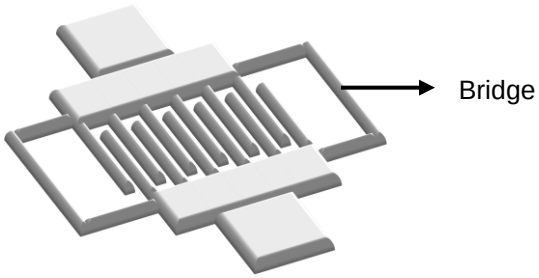

Figure 3.6: IDC cut out after fabrication steps 2 and 3.

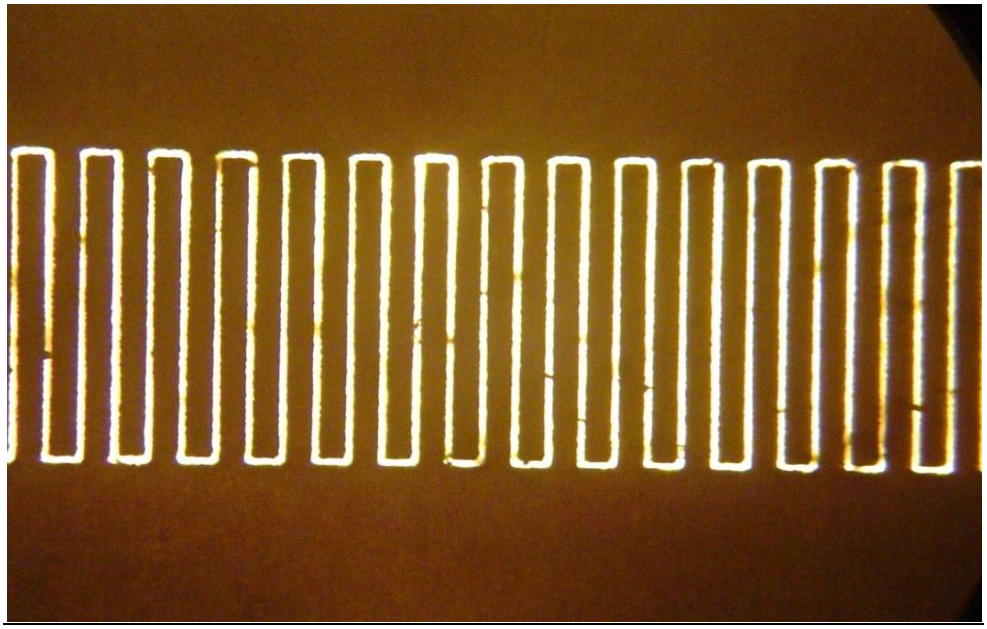

Figure 3.7: IDC fingers under microscope after fabrication step 3.

Step 4- Bottom encapsulation layer

Once the IDCs were made, the cut out was placed on to a nearly cured thin layer of *Sylgard 184* (PDMS) spread uniformly on a glass slide. PDMS was mixed with the curing agent with a 20:1 ratio. This ratio was maintained constant for all the Generation I devices since the flexibility of the completely cured PDMS depends on the percentage of curing agent added [37]. After the

IDC was placed onto the nearly cured PDMS bottom layer, the PDMS was allowed to cure completely after which the IDCs remained firmly attached to the PDMS, which formed the bottom layer of the strain sensor.

Step 5- “Bridge” cutting

After the PDMS was completely cured, the “bridges” were cut off using the laser. The IDCs with the contacts were placed on the laser work plane. An inbuilt function allowing straight line cutting along X-axis or Y-axis was used to perform the cut. These inbuilt functions were used with high power to have a quick cut with low precision. Once the laser cut through the “bridges”, they were removed using tweezers breaking of the conductivity in the two sets of fingers. Firm attachment with the bottom PDMS layer prevented any movements or misalignments between the two finger pairs on the IDC.

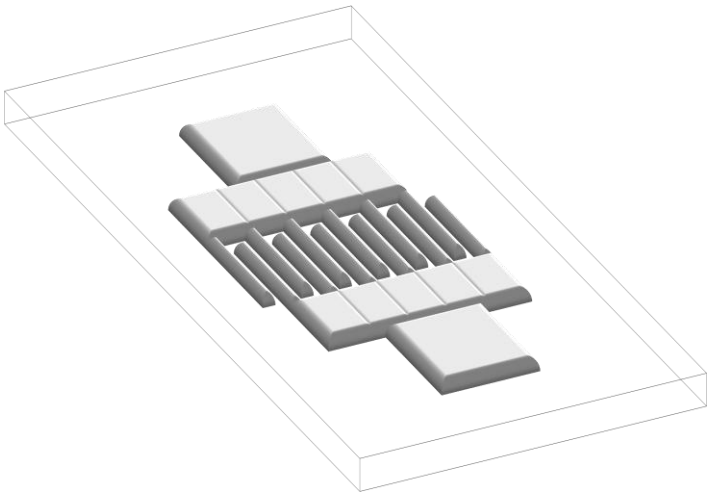

Figure 3.8: Strain sensor after fabrication step 5.

Step 6- Electrical contacts

Once the IDC was firmly attached with the bottom PDMS layer, electrical contacts were made on to the titanium metal surface. The surface of the IDC was scratched lightly with a sharp object like a razor. This allowed better grip and adhesion for the electrical contacts. The

contacts were made by a conductive epoxy consisting of epoxy resin and silver. Copper wires were kept in contact with the scratched surface of the titanium IDC and silver epoxy paste was carefully dropped on to the metal surface. The silver epoxy paste was made after mixing individual silver and epoxy pastes mixed in 1:1 ratio. Once the paste was dropped, it was allowed to cure at a temperature of 90^{o} C for 5 minutes. Heating cured the paste to make strong contacts. It was observed that the ratio of silver to epoxy was crucial. Slight imbalance in the unity ratio caused a large change in the curing time. Very thin 32 AWG copper wires were used.

Step 7- Complete PDMS encapsulation

Once the conductivity was broken and connections were made, the entire titanium IDC was poured with another top layer of PDMS in the ratio 20:1 with 20 parts of PDMS over 1 part of the curing agent. The two layers of PDMS were made as thin as possible so as to have maximum possible stretch.

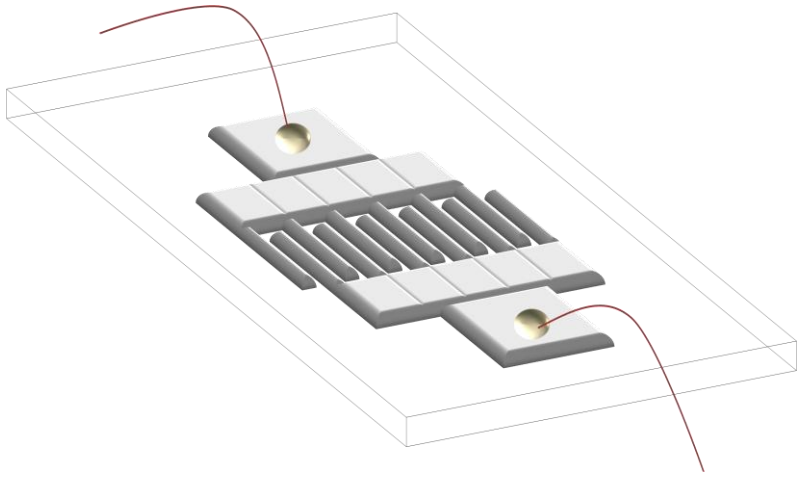

Figure 3.9: Strain sensor after fabrication steps 6 and 7.

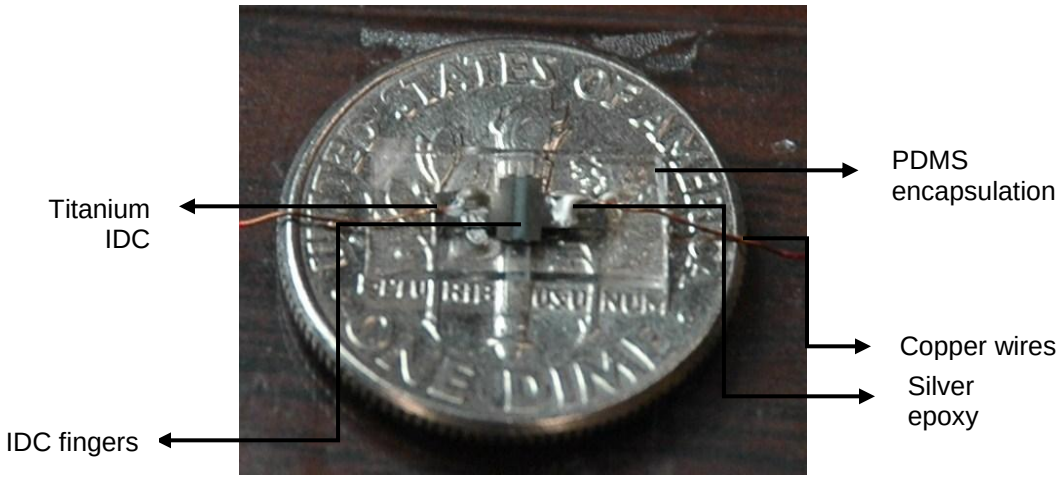

Figure 3.10: Actual titanium strain sensor encapsulated in PDMS layer placed on a dime.

3.4.2 Limitations in the use of Generation I strain sensors

Although the Generation I devices were easy to fabricate, were totally bio-compatible and possessed great stretching ability, they were not used in the targeted applications of structural health monitoring and bladder volume monitoring. They were used for preliminary experiments (as shown in chapter 4). Some of the drawbacks associated with the use or fabrication of the generation I devices are given below.

3.4.2.1 Limitations in use of PDMS bottom layer

In the fabrication steps mentioned above, certain issues were evident when the device was practically tested for applications. Since PDMS formed the bottom layer, it was very difficult for the device to be attached to any structure even with strong glues without any surface modifications due to its low surface energies [33] [34]. Being a transparent rubber type structure, suturing of PDMS on to a substance was also not advisable as it was observed to tear or break easily at the point of suturing.

3.4.2.2 Large time requirements

Apart from the limitations involved in using the PDMS bottom layer, there were some problems associated with the use of titanium for micro-machining the IDCs. Titanium has a very high melting point of about 1800˚ C or about 3260˚ K. During laser micro-fabrication, it was observed that titanium required large amount of time to melt and form a through cut. Each IDC device took about an hour to completely form a through cut. To reduce the time factor, the laser power was increased, which resulted in further melting and ash formation. Moreover, the bio-compatibility of titanium was not a necessity for the strain sensors. As the metal IDC was completely encapsulated within a bio-compatible polymer, it was not mandatory for the metal to be bio-compatible.

3.4.2.3 Large debris formation on titanium

It was observed that a large amount of debris was formed when titanium sheet was repetitively melted by the laser beam during micro-machining. Titanium, being highly tensile and possessing a higher melting temperature, required large laser power and long exposure time. Even though the IDC underwent ultrasonication and immersion in acetone for cleaning, complete debris removal was not possible. Photoresist spin coating also could not permit complete removal of ash formed as a result of solidifying of the melting metal. The solidified ash can be clearly seen from the SEM images below. The laser beam facing end of titanium (Figure 3.11) showed a large amount of debris formation as compared with the back end of titanium sheet (Figure 3.12). This clearly explained why the ash and debris formation was due to the heavy melting of titanium. The main problem associated with the ash was that it could give rise to electric fields which could not be explained logically. Hence, it was desirable to reduce the ash formation.

Figure 3.11: Scanning Electron Microscope image showing debris formed on the IDC surface on the laser beam facing end of the titanium sheet.

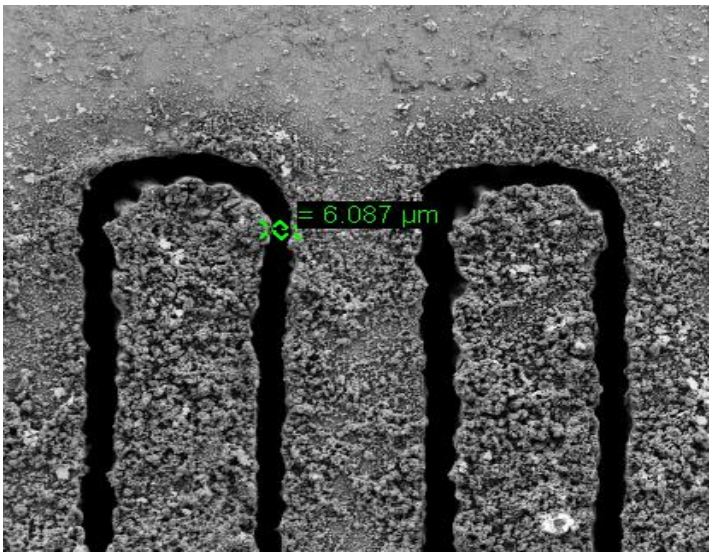

Figure 3.12: Scanning Electron Microscope image showing debris formed on the IDC surface on the back end of the titanium sheet.

Keeping in mind the issues faced with the fabrication, it was decided to slightly modify the fabrication process and use a metal for the IDC which will give rise to less debris on the metal surface.

3.5 Brass strain sensor

Keeping in mind the problems faced with the use of titanium in generation I devices, it was important to use a different metal to fabricate the IDCs. It was important that the new material to be micro-machined should give rise to less debris compared with titanium and at the same time not affect the capacitance of the device. Various metals such as nickel, stainless steel and brass were tested for their performance under the laser during micro-machining. It was observed that nickel was very brittle and could not withstand the high temperature laser beam and the nickel IDCs broke easily. Stainless steel though showed high tensile strength, was found to burn along the finger lengths leading to very charred features. Brass was found to have the best performance of the three metals. Being more brittle as compared with titanium, it took less micro-machining time with no burning. Brass was used for the next generation of devices.

3.5.1 Brass inter- digitated capacitors

As an alternative material for micro-machining IDCs, brass was tested under the laser. Brass has a melting temperature of about 930 ^{o} C which is about half of that of titanium. Hence, it was expected that brass would take less time to cut and lead to less amount of ash. Also brass, being brittle was expected to be easier to cut or micro-machine. It was important that the initial capacitance values were not affected with brass as the IDC. The observations for brass were as follows.

3.5.1.1 Time required for laser micromachining of brass

While laser micro-machining brass, it was observed that brass IDCs took less time to cut as compared with titanium IDCs. In about half the time, similar finger gaps were obtained on brass IDCs which proved that brass was a lot easier to cut in the laser than titanium. This helped in substantially saving micro-machining time and increased the throughput of the strain sensors.

3.5.1.2 Debris formation on brass

Debris formation in brass was observed to be lot less when compared with titanium. This was clearly evident from the SEM images for brass IDCs. The main reason for low debris formation was because brass is brittle and can be cut with fewer efforts and lower temperatures. Also brass required lower laser power leading to less surface melting. The SEM images below show the front and back faces of the brass IDCs.

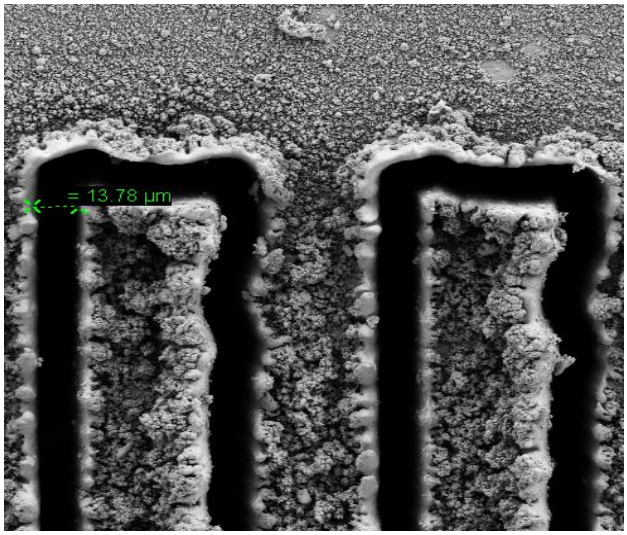

Figure 3.13: Scanning Electron Microscope image showing debris formed on the IDC surface on the laser beam facing end of the brass sheet.

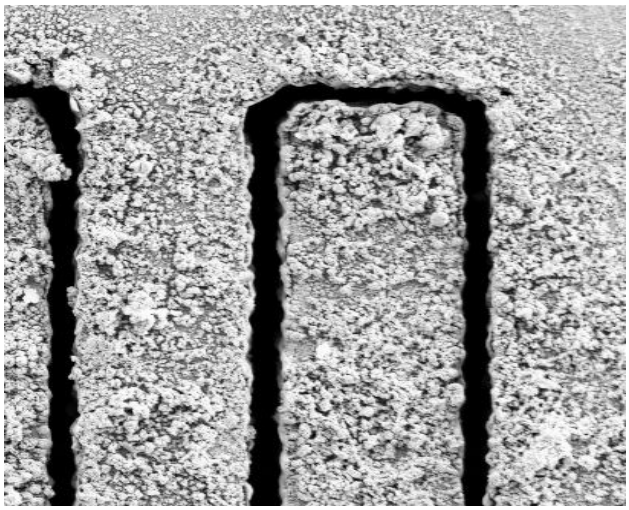

Figure 3.14: Scanning Electron Microscope image showing debris formed on the IDC surface on the back end of the brass sheet.

3.5.1.3 Initial capacitance value comparison

After the performance of the brass IDCs was tested during fabrication, it was required to compare the initial values of the titanium IDCs and the brass IDCs. There was no change expected in the capacitance values. For thorough comparison, it was important that the exact gap between the fingers of each device be known accurately. If the IDCs of the two metals having the same capacitance values were shown to possess the same average finger gap, then it would be fair to conclude that switching from titanium to brass would not affect the IDC capacitance. For the comparison purpose, four sets of IDCs were made for each metal and before the IDCs were placed on the lower PDMS layer, they were run under SEM to find out the gaps between fingers of each device. The table below compares the practically observed capacitance values of each of the devices with the finger gaps for the respective IDCs.

Table 3.1: Comparison between Titanium and Brass IDC capacitance values with respect to finger dimensions.

Device	Average finger gap (μm)	Average finger length (μm)	Practical Capacitance (pF)
Brass_01	10.69	489.315	14.12
Brass_02	9.77	490.23	14.44
Brass_03	10.26	489.73	14.4
Brass_04	10.63	489.36	14.26
Titanium_01	10.499	489.501	14.30
Titanium_02	13.72	486.27	11.94
Titanium_03	15.211	484.789	11.20
Titanium_04	13.066	486.93	12.65

From the table it could be observed that the average gap for the four titanium IDCs was more than the average gap for the four brass IDCs. As a result, the average capacitance for the four titanium IDCs is less than the average practical capacitance for the four brass IDCs. For IDCs of the two metals having comparable finger gaps and finger lengths (devices: Brass_04 and Titanium_01), the capacitance values were also found to be comparable. The SEM images below show the finger gaps of the IDCs having comparable gaps (devices: Brass_04 and Titanium_01). As mentioned previously, the average finger gaps were calculated from the

values of the finger gaps at the laser facing front end and the finger gaps at the back end. Direct comparison also showed that brass IDC (Figure 3.15 (a)) showed much less debris as compared with titanium IDC (Figure 3.16 (a)).

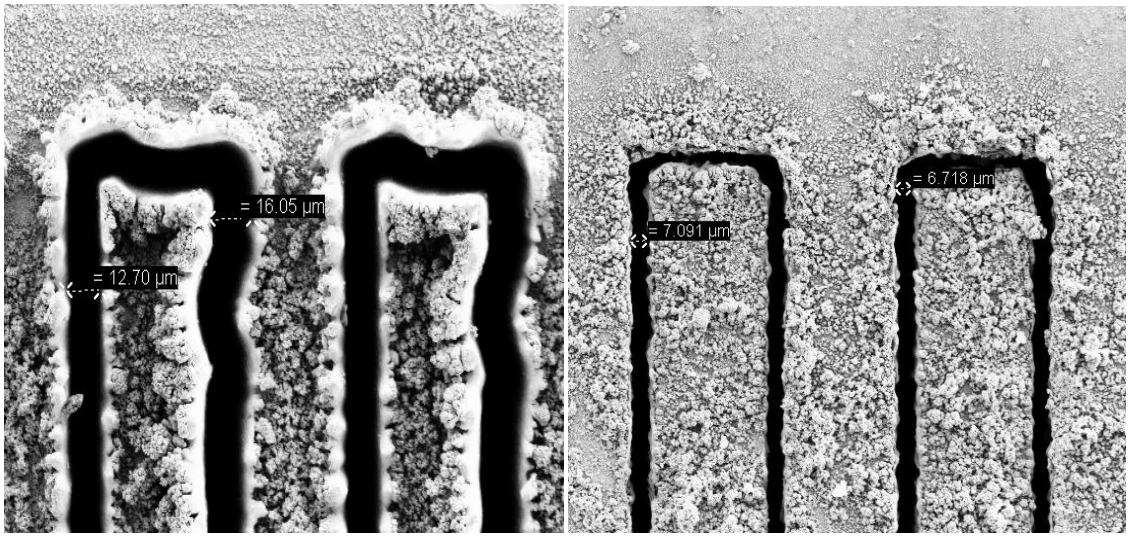

(a) (b)

Figure 3.15: Scanning Electron Microscope image showing (a) front face and (b) back face finger gaps of brass_04 IDCs.

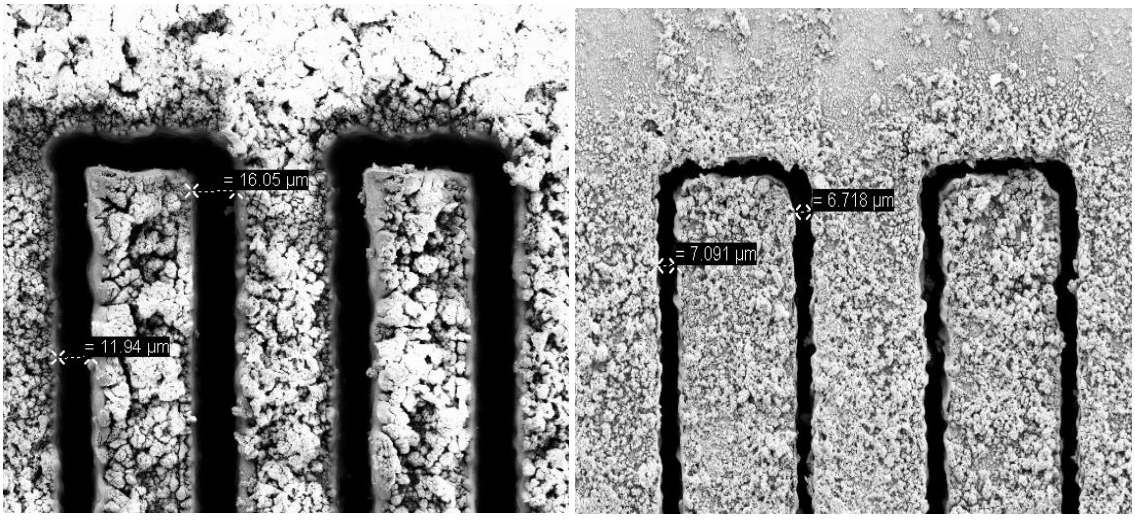

(a) (b)

Figure 3.16: Scanning Electron Microscope image showing (a) front face and (b) back face finger gaps of titanium_01 IDCs.

3.5.2 Brass IDCs with PDMS encapsulation and polyimide bottom layer (Generation II) devices

The basic steps for the fabrication of generation II devices were similar to those for the titanium strain sensors. The major difference during fabrication was that instead of having the entire fabrication done on a glass slide, it was now done on a 50 μm thick polyimide film making the polyimide film as the bottom most layer of the strain sensor. The thinnest commercially available polyimide (*kapton)* film was chosen so that it did not reduce the sensitivity of the strain sensor. This substantially improved the adhesion of the strain sensors to underlying structures. *Kapton* films have good adhesion properties and have been used in strain sensor applications [35].

Generation II devices had the following fabrication steps:

Step 1- Pre micro-machining

To make the removal of debris easier, one face of the brass sheet was spun coated with a layer of *S1813* photoresist before laser micro-machining. This photoresist layer protected the region of brass which was not directly impacted by the laser and allowed easy removal of the debris and ash.

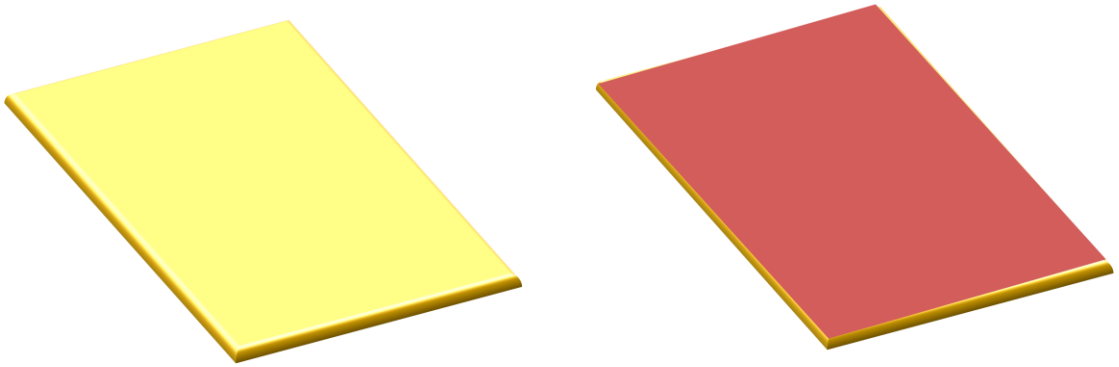

(a) (b)

Figure 3.17: After fabrication step 1 (a) brass sheet before photoresist and (b) brass sheet after photoresist coating.

Step 2- Laser Micro-machining

The photoresist coated brass sheet was placed in the jig position 1 which allowed for uniform metal cut outs. The micro-machining was done as per the steps explained in section 3.1. As in the case of titanium devices, the brass devices also had “bridges” to keep the finger pairs from separating. These were later cut off from the device so as to break the connectivity.

Step 3- Post micro-machining

After the IDCs were cut in the laser, they were kept in a beaker with acetone and cleaned in an ultrasonicator machine for 5-10 minutes. The high frequency vibrations washed away the debris present on the device and also cleaned some of the melted metal in between the fingers. The integrity of the devices was checked under a microscope. Figure 3.18 shows schematic of brass IDC after complete cleaning process.

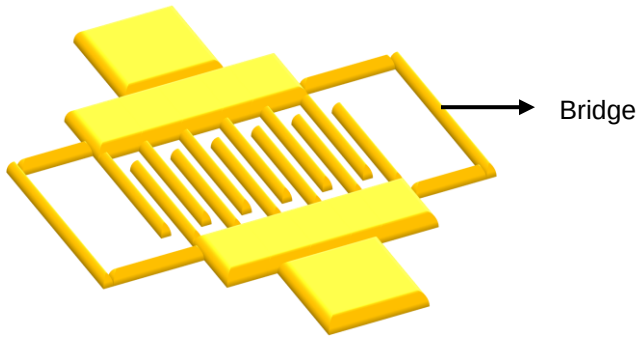

Figure 3.18: Generation II IDC after fabrication steps 2 and 3.

Step 4- Bottom encapsulation layer

Sylgard 184 (PDMS) was spin coated on a 50 µm thick *kapton* film to form a uniform, thin and well adhered PDMS layer. PDMS was mixed with the curing agent with a 10:1 ratio with 10 parts of PDMS over 1 part of the curing agent. This was unlike the case of titanium strain sensors. The change in the ratio was made to reduce the stretch ability of PDMS with respect to *kapton* as it is observed that stretching ability or the Young’s modulus of PDMS depends on the

ratio of PDMS to curing agent. This ratio was maintained constant for all the generation II devices made. The IDCs were placed on PDMS layer just before it cured completely. After complete curing, the IDCs were firmly attached to the PDMS, which in turn was on a think *kapton* film forming the bottom layer of the strain sensor.

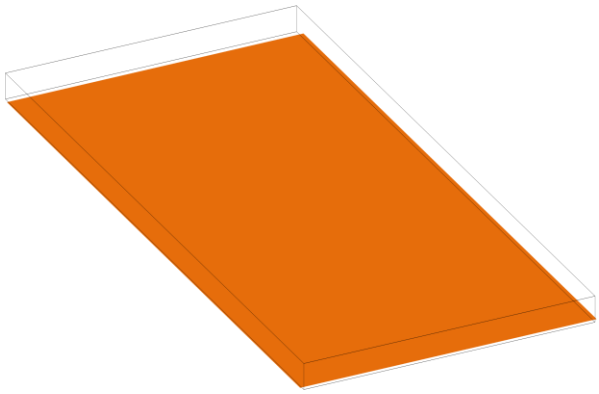

Figure 3.19: Generation II strain sensor during fabrication step 4.

Step 5- “Bridge”cutting

After the PDMS was cured completely, the “bridges” which were included in the device design to hold the opposite finger pairs together, were cut off. This step was also done on the laser similar to the one for titanium strain sensors to have a quick cut with low precision and high power. Once the laser cut through the “bridges”, they were removed using tweezers breaking the conductivity between the two sets of fingers. Firm attachment with the PDMS layer prevented any dislocation of the fingers from the initial position.

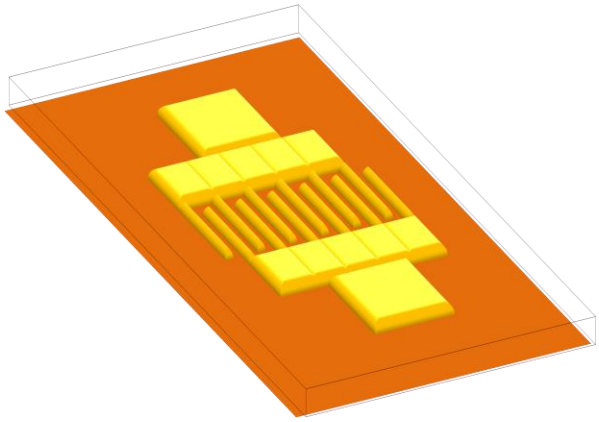

Figure 3.20: Generation II strain sensor after fabrication step 5.

Step 6- Electrical contacts

Once the IDC is firmly attached with the bottom PDMS layer, electrical contacts were made on to the brass surface. The brass surface was scratched lightly with a sharp object like a razor allowing better grip and adhesion for the electrical contacts. The contacts were made by a conductive epoxy consisting of epoxy resin and silver as in the case of titanium strain sensors. The process followed for making the contacts was same as the one for titanium strain sensors.

Step 7- Complete PDMS encapsulation

Once the conductivity was broken and connections were made for each set of fingers, the entire brass IDC was poured with another top layer of 10:1 PDMS. The two layers of PDMS were made as thin as possible so as to have maximum possible stretch.

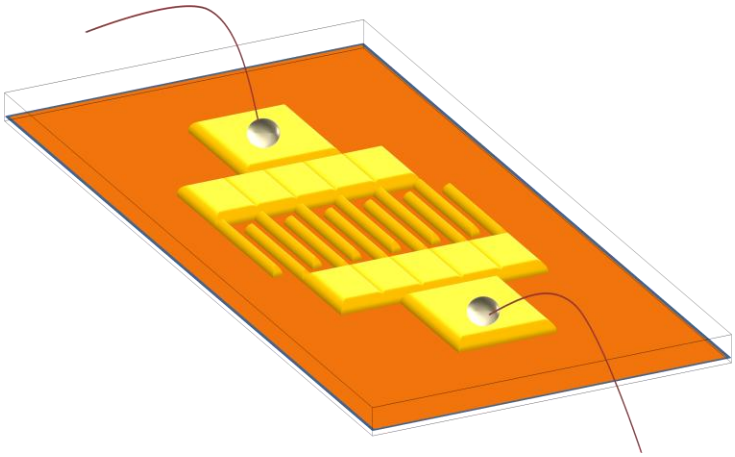

Figure 3.21: Generation II strain sensor after fabrication steps 6 and 7.

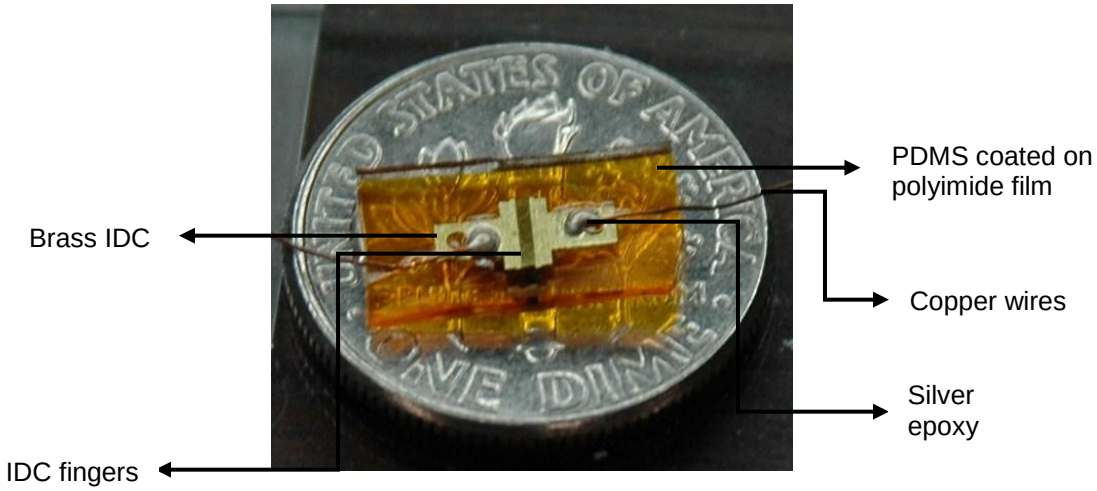

Figure 3.22: Actual brass strain sensor encapsulated in PDMS and with a polyimide bottom layer placed on a dime.

3.5.3 Disadvantages of brass IDCs with PDMS encapsulation and polyimide bottom layer (generation II) devices

3.5.3.1 Reduced stretch ability

It was shown from the previous section that generation II devices were more advantageous than the generation I devices. But there was one obvious drawback in using

these devices. Even thought the polyimide film used as the bottom layer in these devices was about 50 μm in thickness which was the thinnest commercially available polyimide film, it did not possess the ability to stretch as much as PDMS [36] [37]. In other words, the stretching ability of the generation II devices was limited due to the polyimide film. As a result, the generation II devices could not stretch as much as the generation I devices. This limitation however, did not affect the performance of the strain sensors as the applications required strain sensing below 1% strain levels. For such strain levels, high stretching ability was not required and the polyimide film did not limit the detection of strains in this range.

3.5.3.2 Inability to be used for spherical structures

The generation II devices were shown to be sensitive to strains over structure with minimum curvatures or planar structures. In the case of spherical structures where the diameter of the structure changed, these sensors lost their sensitivity. This loss was due to two different reasons acting at the same time but in opposition to each other. As mentioned in chapter 2, the application of strain on the sensor causes the overlapping finger length of the IDC to reduce resulting in reduction in capacitance. In the case where the sensor was placed on a small spherical structure, the rigid metallic fingers of the IDC could not bend along the shape of the sphere making the fingers cross each other (at an angle) reducing the overlap area of the fingers. Even though the complete strain sensor was flexible, the actual IDC itself was rigid making it unable to adapt to the shape of a spherical structure below it. When the spherical structure below the sensor deformed, expanded or contracted slightly, the sensor could no longer follow the changes uniformly. The happenings can be better explained with an example. Consider a small cylinder with the strain sensor attached on its circular walls. The fingers of the IDC will not follow the same cylindrical shape as they cannot bend but will show a reduced capacitance because the fingers cross each other and the overlap finger area (shaded) is small as shown in Figure 3.23.

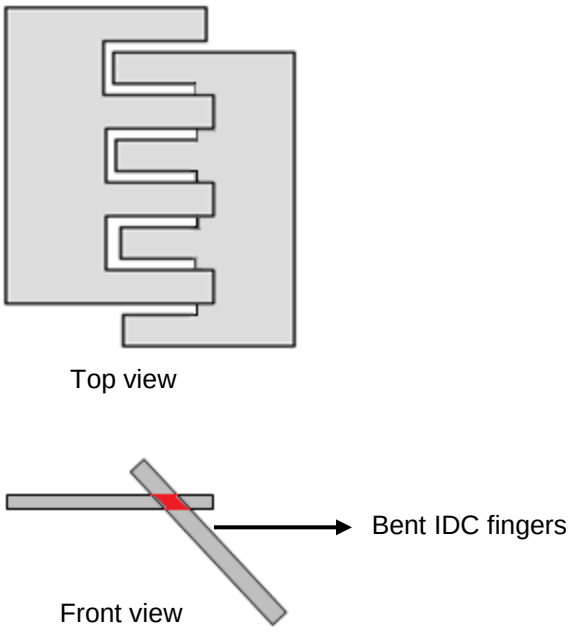

Figure 3.23: The bending of the IDC when placed on a curved surface with high curvature. Front view showing the crossing of the fingers due to the inability of the metal fingers to bend.

Now if the cylinder were to expand, the strain sensor would stretch causing the fingers to move away from each other thus reducing the capacitance. At the same time, the curvature of the cylinder will reduce, in turn reducing the bend in the fingers, thus causing the overlap area of the fingers to increase. This would in turn cause the capacitance output of the strain sensor to increase. These two operations will take place at the same time yielding a very small net change in the output capacitance. This is shown in Figure 3.24. In the case where both the working principles were to be equal in effect, the net change in capacitance would be zero. If both the effects are not equal, it is difficult to predict whether the capacitance will increase or decrease with decreasing capacitance. Hence, for applications involving spherical structures, it was decided to make the IDC fingers themselves flexible and for this newer materials were used. The new strain sensor fabrication technique is explained in the Section 3.6.

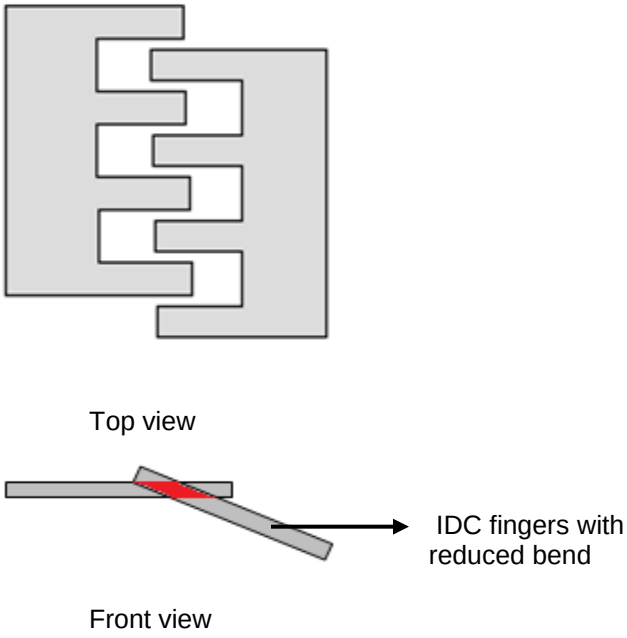

Figure 3.24: The IDC placed on an expanded curved surface with reduced curvature. Top view showing reduced overlap finger length. Front view shows the increased overlap area (in red) due to reduced curvature.

3.6 Aluminum sputtered *kapton* IDC strain sensor

In order to nullify the loss of sensitivity of the brass IDC strain sensors over spherical or curved surfaces, it was important to make the fingers flexible. In both the previous designs, the actual IDC fingers were rigid since they were metallic. A new idea for fabrication was implemented in which the IDCs were laser micro-machined out of 120 μm thick commercially available polyimide (*kapton)* film. Even though *kapton* was flexible, it was non metallic thus requiring an additional step for metal deposition or coating. Being a polymer, it was very easy and quick to laser micro-machine the *kapton* and form the IDCs. However, the overall time for fabrication did not change since the additional metal coating step introduced a substantial amount of time requirements. The detailed fabrication steps for generation III devices are given below.

3.6.1 Aluminum sputtered polyimide IDCs with PDMS encapsulation and polyimide bottom layer (Generation III) devices

The overall fabrication step flow was unchanged. An additional step for sputtering aluminum film was introduced to obtain a conductive film over the *kapton* IDC.

Generation III devices had the following fabrication steps:

Step 1- Pre micro-machining

Devices having polyimide IDCs were fabricated using a 120 µm thick *kapton* film. For polyimide devices, it was not required to spin coat a layer of *S1813* photoresist because the amount of debris formed after laser micro-machining were negligible. The reason behind the clean micro-machining was because *kapton* is a flexible polymer and the power required to make a through cut was minimum. Prior to clamping on the platform for micro-machining, a wipe with iso-propyl alcohol was used to clean the polyimide sheet. After laser cut, regular iso-propyl alcohol immersion for 3 minutes was enough to clean the device completely.

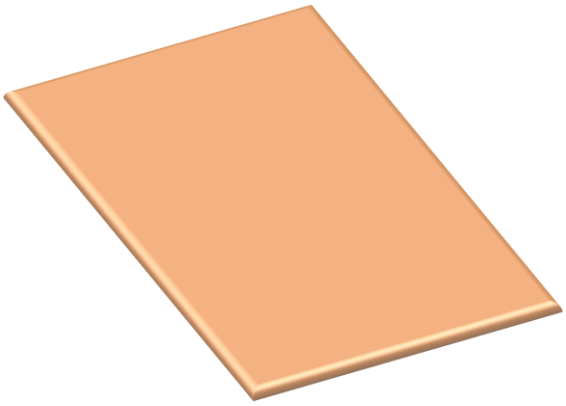

Figure 3.25: Generation III strain sensor during step 1.

Step 2- Pre micro-machining

The polyimide sheet was placed in the jig position 1 which allowed for uniform metal cut outs. The micro-machining was done as per the steps explained in Section 3.1. As in the case of

previous metal IDCs, the polyimide devices also had “bridges” to keep the finger pairs from separating. These were later cut off from the device so as to break the connectivity.

Step 3- Post micro-machining/Aluminum sputter

After the IDCs were cut in the laser, they were kept in a beaker with isopropyl alcohol for 3 minutes and wiped dry. The integrity of the devices was checked under a microscope. The good devices were sputtered with aluminum on the *AJA ATC Orion Series UHV* sputtering system. Conformal metal deposition on the front faces and the side walls of the fingers was achieved with sputtering. Aluminum was the chosen metal for the purpose as it was cheap and easily available.

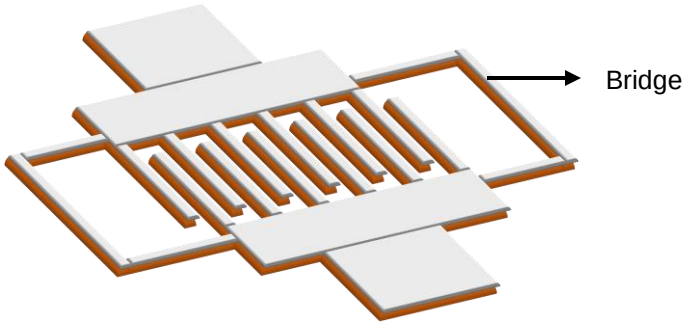

Figure 3.26: Generation III IDC after fabrication steps 2 and 3.

Step 4- Bottom encapsulation layer

Sylgard 184 (PDMS) was spin coated on a 50 µm thick *kapton* film to form a uniform, thin and well adhered PDMS layer. PDMS was mixed with the curing agent in a 10:1 ratio. This process is identical to the fabrication process step 4 in the generation II sensors. This is shown in Figure 3.27.

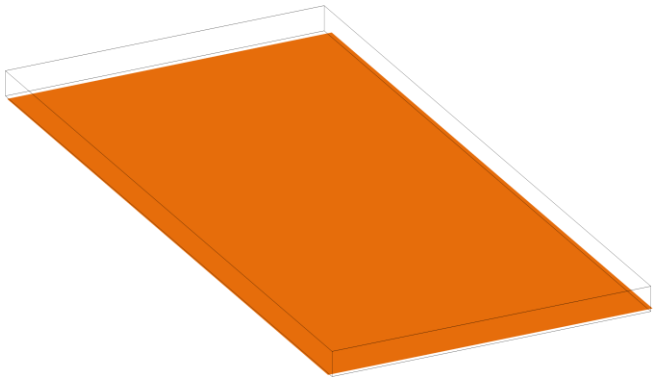

Figure 3.27: Generation III strain sensor during fabrication step 4.

Step 5- “Bridge”cutting

The polyimide IDCs sputtered with aluminum were placed on a PDMS layer just before it cured completely. After complete curing, the IDCs were firmly attached to the PDMS, which in turn was attached onto the thin *kapton* film forming the bottom layer of the strain sensor. After the PDMS was cured completely, the “bridges” which were included in the device design to hold the opposite finger pairs together, were cut off. This step was also done on the laser similar to the one for metal IDC strain sensors to have a quick cut. Once the laser cut through the “bridges”, they were removed using tweezers breaking the conductivity between the two sets of fingers. Firm attachment with the PDMS layer prevented any dislocation of the fingers from the initial position.

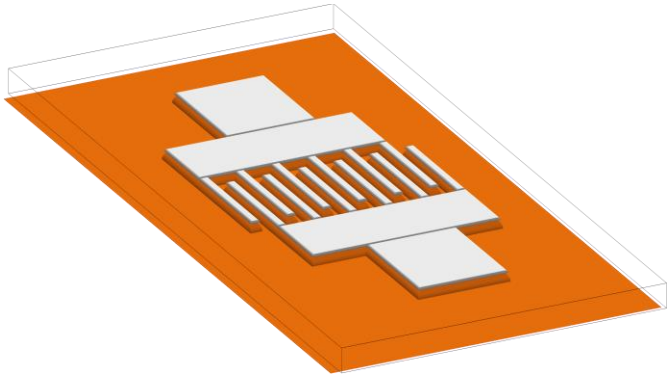

Figure 3.28: Generation III strain sensor after fabrication step 5.

Step 6- Electrical contacts

Once the IDC was firmly attached with the bottom PDMS layer, electrical contacts were made on to the sputtered aluminum surface. The aluminum surface was scratched lightly with a sharp object like a razor allowing better grip and adhesion for the electrical contacts. The scratching was lighter than that done for brass or titanium as heavy scratching for adhesion could result in peeling off of aluminum layer. The contacts were made by a conductive epoxy consisting of epoxy resin and silver as in the case of titanium and brass strain sensors. Once the paste was poured on to the sensor for bonding, it was allowed to cure on a hot plate at 100 ˚C for 5 minutes.

Step 7- Complete PDMS encapsulation

Once the conductivity was broken and connections were made for each set of fingers, the entire brass IDC was poured with another top layer of 10:1 PDMS with 10 parts of PDMS over 1 part of the curing agent. The two layers of PDMS were made as thin as possible so as to have maximum possible stretch.

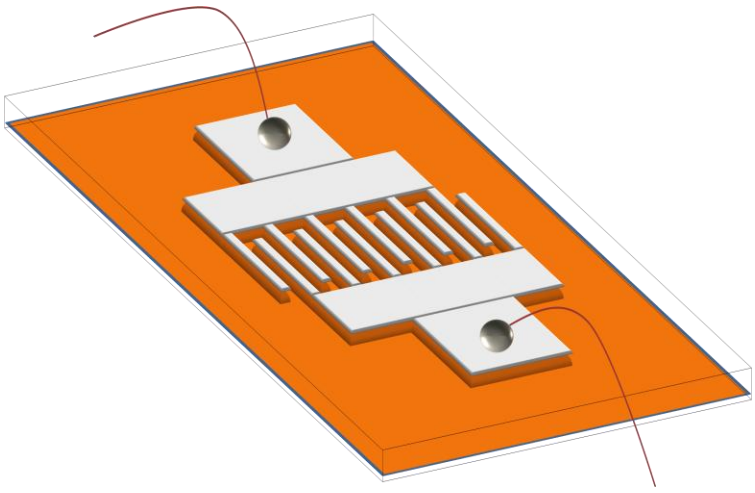

Figure 3.29: Generation III strain sensor after fabrication steps 6 and 7.

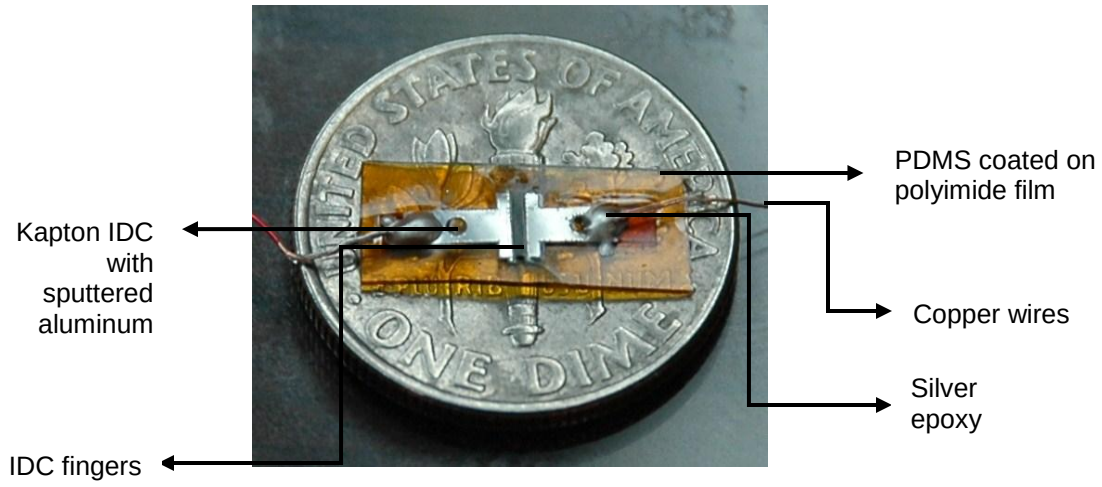

Figure 3.30: Actual polyimide generation III strain sensor encapsulated in PDMS and with a 50 μm thick polyimide bottom layer placed on a dime.

CHAPTER 4

PRELIMINARY EXPERIMENTS

It was mentioned in chapter 1 that the strain sensors developed were sensitive to stretching as well as bending resulting in change in capacitance. To verify the working principle, it was important to learn the performance of the sensors for stretching and bending. In this chapter, discussion will focus on the experiments which were carried out to check the performance of the generation I sensors on stretching and bending. Generation I devices were used for this purpose since they were the first devices to be fabricated. After the initial tests were carried out on these devices, limitations of generation I devices were overcome in generation II devices which were then used for the actual applications.

4.1 Experiments to verify sensor working principle

In this part of the chapter, discussions have been focused on the performance of the generation I devices on stretching and bending. The main focus of the experiments was to check if the sensors showed the expected performance and to understand the changes which were required to be made to make the sensors suitable for the targeted applications.

4.1.1 Experiment to determine linearity of strain sensor

In order to test the working of the sensor on stretching, the ends of a titanium sensor were clamped using metal clamps and screws and were stretched using a micro-meter gauge. This allowed for uniform stretch on the sensor as the clamped PDMS was pulled equally in each step. The setup is shown in the Figure 4.1.

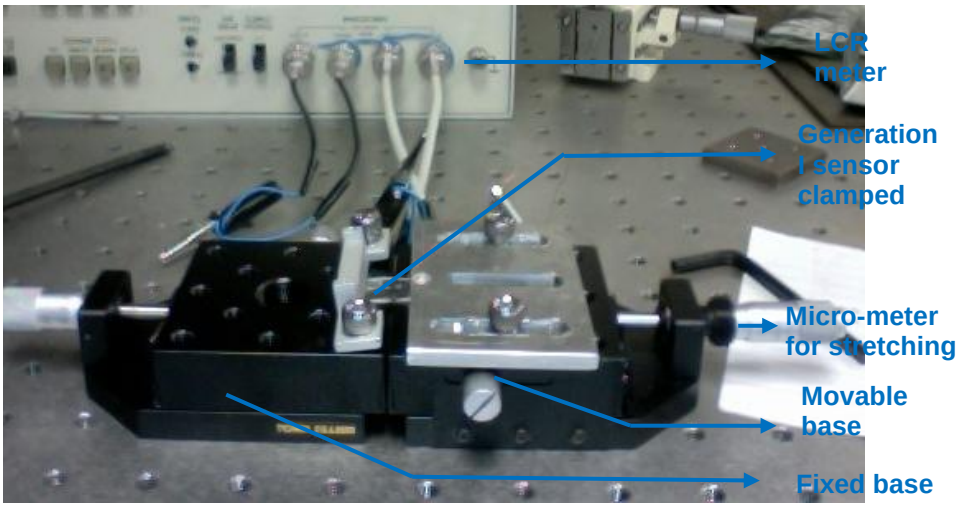

Figure 4.1: Micro-meter gauge for Generation I sensor stretching.

Each complete rotation of the micro-meter corresponded to stretch of 500 µm. The micro-meter had the least count of 10 µm. As can be seen from the setup, micro-meters were present on the ends of both the clamps. One of the micro-meters was kept fixed while the other was rotated in steps of 50 µm causing the sensor to stretch. The copper wires of the strain sensor were connected to a LCR meter shown in the background and the capacitance of the sensor was measured at 100 kHz. The results obtained are shown in Figure 4.2.

It was clear that the capacitance changed linearly and repeatedly on stretching. One obvious observation from the above results was the amount of stretch given to the sensor. Even if the sensors had finger lengths of 500 µm, the stretching was well beyond 500 µm. At such high stretches, it would be expected that the fingers would come out of the grooves and the capacitance drops substantially. No sudden drop in the capacitance was observed and the fingers were still well grooved. This was observed because even though the entire sensor was stretched up to 3 mm, it was the PDMS encapsulation which was stretched up to 3 mm and not the actual IDC fingers. The PDMS was not strong enough to pull the metal IDC along with it on stretching. Although this setup showed very linear performance, it was difficult to understand the potential sensitivity of the strain sensor. For this purpose, slight modification was introduced in the fabrication steps and the clamping methodology.

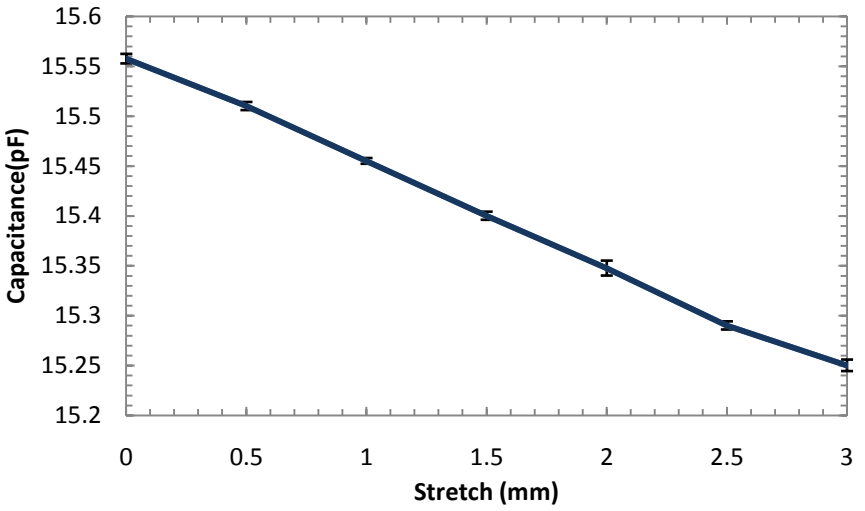

(a)

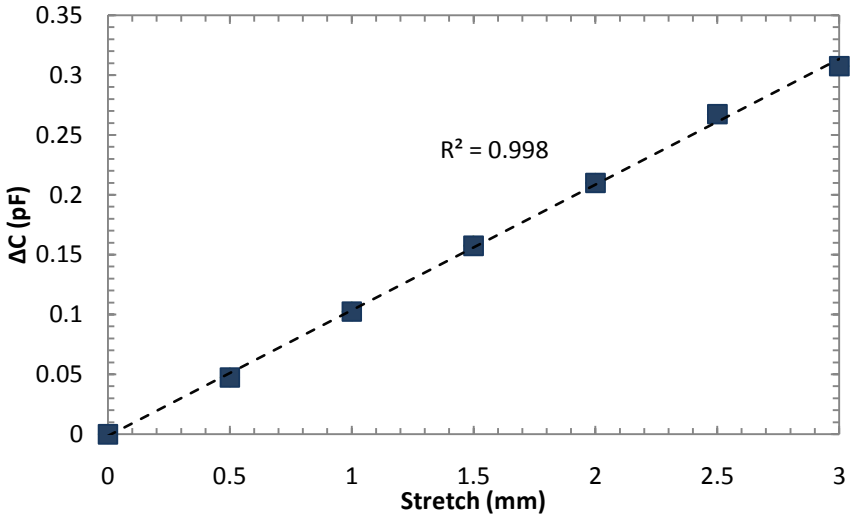

(b)

Figure 4.2: Stretching experiment (a) Capacitance with respect to stretching (b) change in capacitance with respect to stretching.

4.1.2 Experiment to determine sensitivity of the strain sensors to stretching

To stretch the actual IDC fingers, holes were made on the titanium cut out during the laser micro-machining. Wires were passed through these holes and were clamped on the

micrometer stages instead of the PDMS. This allowed direct stretching of the IDC fingers since the wires were directly passed through the metallic IDCs. It was expected that stretching the wires would cause equal amount of stretch on the fingers. This experiment was also performed on the same micro-meter stage as shown in Figure 4.1. The actual IDCs with wires passing through them are shown in Figure 4.3.

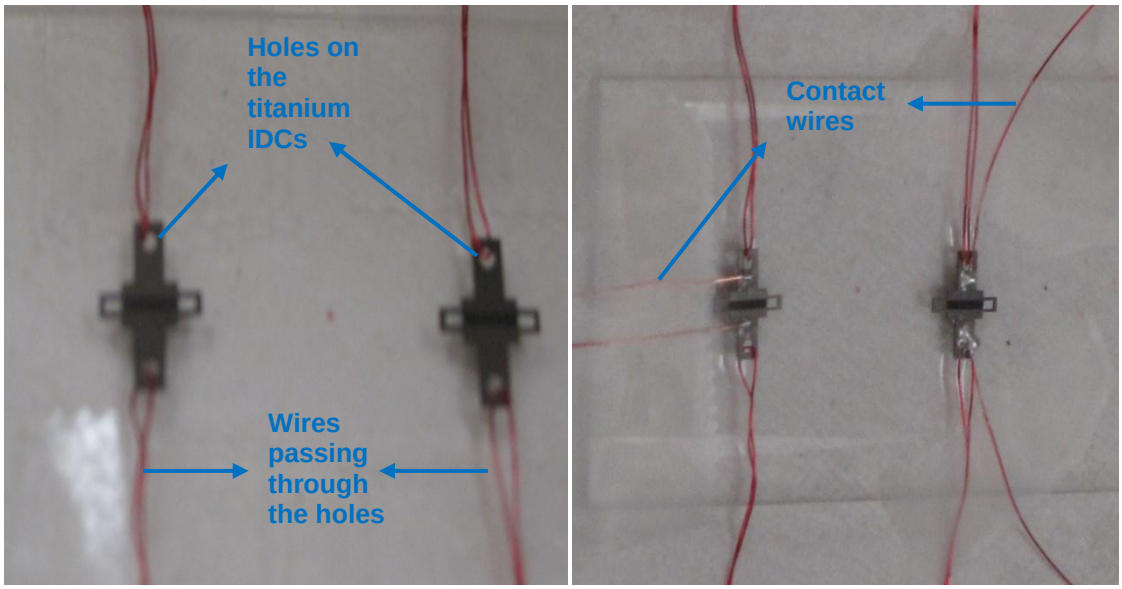

(a) (b)

Figure 4.3: Generation I sensor with (a) Titanium IDCs with wires passing through holes for stretching (b) Contacts made to the IDCs with wires passing through the holes.

Capacitance of the IDC was measured using the LCR meter as before. It was observed that the sensor showed a much larger change in capacitance on a smaller stretch clearly indicating that the stretch was directly affecting the finger overlap length. Figure 4.4 shows the performance of the sensor with clamped wires. From the Figure 4.4 the large change in capacitance for a smaller stretch compared to the previous experiment can be noticed. This showed that clamping the wires clearly caused more finger displacement as compared with clamping the PDMS. From the result it could be concluded that even at a stretch of 500 µm, a large capacitance drop was not observed. This meant that even at the stretch of 500 µm the

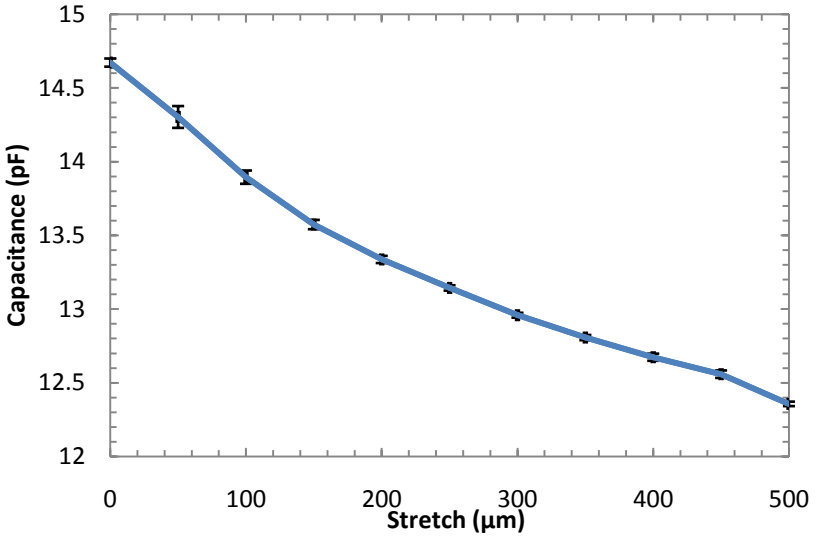

(a)

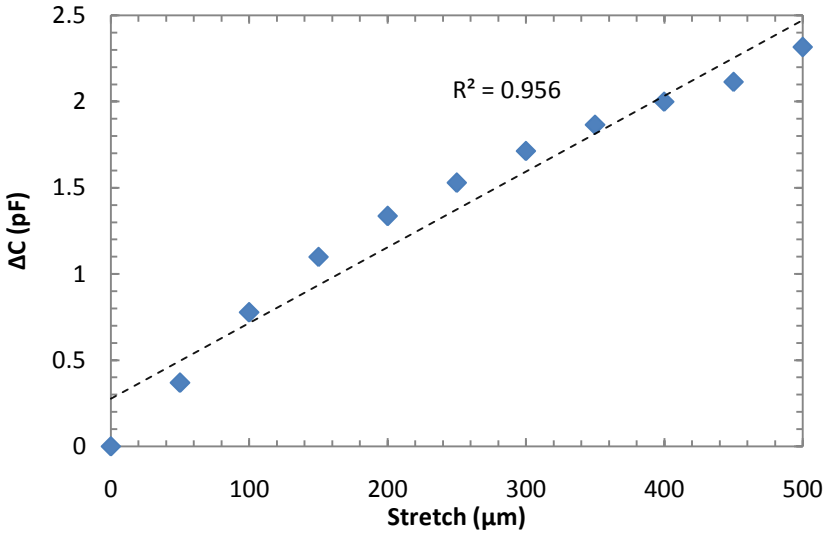

(b)

Figure 4.4: Stretching of clamped wires passing through holes on the IDC (a) Capacitance with respect to stretching (b) capacitance change with respect to stretching.

fingers remained grooved. The amount of stretch shown on the gauge was more than the actual stretch at the fingers. Moreover, the linearity was lost during the stretching. The reasons for the

non-linearity were studied and it was found that during each of the stretching steps of 100 μm of the mirco-meter gauge, the stretch at the fingers was not the same. The wires did not pull the IDC equally each time they were pulled. As seen from the image of the wires passing through the holes on the IDC, the wires were not exactly straight after the PDMS was cured. Hence, during the stretches of the wires, some amount of stretch was lost in straightening of the wires. Even though the wires were pulled by the clamps on the micor-meter gauge for 500 μm, the IDC fingers did not move away by 500 μm. The actual movement of the IDC fingers was much less. From the observations after stretching, it was estimated that the fingers actually moved away only about 100 μm. The non-linear stretching resulted in a non uniform capacitance change. From the curve, it could be concluded that for stretch between 100 μm to 300 μm was linear compared with the stretch for the first 100 μm and the last 100 μm. This meant that the wires actually pulled the fingers more during the initial 100 μm and less in the final 100 μm as compared with the intermediate 300 μm of stretch. With this experiment a capacitance change of about 14 percent was observed for an approximate stretch of 100 μm. With this experiment, it could be infered that in reality the IDCs were a lot more sensitive to stretching than observed from the previous experiment. A 14 percent change for 100 μm meant a 0.2 pF capacitance change for an approximate stretch of 10 μm. Even though the observed results were approximate, the IDC was very sensitive to stretching at the fingers. From the results of the two experiments carried out (Figures 4.2 and 4.4), it can be concluded that the IDCs showed linear change in capacitance on stretching uniformly and the change in capacitance was very high when the fingers were actually stretched. Hence, these IDCs were very suitable for the structural health monitoring experiments which needed the sensors to be sensitive for strains below 1 percent.

4.1.3 Experiment to determine sensitivity of strain sensor on bending

To prove the working principle, it was important to determine the capacitance change of the sensor on bending. This experiment was also performed as a proof of the concept and did not show the most accurate result but it helped in determining the performance of the strain sensor on bending. The titanium sensor was attached on to two vertical plates which could be turned around a hinge allowing different bending angles. A protractor allowed approximate measurement of the angles and was placed below the plates such that the hinge was exactly at the center of the protractor. One of the plates was kept fixed while the other was rotated at different angles and capacitance was measured. The schematic below shows the bending principle.

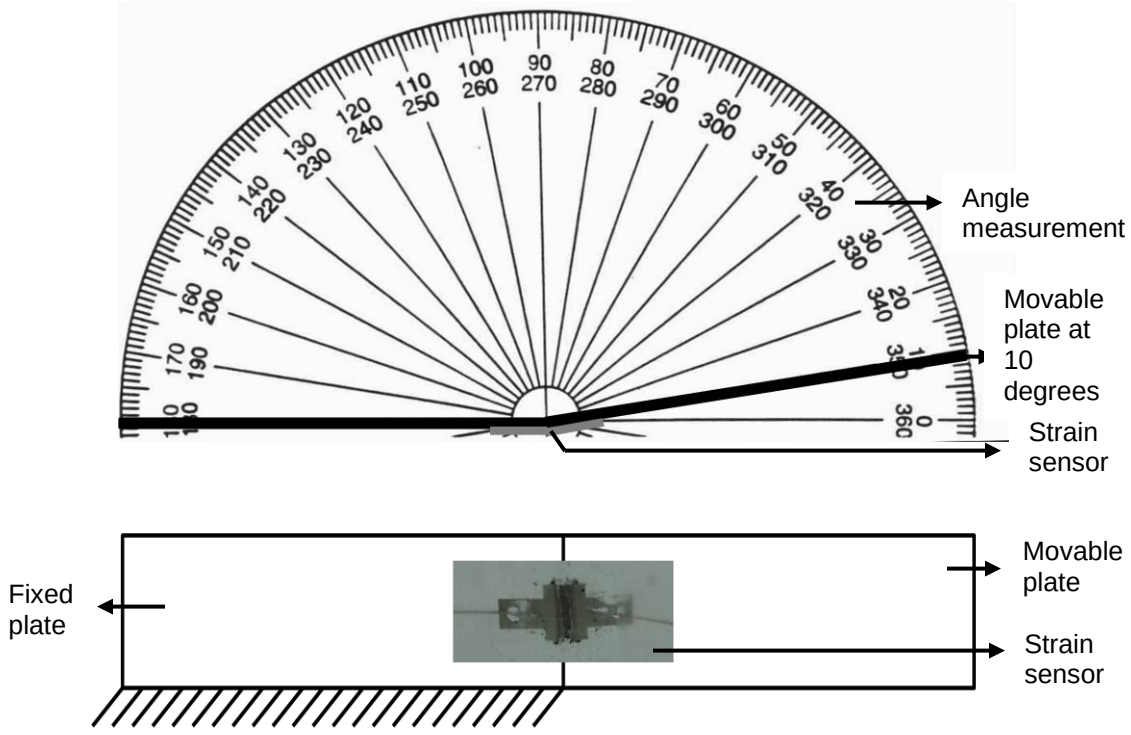

Figure 4.5: Diagrammatic representation for the bending principle of titanium IDC.

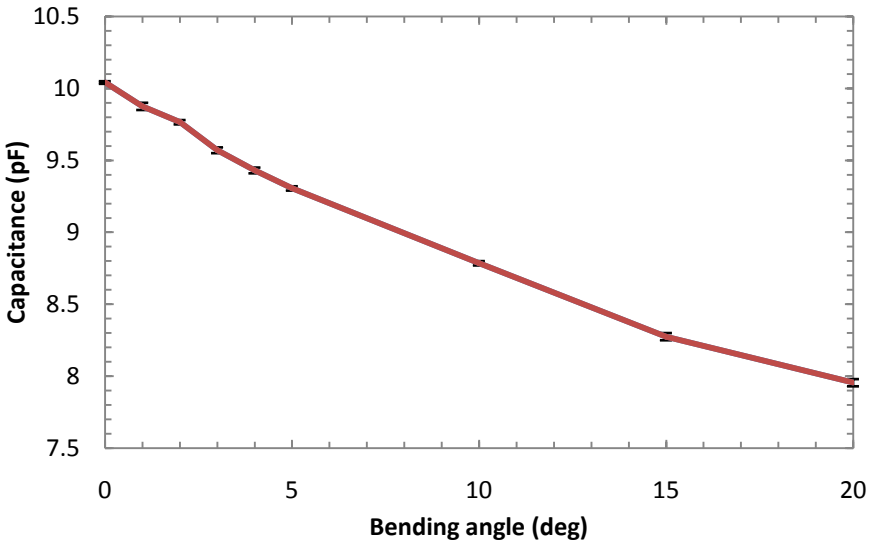

(a)

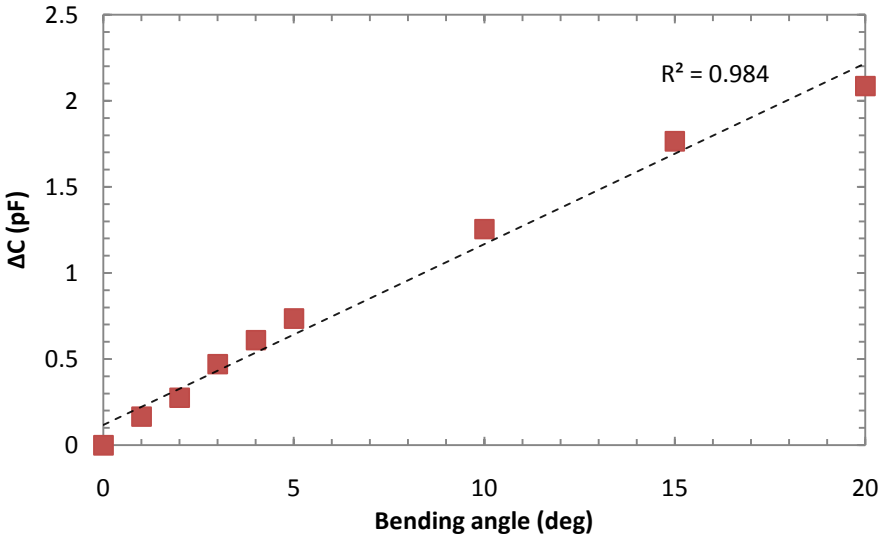

(b)

Figure 4.6: Bending experiment (a) Capacitance with respect to bending angle (b) Capacitance change with respect to bending angle.

From the Figure 4.6, the change in capacitance of the sensor was linear with the change in bending angle. For this experiment, the angles at which the plates were turned were measured. This did not mean that the fingers were actually bent at the same angles. It was obvious that PDMS limited the IDC fingers from bending as much as the vertical plates. Since the bending was done at uniform steps, it was safe to assume that the angles at which the fingers were bent were also in uniform steps even though it was not the same angle as the plates. This showed that the change in capacitance was linear with respect to the angle at which the entire sensor was bent.

CHAPTER 5

APPLICATIONS: STRUCTURAL HEALTH MONITORING AND BLADDER VOLUME MONITORING

The experiments explained in the previous section laid the background for the sensors to be used for actual applications. They were done as a part of preliminary performance testing of the strain sensor and to make the necessary fabrication changes. From the observations made while implementing the generation I sensors for strain measurements, it was required that some modifications be made in the materials used, fabrication and experimental procedure. Detailed explanation on the limitations of generation I devices and how they were overcome in the generation II devices has been provided in the chapter 3 on fabrication. Keeping these in mind, generation II devices were used for structural health monitoring applications and their performance has been elaborated in the sections of this chapter.

5.1 Structural health monitoring

Cantilever beam setup is considered to be a standard for performance verification of strain sensors for structural health monitoring. In this work, an aluminum cantilever for strain sensors testing was used.

5.1.1 Cantilever strain equation

Cantilever beam is a thin, long structure which is fixed at just one end while the other end is kept free. The schematic for a cantilever has been shown in Figure 5.1. Loads were applied on the free end of the cantilever which resulted in straining the cantilever. For a

cantilever of length L with sensor placed at a distance x from the fixed end, a load P applied at the free end will cause a moment M at the point at which the sensor is placed. The moment M is given as [38]

$$M = -P(L - x) \tag{5.1}$$

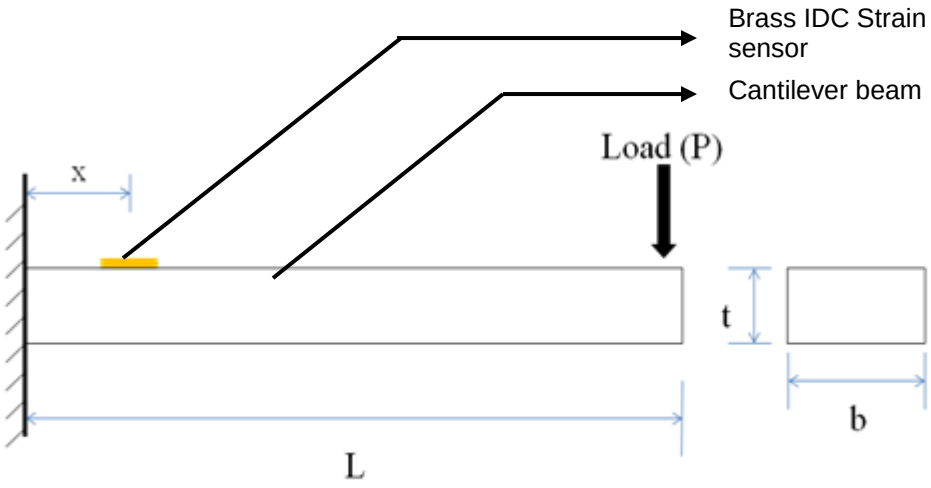

Figure 5.1: Cross section of the load bearing cantilever beam with various dimensions.

The strain on the sensor is expressed as

$$\sigma = -\frac{My}{I} \tag{5.2}$$

where I is the moment of inertia of the cantilever beam, y is the distance between the neutral of the cantilever axis and the surface at which the strain sensor is mounted and σ is the stress on the cantilever. To be precise, y is written as $t/2$ where t is the thickness of the cantilever. Now, the moment of inertia I can be expressed as

$$I = \frac{bt^3}{12} \tag{5.3}$$

where B is the breadth of the cantilever beam. Now, on combining Equations (5.2) and (5.3), we can obtain the stress on the cantilever beam as

$$\sigma = 6P(L - x)/bt^2 \tag{5.4}$$

Now, from Hooke's Law, stress σ is proportional to strain ε_x with proportionality constant E which is the modulus of elasticity of the material, in this case the material of the beam.

This means,

$$\sigma = E\varepsilon_x \tag{5.5}$$

From Equations (5.4) and (5.5), the strain on the cantilever beam is obtained as [38]

$$\varepsilon_x = 6P(L - x)/Ebt^2 \tag{5.6}$$

From Equation (5.6), the amount of strain on the sensor placed at a distance x from the fixed end can be found for a cantilever of length L and with load P applied at the free end. The variation of strain with load is linear and can be shown in the plot below.

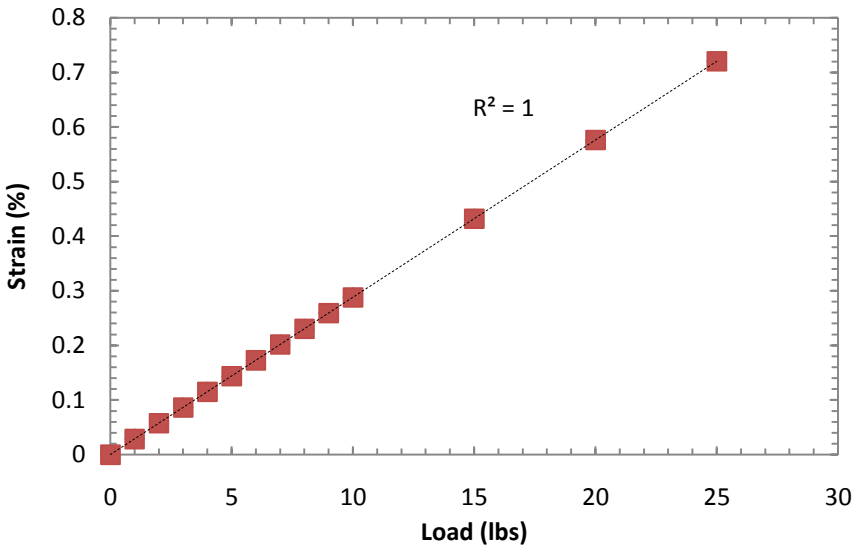

Figure 5.2: Strain with respect to load variations.

5.1.2 Cantilever specifications

The dimensions of the cantilever have been chosen to give less than 1% strain for a weight of up to 25 pounds. Aluminum has been chosen as the material because of its high Young's modulus and easy availability. The cantilever is clamped on a workbench at a distance

of 2 inches from one end. To prevent slipping of weights, a metallic block is screwed at a distance of 1 inch from the fix end. Hence, the total working length of the cantilever is 18 inches. The schematic of the cantilever has been shown below. All the dimensions are in inches.

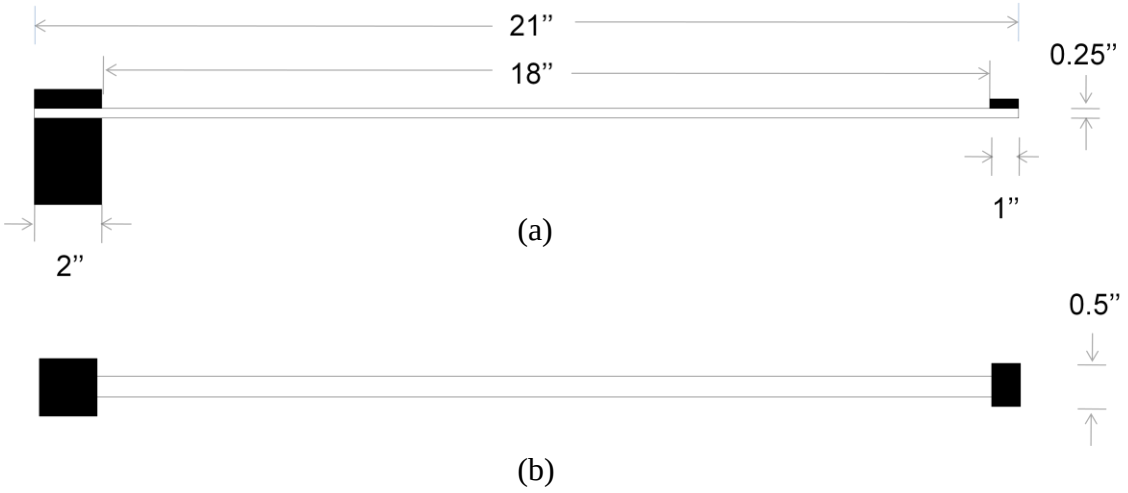

Figure 5.3: Schematic of the load bearing cantilever beam with actual dimensions.

5.1.3 Experimental setup

The strain measurement experiments were done by attaching the sensor at a distance of 3 inches from the fixed end. From equation (5.6), it was observed that as x is increased, the strain reduces. To achieve higher strains, it was required to attach the sensor closer to the fixed end. With a distance of 3 inches, overall working length of the cantilever as 18 and maximum weight of 25 pounds, a strain of 0.72 percent was obtained. Figure 5.4 shows the experimental setup of the cantilever with sensors attached at different locations. The cantilever setup is standard for verification of strain sensor performances.

5.1.4 Experiments with sensors placed at different locations

To check the performance, initially the weight was increased in steps of 5 pounds with sensor at 3 inches from the fixed end. The results for capacitance and change in capacitance with respect to strain are as shown in the Figure 5.5. In this experiment, the increment in

weights was large. To observe if the strain sensor could respond to smaller weights, the strain sensor was tested for 10 weights of 1 pound after an initial load of 5 pounds. From the results, it was observed that the sensor responded well to strain levels as small as 0.0288 percent corresponding to weights of 1 pound. From Figures 5.5 and 5.6, it was observed that the linearity of the strain sensor was very low. This was because the sensors were placed at 3 inches from the fixed end and it was observed that on loading, the cantilever showed heavy bending at about 2-4 inches from the fixed end. This is evident from the Figure 5.4. This resulted in additional change in capacitance of the strain sensor. This is a good indication that in real applications, the increased sensitivity to bending can help detect bending as well as longitudinal stresses.

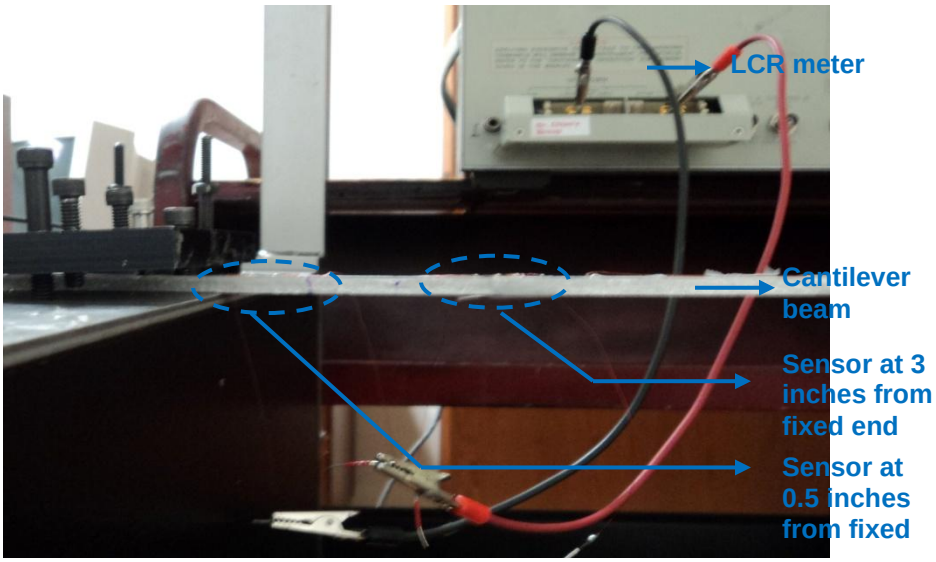

Figure 5.4: Image of side view of unloaded cantilever showing sensors at 0.5 inches and 3 inches from the fixed end.

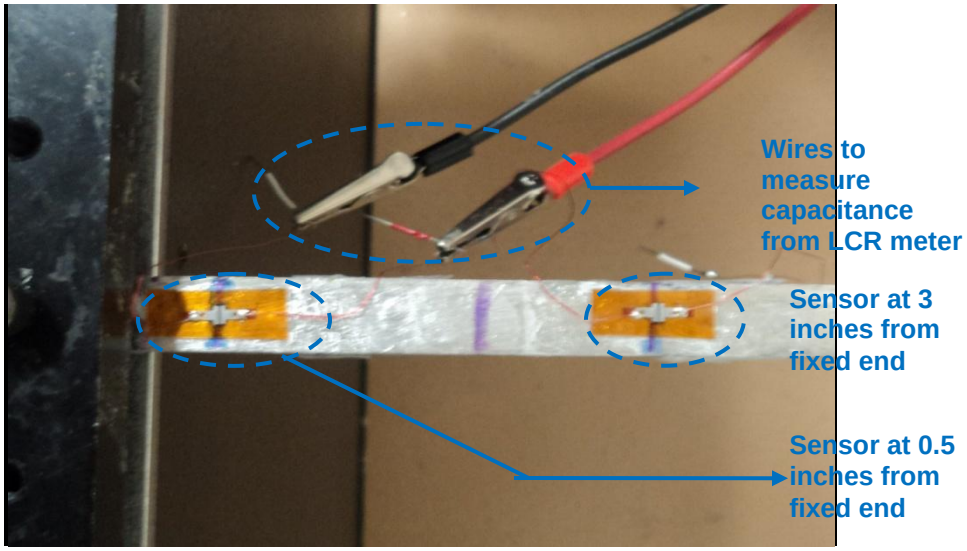

Figure 5.5: Image of top view of unloaded cantilever showing sensors placed at 0.5 inches and 3 inches from the fixed end.

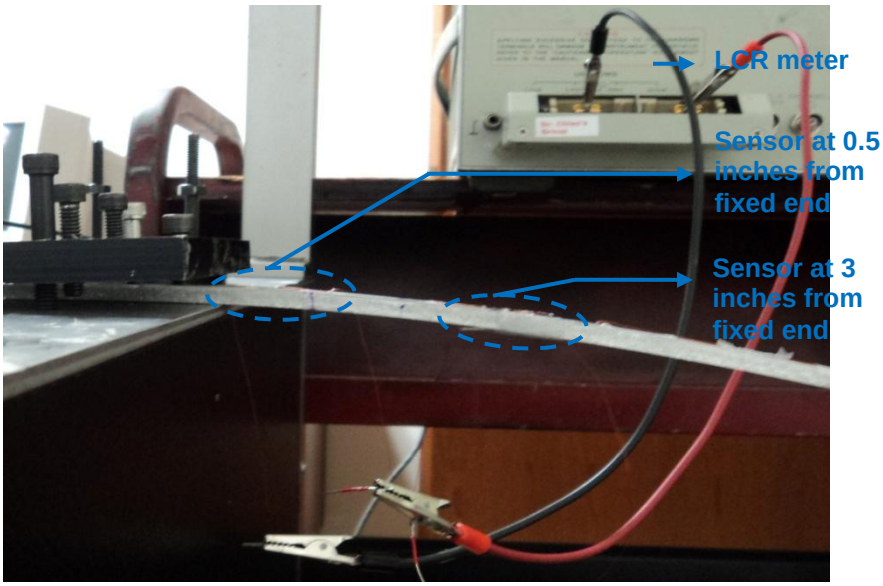

Figure 5.6: Image of side view of loaded cantilever showing sensors placed at 0.5 inches and 3 inches from the fixed end.

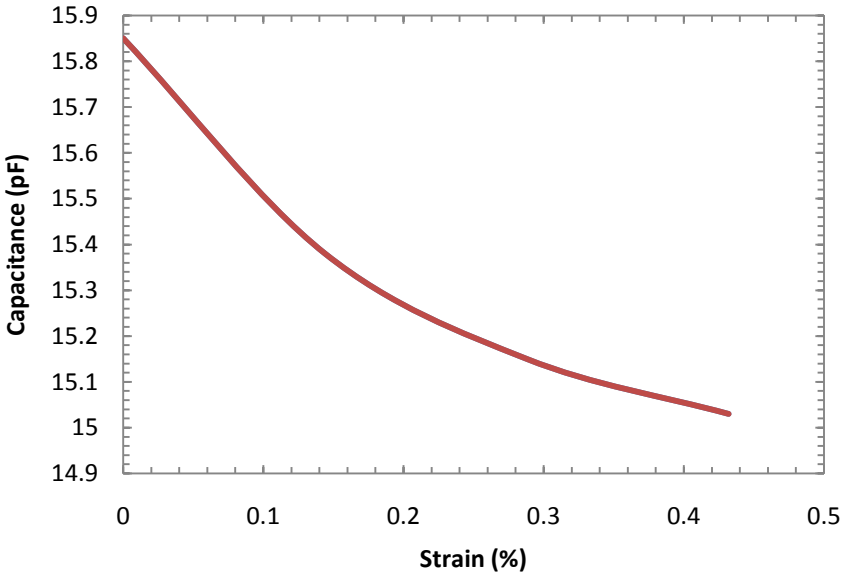

(a)

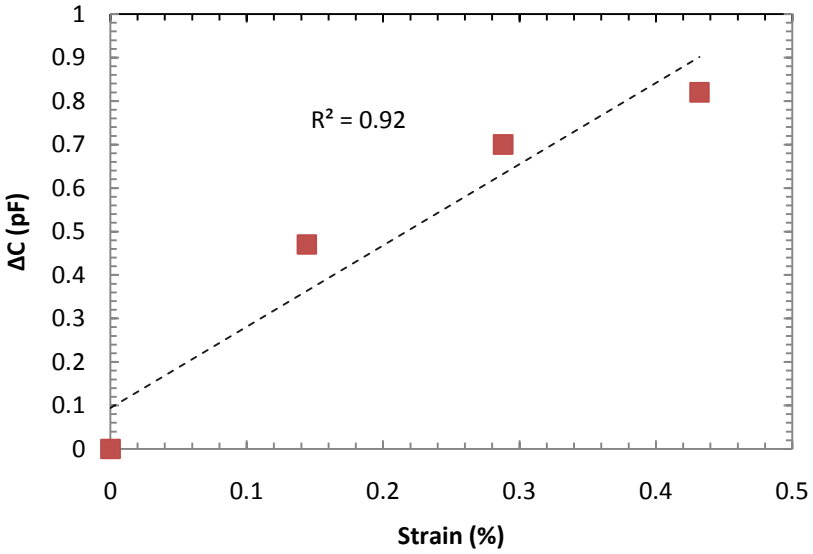

(b)

Figure 5.7: Load increments of 5 pounds with strain sensor at 3 inches from fixed end (a) Capacitance with respect to strain (b) change in capacitance with respect to strain.

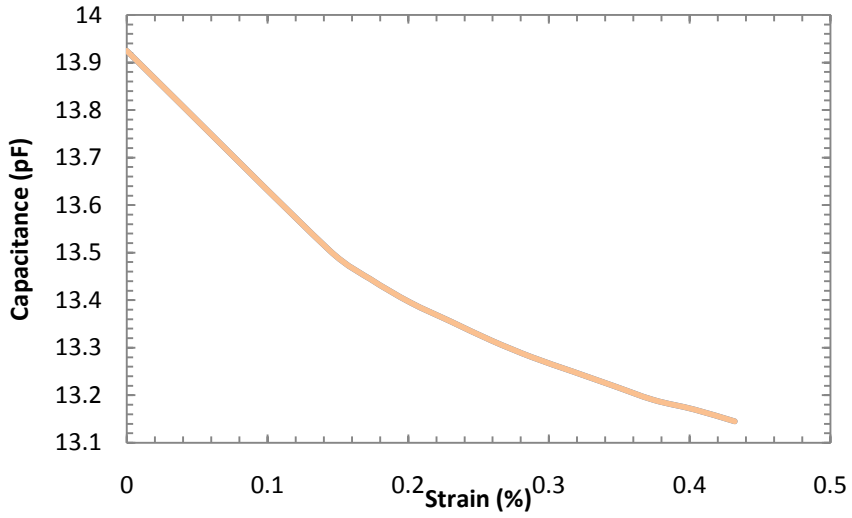

(a)

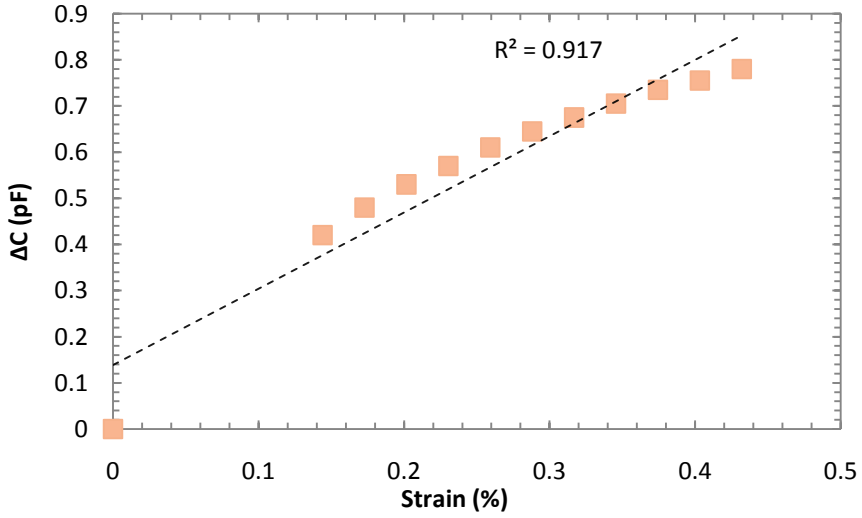

(b)

Figure 5.8: Load increments of 1 pound after initial load of 5 pounds with strain sensor at 3 inches from fixed end (a) Capacitance with respect to strain (b) Change in capacitance with respect to strain.

To observe the performance of the strain sensor at a different location on the cantilever, the sensor was placed at 5.2 inches while keeping the loading point at the same location

resulting in (L-x) to be 12.8 inches. This reduced the strain levels on the sensor. The performance of the strain sensor is shown in Figure 5.7 below.

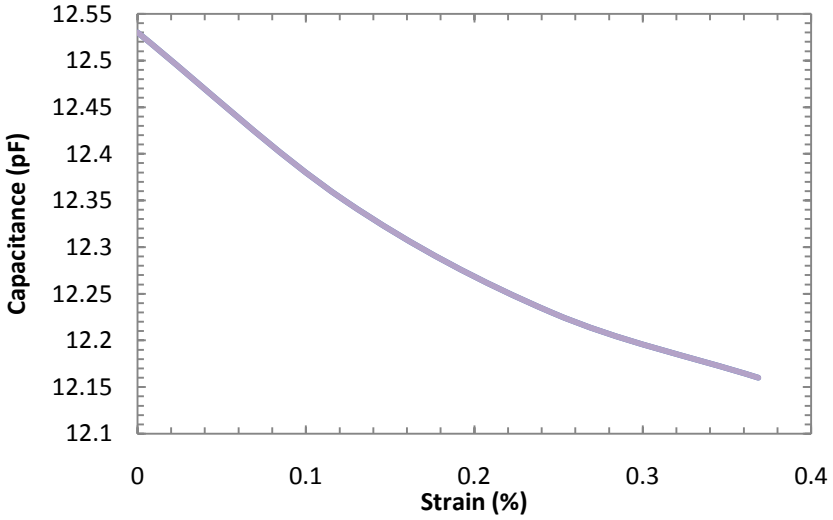

(a)

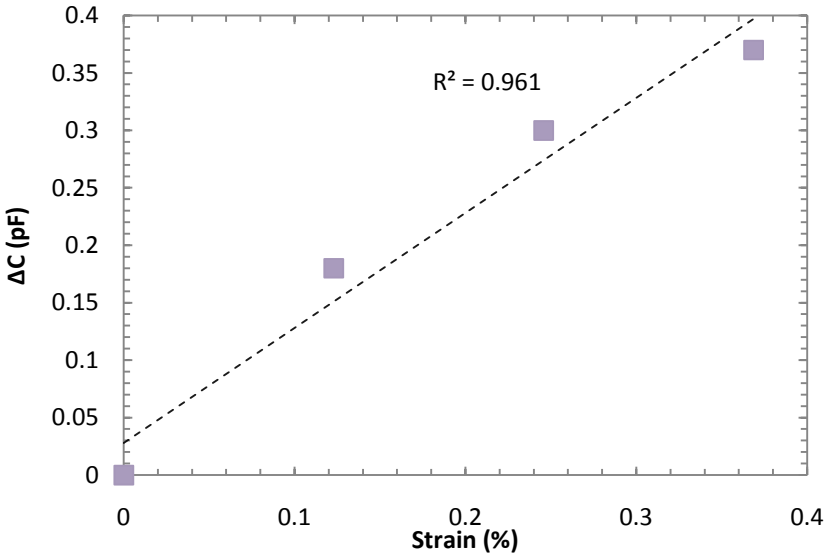

(b)

Figure 5.9: Load increments of 5 pounds with strain sensor at 5.2 inches from fixed end (a) Capacitance with respect to strain (b) Change in capacitance with respect to strain.

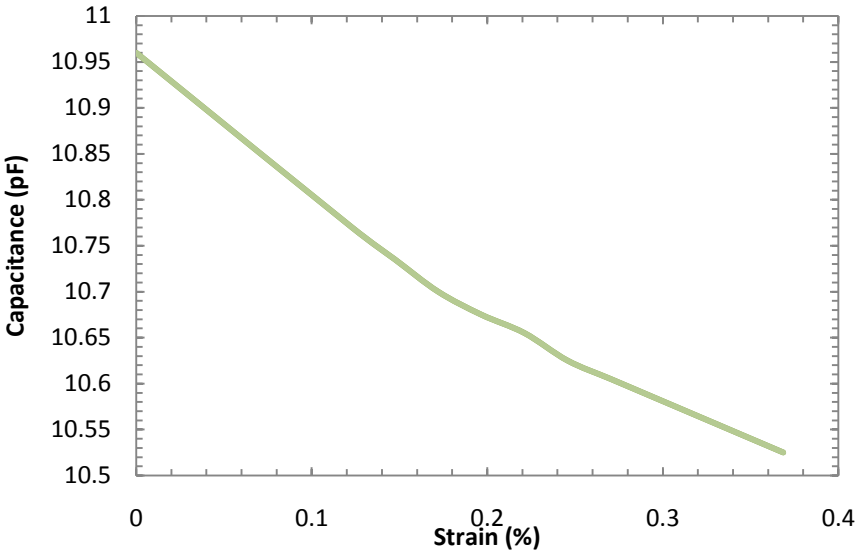

(a)

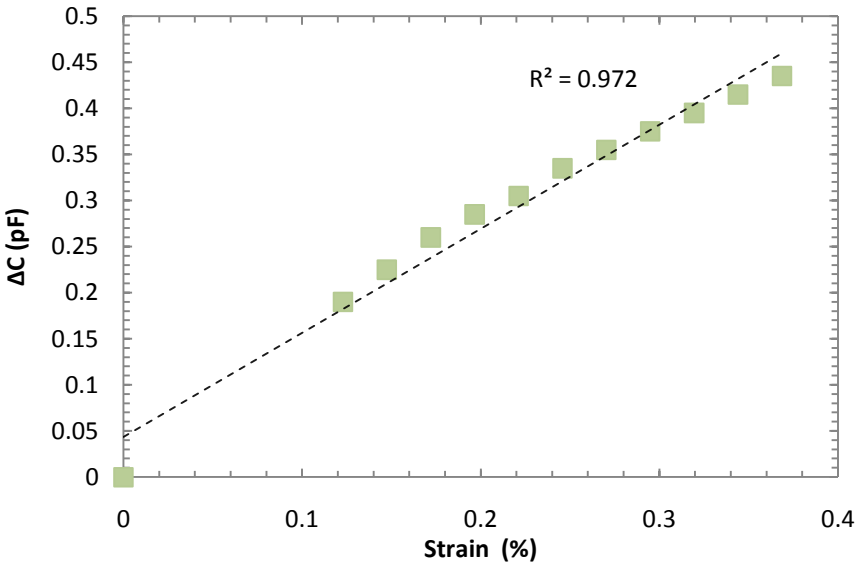

(b)

Figure 5.10: Load increments of 1 pound after initial load of 5 pounds with strain sensor at 5.2 inches from fixed end (a) Capacitance with respect strain (b) Change in capacitance with respect strain

On comparing Figure 5.8 with Figure 5.5 for sensor at 3 inches, it can be observed that the strain levels along the X-axis have been reduced. The sensor could very well detect strain changes as low as 0.0245 percent. Also, it is evident that the linearity of the curve has improved. The reason for improved linearity was that the bending of the cantilever at 5.2 inches from the fixed end was very much lower than the bending at 3 inches. It has already been shown that the strain sensor is sensitive to bending along with stretching. Although the capacitance change increases due to increased bending, the linearity of the strain sensor reduces.

In order to check the performance of the strain sensor for purely linear strains, it was necessary to remove the cantilever bending effect. Hence, the sensor was placed at a distance of 1 inch from the fixed end. It was evident from Figure 5.9 that the bending of the cantilever was very low at 1 inch from the fixed end. To keep the strain levels the same, the loading point was moved closer so that the (L-x) factor in Equation (5.6) remained same at 15 inches as in the case with sensor at 3 inches. The weights were increased in steps of 1 pound up to 10 pounds followed by a 5 pound step increase. It was observed from the graphs below that the sensor showed very linear results for change in capacitance when pure linear strain was applied. The gauge factor of the strain sensor, which is the change in capacitance over total applied strain [22], was about 7.5 which was high as compared to the metallic resistive strain sensors.

5.2 Performance tests

In order to check the suitability of the sensor for structural health monitoring applications, it was important to determine the performance of the sensor. Different tests were performed on the sensor to detect the performance under repeating loads, repetitive loading and unloading and strain sensitivity at different temperatures as discussed below.

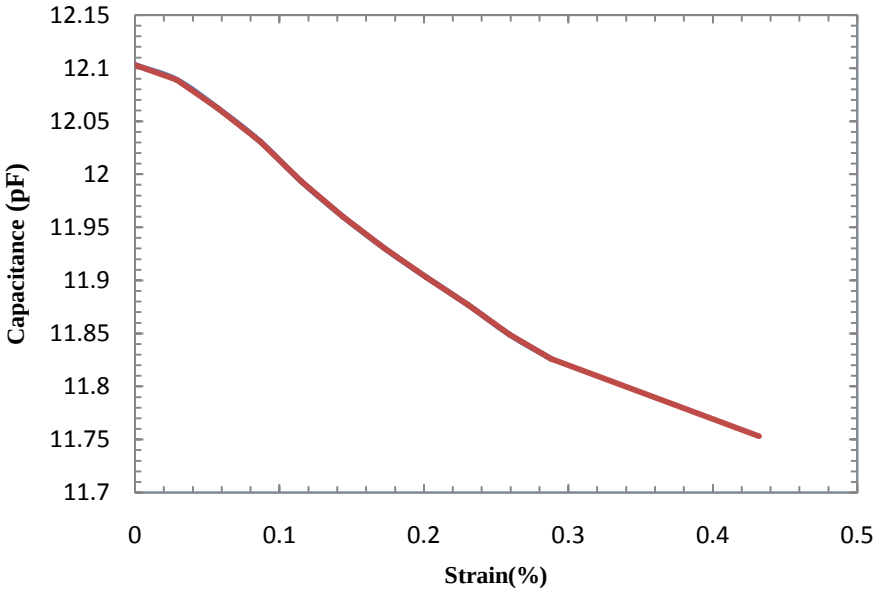

(a)

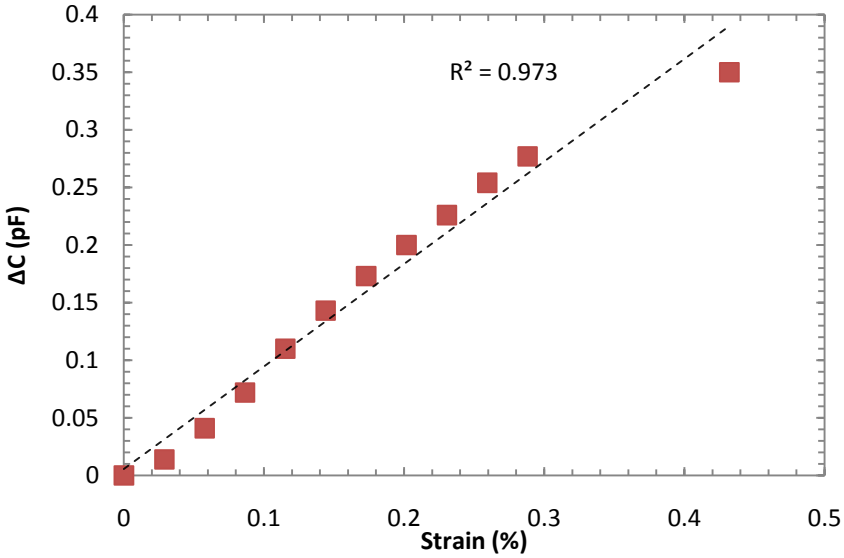

(b)

Figure 5.11: Load increments of 5 pounds with strain sensor at 5.2 inches from fixed end (a) Capacitance with respect to strain (b) Change in capacitance with respect to strain

5.2.1 Repeatability test

To check the repeatability of the strain sensor, a Generation II sensor was mounted at 5.2 inches on the cantilever and loaded with weights of up to 10 pounds in steps of 1 pound. The sensor was placed at 5.2 inches as the strain levels at that location were less with less bending. Repetitive performance of the strain sensor for small strains could be checked at this location. The performance of the strain sensor was checked by loading the cantilever repeatedly to determine its ability to show same the capacitance values at same strain levels. The loading was repeated 5 times and the average result has been plotted in the graph below. Unloading was done by removing all the weights at once. Error bars on each point in Figure 5.12 (a) show the net variation from the average value. From the Figure 5.12 (b), we can observe that the maximum variation in capacitance is at the point of 0.09% strain between the 1^{st} and the 4^{th} loading. The maximum variation in the capacitance value was found to be around 0.06 pF which was about 0.5% from the absolute capacitance value at that strain showed highly repeatable performance.

5.2.2 Hysteresis test

In practice, it is possible that the strain levels may increase and decrease repeatedly. It is important that such increase and decrease be recorded accurately and that there is no variation in the capacitance at the same strain levels during the gradual increase and decrease. In other words, the hysteresis effects should not be large in the strain sensors. To record the hysteresis effects in the strain sensor, repeated loading and unloading of the cantilever beam was carried out and the capacitance of the strain sensor was monitored. The graph showing the change in capacitance over strain for hysteresis effects is shown below. The cantilever beam was loaded for 20 pounds with steps of 1 pound up to 10 pounds followed by 2 steps of 5 pounds. Obviously, the strain levels recorded were higher than those in the previous

experiments. The loading and unloading of the cantilever was repeated 3 times. The performance is shown in Figure 5.13.

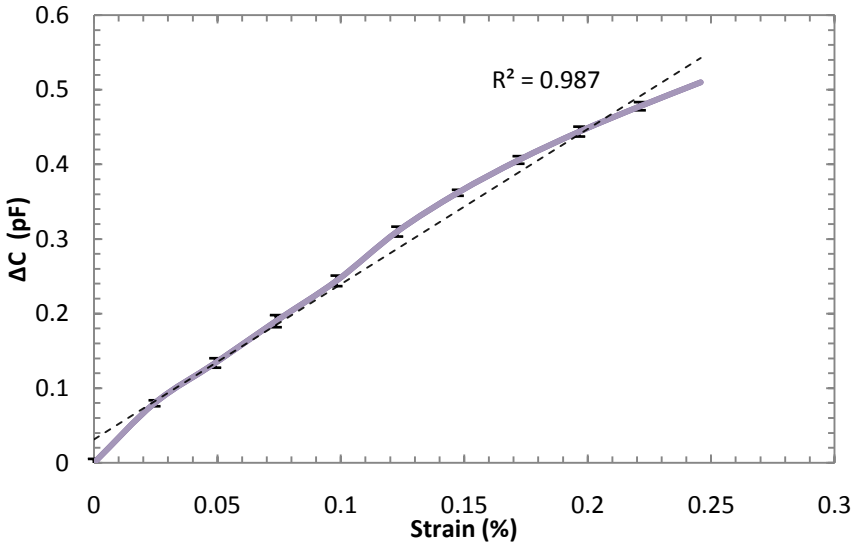

(a)

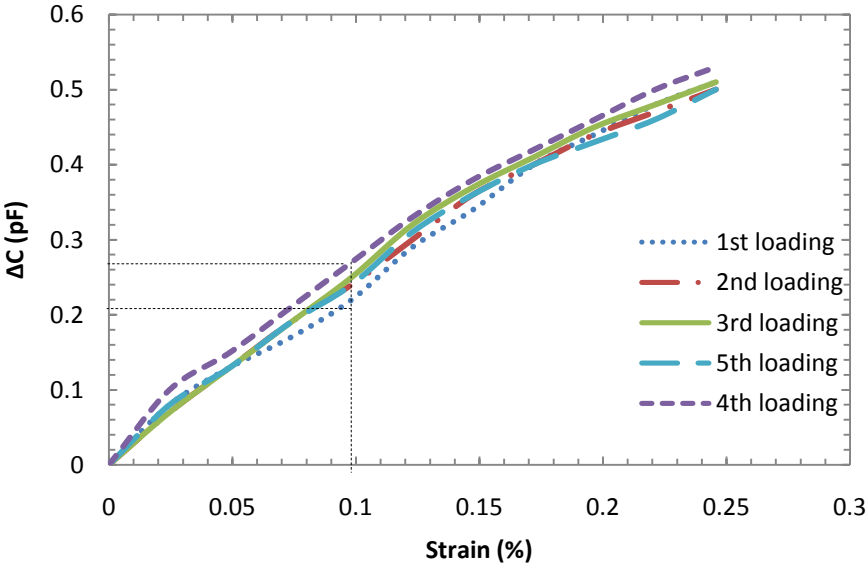

(b)

Figure 5.12: Repeatability test (a) Change in capacitance with respect to strain plot and (b) Change in capacitance with respect to strain.

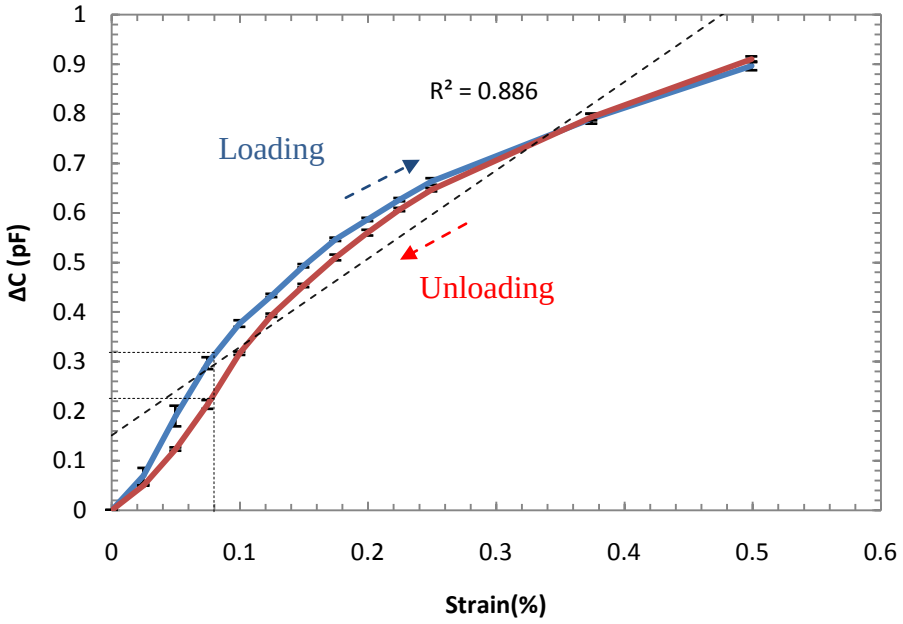

Figure 5.13: Change in capacitance with strain for hysteresis test.

From the Figure 5.13, it is observed that the maximum variation while loading and unloading is about 0.1 pF at the strain of 0.08 % strain (as marked in the graph). The average capacitance observed at this strain is 14.27 pF and hence the percentage error at this strain level was 0.7 % which is very low and can be often neglected. The bend in the curve is observed because the strain sensor was placed at 3 inches from the fixed end at which point the bend in the cantilever was high.

5.2.3 Temperature test

Surrounding temperatures vary during the course of a day, a month and a year. In case of metallic structures such as bridges, the temperature variations can be even higher as the metals tend to heat to very high temperatures. It is important to understand the behavior of the strain sensor under different temperatures and to verify if its performance is affected. To observe the capacitance change under different working temperatures, the strain sensor was

mounted on the cantilever as in the previous experiments. Along with increase in loads, the temperature variations were introduced to detect if the sensor retains its ability to detect strain changes for abnormal temperatures. Hot air was blown on the strain sensor using a hair dryer. Temperature variations were made using different settings on the hair dryer and two different temperatures of 50 ˚C and 90 ˚C were achieved. For obtaining cooler temperatures, ice at -19 ˚C was placed in front of an air blower to achieve air at about -10 ˚C which was similarly blown over the sensor. The sensor was placed at a distance of 3 inches from the fixed end with the weights placed at a distance of 16 inches from the fixed end. Hence, the effective distance (L-x) between the sensor position and location of the weights was 13 inches as compared with 15 for previous experiments. This was done to accommodate higher load on the loading end and avoiding excess bending of the cantilever. This reduced the strain for a particular weight but the loading weight was, however, increased up to 25 pounds resulting in an increase in the overall strain range for a thorough testing. Figure 5.14 shows the performance of the strain sensor at different temperatures. The non-linearity observed is because the sensor was placed at 3 inches from the fixed end, the point showing high cantilever bending. The nature of the curve does not vary with the variation in temperature. The change in capacitance (ΔC) also does not show substantial variation for different temperatures. This means, the strain sensor does not show any performance ambiguity with changes in temperatures. But it is observed that reduction in temperature causes an increase in the capacitance value and vice-versa. Hence, in order to be used for structural health monitoring applications, it would be required to provide a close loop temperature feedback.

5.2.3.1 Possible reasons for variation in initial capacitance with temperature

1) As in the case of resistors where the resistance depends on the temperature through the temperature coefficient of resistance (TCR), temperature coefficient of capacitance (TCC) of the dielectrics plays an important role in the change of capacitance with temperature. With

increase in temperature, the TCC of a dielectric reduces, causing a reduction in capacitance. The dielectric constant of PDMS changes from 2.5 to 2.3 for a temperature increment of about 100 ˚C [39]. The variation in the dielectric constant of PDMS is the most important reason for the change in the initial capacitance values with temperature.

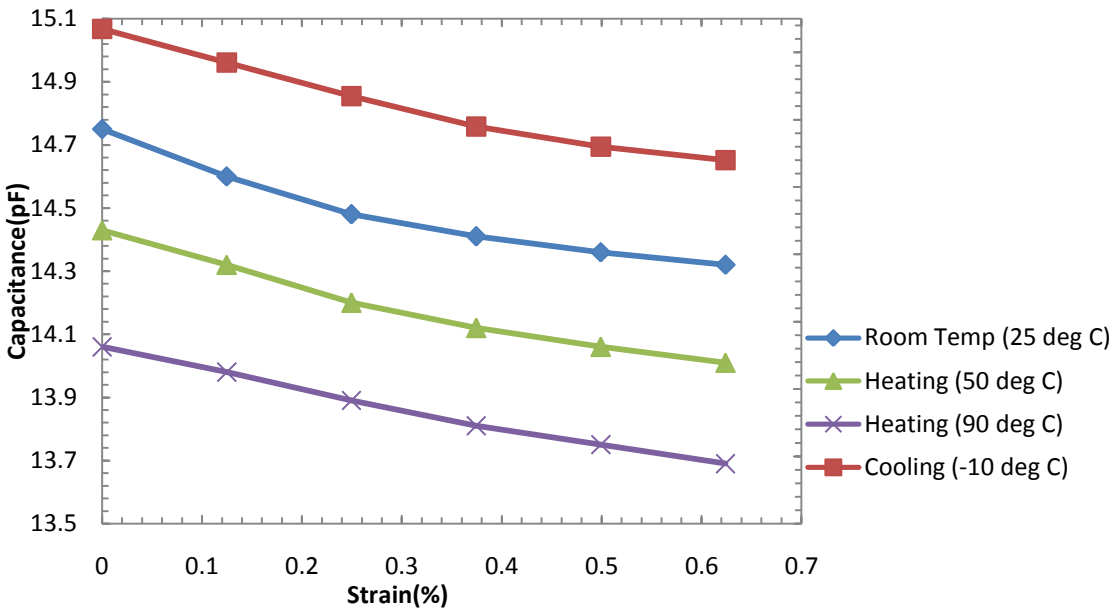

Figure 5.14: Change in capacitance with respect to strain for strain test at different temperatures.

2) Another reason for the change in capacitance can be because of the expansion of the bottom *kapton* layer attached on the cantilever beam on increased temperature. The expansion of the *kapton* will result in the IDC fingers moving away from each other causing a reduction in capacitance.

3) It is also possible that the metal IDC may expand on heating resulting in the metallic fingers moving away from each other causing reduction in capacitance. Reverse of the above will happen when the ambient temperature is reduced.

5.3 Remote data acquisition system

In the previous section, the suitability of the strain sensor for structural health monitoring was shown. For such applications, it is often essential that the sensors are placed at remote locations on the structures such as bridges, tall buildings and these locations are often inconvenient for regular access. Hence, it is required to implement a wireless data transmission system for remote data acquisition.

5.3.1 Capacitance to frequency conversion

In order to be able to transmit the data over long distances for wireless strain sensing, it was essential to convert the capacitance change of the strain sensor in to a proportional electrical signal such as a frequency or a voltage signal. For this purpose, a simple relaxation oscillator circuitry was implemented which converted the capacitance change of the IDC into a proportional square wave output. The frequency of the circuit was dependent on the capacitance of the IDC and on the values of the resistances used in the system. The circuit was implemented as shown below.

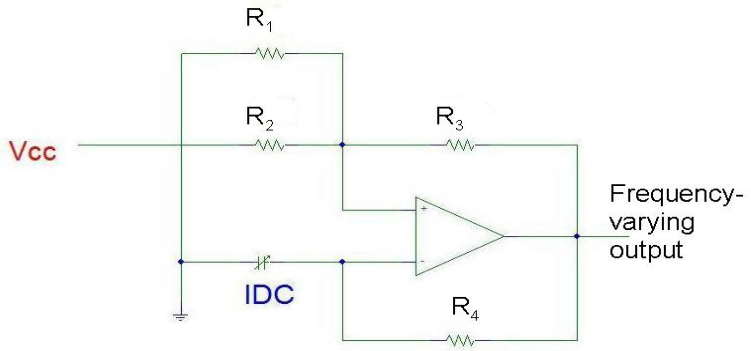

Figure 5.15: Relaxation oscillator circuit.

For the above circuit, the values of resistors R1, R2 and R3 was chosen to be 1 M Ohm while for R4, the value was 2.5 M Ohm. The IDC was connected across the inverting terminal of the

Op-amp TLV 3012 from *Texas Instruments.* The frequency output of the circuit could be given as

$$f = 1/[2R_4C_{IDC}\ log_n\{\frac{1+\varphi}{1-\varphi}\}] \quad (5.7)$$

where f is the frequency output and φ is the desired duty cycle which is 50%. For the values of capacitances of about 12- 15 pF, the frequency output was around 15-12 kHz according to (5.7) as shown in the Figure 5.14.

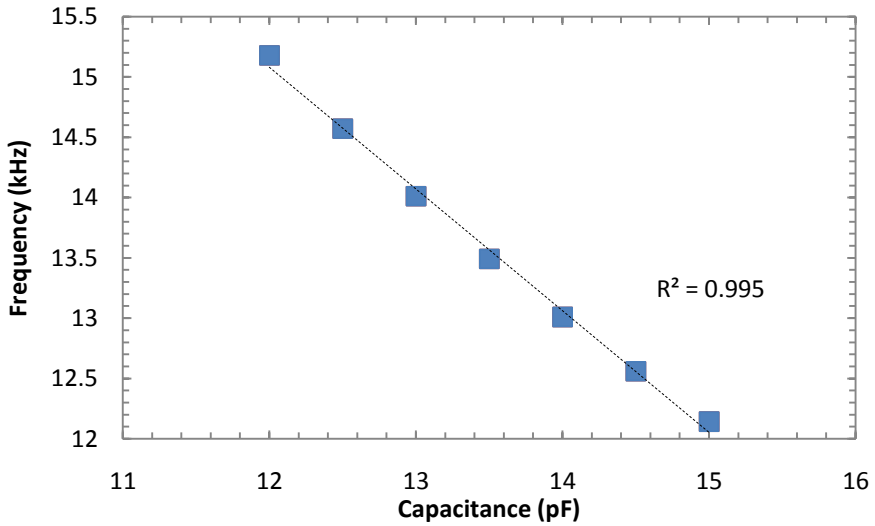

Figure 5.16: Change in frequency with respect to capacitance.

From the above plot, it was clear that the frequency was inversely proportional to the capacitance and hence, reduction in capacitance on stretching gave increase in the frequency output.

5.3.2 Remote data transmission

Once the capacitance output was converted into a proportional frequency output, it was required to transmit the data wirelessly for remote data acquisition. For this purpose, an *EZ430RF2500* (*Texas Instruments* - TI) 2.4-GHz RF transceiver supported by a low-power

MSP430 microcontroller (TI) was used as the wireless module. This module had an embedded MSP430 microcontroller, a 10/12 bit ADC, a CC2500 transceiver chip and a small on-chip antenna. The programmable CC2500 transceiver with the working frequency in the range of 2400−2483.5 MHz supports a sleep mode (400 nA current consumption) with fast start-up time (240 μs from sleep to transmit or receive modes). The wireless communication uses *SimpliciTI* which is a standard RF network protocol. This simple and low-power protocol is capable of both star and peer-to-peer networks. The *MSP430* was programmed such as to count the square wave pulses at the output of the relaxation oscillator circuit for a period of one second. The count, which directly corresponded to the frequency output of the relaxation oscillator circuitry, was wirelessly transmitted over to another *EZ430RF2500* module connected to a PC. Data logging or real time monitoring with a graphical user interface (GUI) programmed in *Labview* could be achieved. Efficient wireless transmission up to 75 meters could be observed for outdoor implementation. The block diagram of the system is shown below.

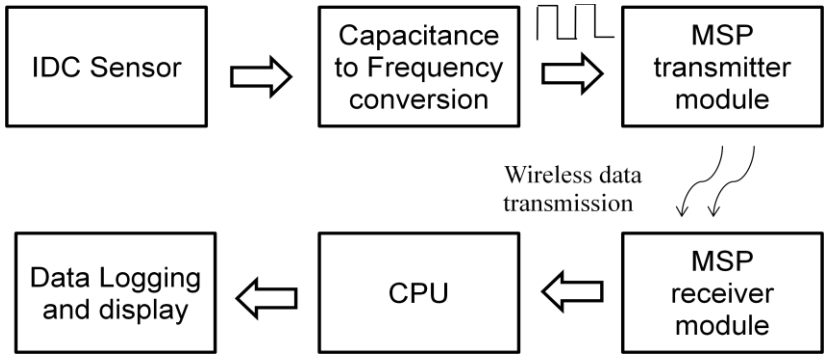

Figure 5.17: Complete block diagram of the data acquisition system for structural health monitoring application.

With variation in strain, the capacitance output of the strain sensor varied resulting in proportional change in frequency at the output of the relaxation oscillator. The wirelessly transmitted frequency count was then displayed in *Labview* for real time monitoring or logged in to files for storage. The frequency output of the relaxation oscillator, with the strain sensor

connected to it, as obtained at the receiver end is shown in figure 5.16. The data was logged on to a *Microsoft Excel worksheet* with the help of the *Labview* interface.

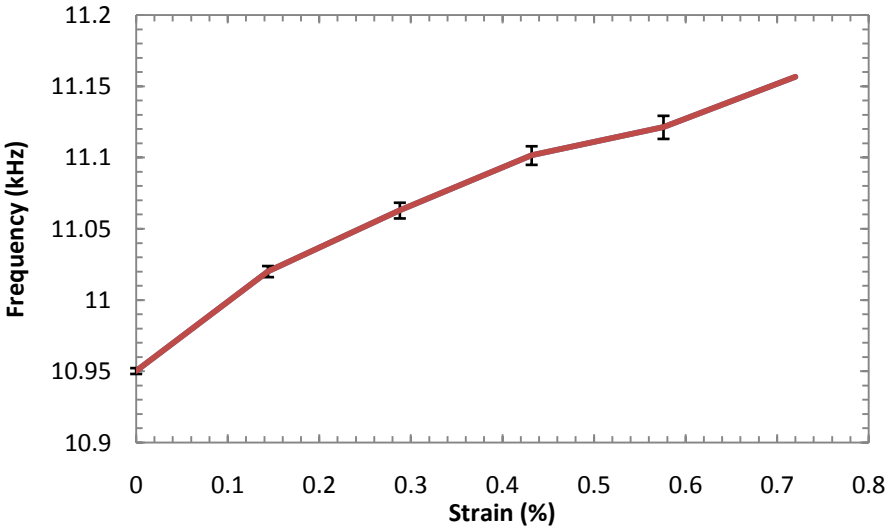

(a)

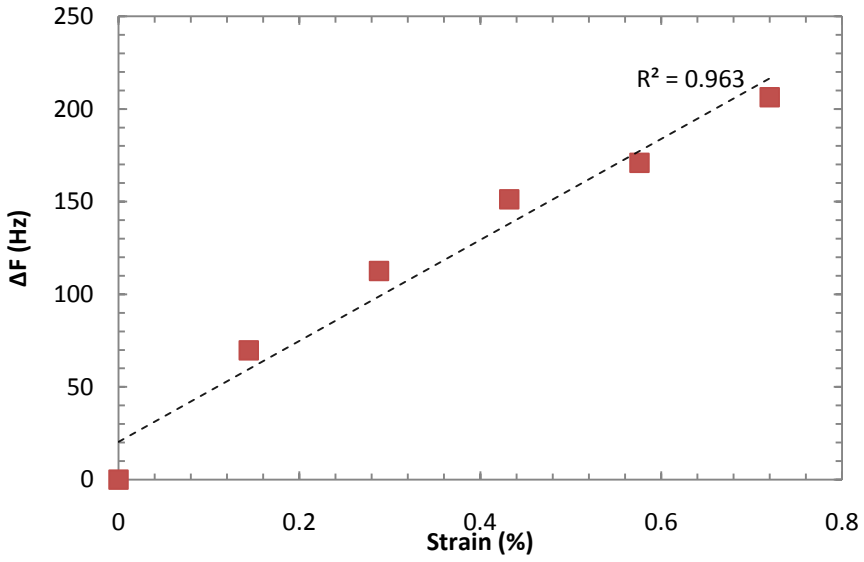

(b)

Figure 5.18: Structural health monitoring (a) Frequency with respect to strain (b) Change in frequency with respect to strain as observed at the receiving end.

5.4 Bladder volume monitoring

As mentioned in the earlier sections, in case of Urinary Incontinence (UI), the patients lose their control over the bladder causing involuntary loss of urine. In order to prevent UI, it is necessary to provide manual feedback to the patient so as to initiate bladder voiding. This requires monitoring the volume of the bladder so as to inform the patient to void the bladder or to stimulate the bladder artificially. In order to achieve continuous monitoring of the bladder, the developed capacitive strain sensor was integrated with a previously developed passive transduction mechanism and a wireless system to monitor *in vivo* the bladder volume in a patient continuously. The entire system consisted of three components:

1) an implanted transponder with the strain sensor

2) a wearable unit that transferred electromagnetic energy to the implant and in turn received the sensor signals from the implant and processed the signals in a microprocessor before sending out wirelessly and

3) a base station receiving and recording the wireless data.

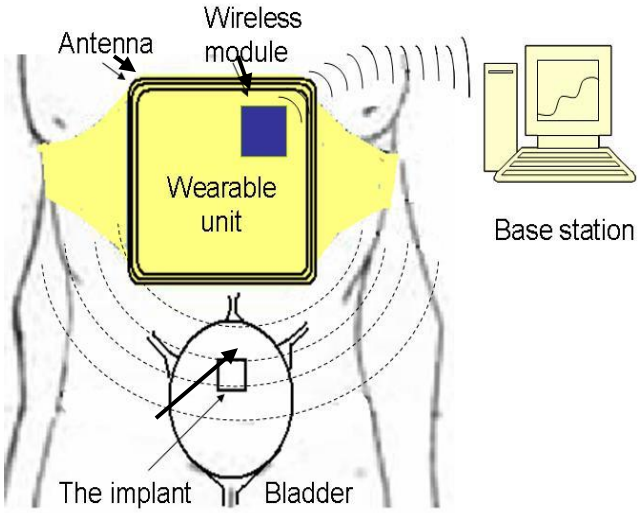

Figure 5.19: Conceptual schematic showing the location of the implant, wearable unit on the body and the base station.

Figure 5.17 shows the concept of our bladder volume monitoring system. The implant receives power from the wearable unit through inductive coupling. The wearable unit has a replaceable battery pack and ports to access the data directly.

5.4.1 Telemetric system for bladder volume monitoring

In order to propose the sensor for *in-vivo* bladder volume monitoring applications, a previously designed wireless battery-less telemetry with minor modifications was used. The block diagram or the circuitry is as shown below.

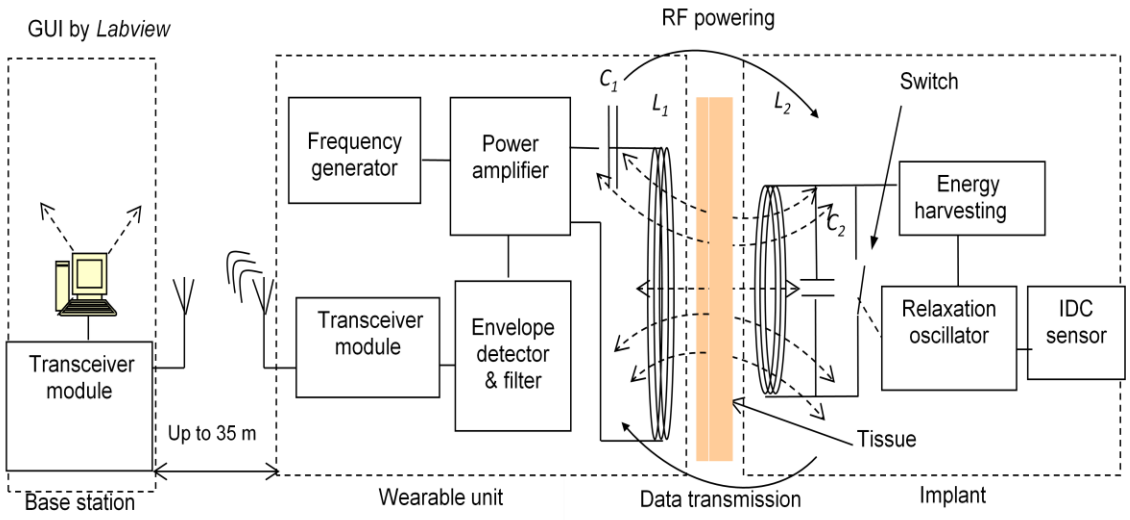

Figure 5.20: Block diagram of the telemetric bladder strain sensing system.

The system blocks are illustrated in Fig. 4 above. The wearable unit powered the implant through an RF link at operating frequency of 1.3 MHz with a 30% duty cycle. The sensor signal transduction was conducted with load-modulating at the same operating frequency. The communication between the wearable unit and the base station was based on two eZ430RF2500 (*Texas Instrument*) modules which are the same as the ones used for structural health monitoring applications.

(1) The implant

The passive implant consisted of a coil antenna (L_2), a 1-nF capacitor (C_2), a switch, an energy harvesting circuit, a relaxation oscillator and the IDC strain sensor. A 24-turn coil antenna made of 30 AWG magnet wires had a size of 1×2 cm^2 giving an inductance of 15 μH and it formed a resonance with C_2. The resonance frequency was also at 1.3 MHz in order to maximize the power received in L_2. A voltage multiplier was utilized with a series of diodes and capacitors to increase the transduction distance [40]. The output of the 4-stage voltage multiplier was connected to a 2.5-V CMOS regulator with current consumption less than 2 μA. A 12-V Zener diode was added to protect the regulator from high voltages in case the transponder was very close to the reader. A 1-μF storage capacitor was placed at the regulator output to keep the voltage stable during modulation. A relaxation oscillator circuit, similar to the one used in Section 5.3.1 was used to convert the changes in capacitance of the IDC sensor to frequency variations. A low-power op-amp LPV321 (*Texas Instrument*) was used as a comparator. The resistors R_1, R_2, R_3, and R_4 were 1 MΩ, 1MΩ, 1 MΩ and 2.5 MΩ, respectively (same as in Figure 5.13). The frequency generated was calculated using the formula in Section 5.3.1 with the modulated frequency in the range of 12−15 kHz.

(2) The wearable unit

The 7-turn coil antenna (L_1) was made from magnet wires wound around a foam board having an area of 12×15 cm^2 with an inductance of 17 μH. The capacitor C_1 was chosen to be 900 pF for resonance at 1.3 MHz so as to match the resonant frequency with the implant circuit. The wearable unit included a class-E power amplifier which generated high voltages across the coil antenna for electromagnetic fields coupling into the implant. An envelope detector was used to read the load-modulation signals along with a wireless transceiver to send the sensor data to the base station [41]. At the implant, load-modulation by the relaxation oscillator, in which the frequency was controlled by the IDC capacitance, varied the voltage levels at the reader coil

antenna. The modulated signals were extracted by an envelope detector and fed through a band-pass filter to suppress the high frequency carrier data. The sensor signals were then amplified and fed to the input port of the microcontroller in the eZ430RF2500 wireless module. The MSP430 in the wireless module was programmed to receive the modulated-frequency signals by counting the number of pulses for duration of 0.25 s. The modulated-frequency was loaded into the data packet and transmitted wirelessly to the base station.

(3) Base station

The base station consisted of another eZ430RF2500 module and interfaces. The received data was sent to a computer by the MSP430 microcontroller through a serial port and displayed in real time with a graphical user interface (GUI) programmed in *Labview*. The data was also logged into text files for off-line diagnosis.

5.4.2 Balloon model

In order to study the suitability of our strain sensor for bladder volume monitoring, an air balloon model was used as a proof of concept setup. It was assumed that the human bladder was a perfect sphere and the shape and size of the model was made similar to the actual bladder. Since it had a spherical shape, the volume of the model could be calculated from the balloon diameter 'D'. Knowing the change in diameter for each air injection, strain could be calculated as ratio of change in diameter over initial diameter and co-related with the volume. It was proposed that the IDC strain sensor was to be attached on the serosal wall of the bladder. To mimic this, a strain sensor was glued on the latex balloon outer wall with a medical epoxy. The schematic of the bladder model is shown in Figure 5.21. Typically, the maximum volume of a human bladder is about 550 ml and the volume at which patients should trigger voiding is 400 ml. Strain measurement should start when the bladder volume goes beyond 390 ml. An alert message will be sent out at 390 ml volume and the modulated frequency output will indicate the

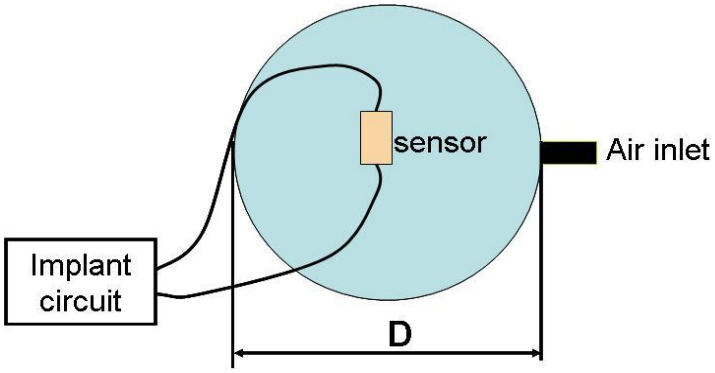

Figure 5.21: Schematic of the experimental setup with the balloon model.

strain/volume information. The balloon used for the bladder had an initial diameter (*D*) of 9.06 cm corresponding to a volume of 390 ml. Air was pumped in 3 steps with the corresponding volumes of 410, 430 and 450 ml while the base station continuously displayed and recorded the modulated frequency. The volume changes corresponded to strains of 1.68, 3.31 and 4.89%, and the modulated frequency output was as shown in the plot below. The sensitivity of the complete system was 8 Hz per percentage of strain.

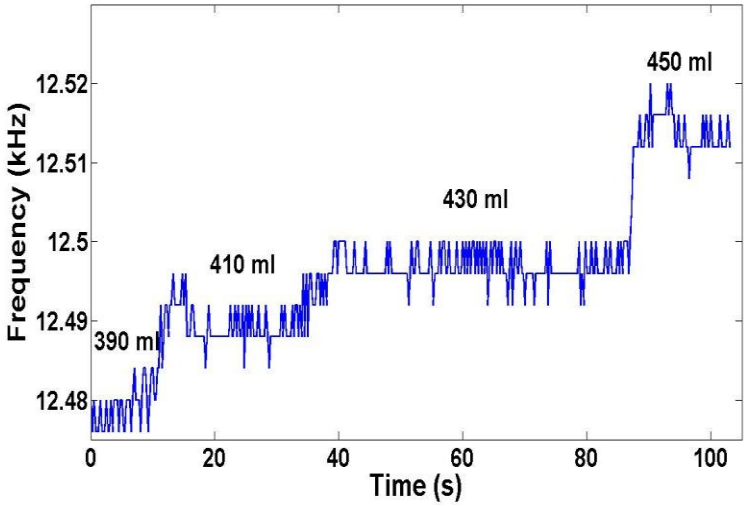

Figure 5.22: Frequency output of the implant as observed at the base station.

The real-time fluctuations in frequency outputs were due to the motion artifacts when the air was pumped into the balloon and the resolution limit in the strain detection. By increasing the

period to count pulse numbers in MSP430, a more stable output could be achieved. However, it will reduce the response time. It may not be a serious issue considering that it takes minutes for urine production before it enters the bladder. To reduce the fluctuations, the resolution (frequency shift per strain change) could be increased by increasing the frequency range of the relaxation oscillator in the implant.

CHAPTER 6

CONCLUSION

A novel laser micro-machining technique for fabrication of inter-digitated capacitors (IDCs) having high aspect ratios has been implemented. The design for the IDCs was finalized after studying different designs for repeatable and precise fabrication, high initial capacitance and low fringe effects. Three generations of devices were fabricated with the chosen design. Generation I devices were the first ones to be fabricated with titanium IDCs encapsulated with PDMS which was also the dielectric. These devices were used to check the working principle of the strain sensors. Sensitivity of the generation I devices to stretching and bending was verified proving the working principle of the strain sensors. Faced with laser micro-machining issues for titanium and adhesion issues with PDMS, the generation II sensors were fabricated. These devices used brass for IDC micro-machining which reduced the cut out time and laser power. A 50 μm thick polyimide film was used to form the bottom layer of the generation II strain sensor thus overcoming the adhesion issues with generation I strain sensors. The generation II strain sensors were tested extensively on the cantilever for linearity, repeatability and hysteresis. The gauge factor of these devices was found to be 80 which was substantially higher than the metallic resistive strain gauges. Performance at different temperatures showed that these sensors did not lose their sensitivity at different operating temperatures. The performance of these strain sensors was tested for remote strain sensing for structural health monitoring applications with the help of circuitry and microcontrollers. The generation II strain sensors were also tested for bladder volume monitoring with the help of a balloon model and wireless, batteryless telemetry system. Limitations in terms of sensitivity were observed for generation II

devices for the bladder volume monitoring because of their responses to bending. These limitations were overcome with IDCs having flexible fingers fabricated from 120 μm thick polyimide film sputtered with aluminum. The results of generation III devices show reduced sensitivity to bending which was in good agreement with the expectations.

CHAPTER 7

FUTURE WORK

It was observed from Figure 5.20 that the changes in frequency and hence capacitance were low for the spherical structures. This was because of the reduction in sensitivity for brass IDC strain sensors for spherical structures as explained in Section 3.4.2 in Chapter 3 dealing with fabrication. Taking in to consideration the issues with generation II devices for spherical structures, generation III devices with flexible IDC were fabricated as explained in chapter 3. The performance of these generation III devices with polyimide IDCs was checked for bending on the cantilever. In the future work, we propose the use of generation III, polyimide IDCs with aluminum sputtering for the use of bladder volume monitoring on the balloon model along with the telemetric system.

7.1 Performance of Generation III devices

7.1.1 Cantilever experiment

It was expected that the generation III devices be less sensitive to bending and show variation in capacitance with increased linear strain. To verify the response of these sensors to bending, a cantilever setup was again used. Two generation III devices were placed on the cantilever, one at 3 inches from the fixed end and the other at 0.5 inches from the fixed end to compare the changes in capacitance. As previously observed, the cantilever showed heavy bending at about 2-4 inches and negligible bending below 1 inch from the fixed end (refer Figure 5.4). With the new fabrication and flexible IDC fingers, both the sensors at different

locations were expected to show linear variations unlike the generation II devices. Initially, loading was carried out with 5 pound load steps up to 20 pounds.

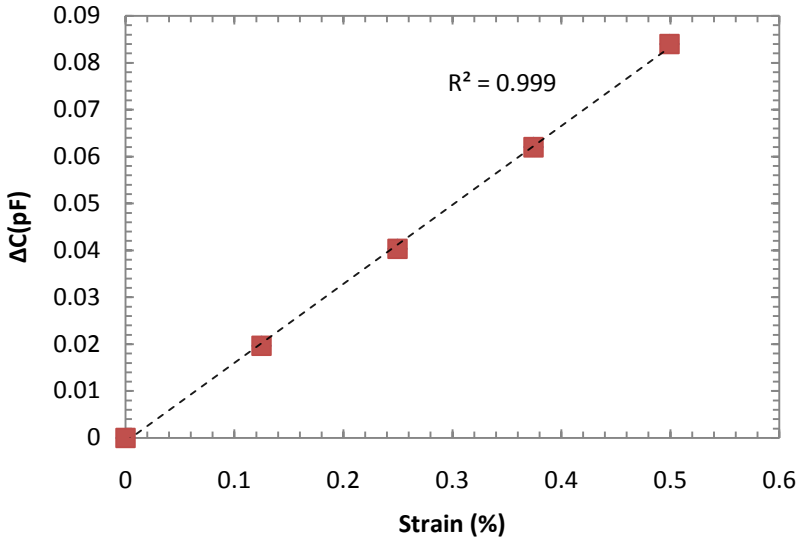

(a)

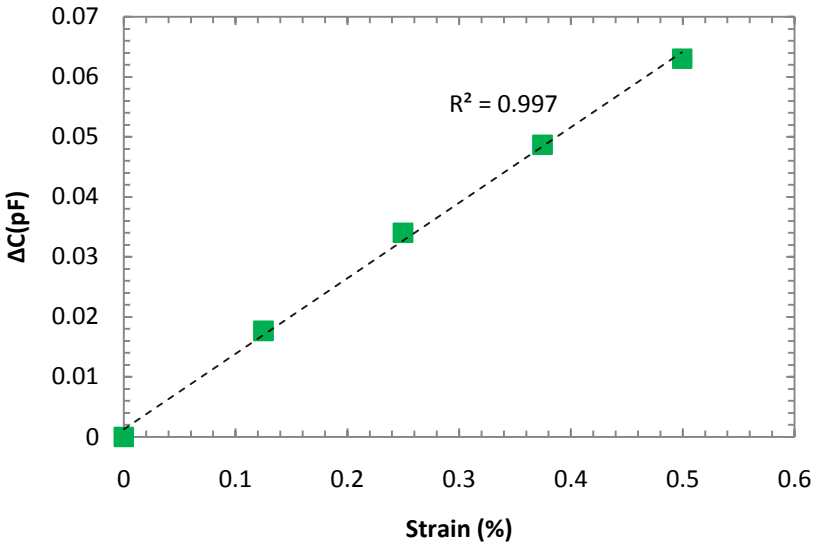

(b)

Figure 7.1: Performance of the generation III strain sensors for initial 5 pound loads for a sensor (a) placed at 0.5 inches from the fixed end and (b) 3 inches from the fixed end on the cantilever.

The changes in capacitance with strain are shown in the Figure 7.1. It was evident that even though the location of the strain sensors was different on the cantilever, both the sensors showed very linear variations in capacitance. The non-linearity shown by the generation II devices due to bending of the cantilever at 3 inches from the fixed end was absent for generation III devices.

To determine the sensitivity of the strain sensors for smaller weights, 10 weights of 1 pound were added followed by two 5 pound weights. The results are shown in Figure 7.2. The linearity was again very clearly evident for sensors placed at both the locations. This was a clear indication of the fact that generation III devices were not sensitive to bending and could be used for strain measurements for spherical structures. It was clear that generation III devices were good enough to be used for bladder volume monitoring applications.

It was observed that the change in capacitance was small as compared with the generation II devices. This was because the initial capacitance value of generation III devices was about 3-6 pF which was smaller than the previous generation devices. Less absolute capacitance was expected because the sputtered aluminum film on polyimide IDCs was only about 5 μm thick on the top and side walls. The previous generation devices were completely metallic and hence had a higher initial capacitance of about 13-15 pF. This limitation could be overcome with a highly sensitive oscillator circuitry. With the observed results, the generation III sensors for bladder volume monitoring applications after further testing and experiments could be used with better sensitivity.

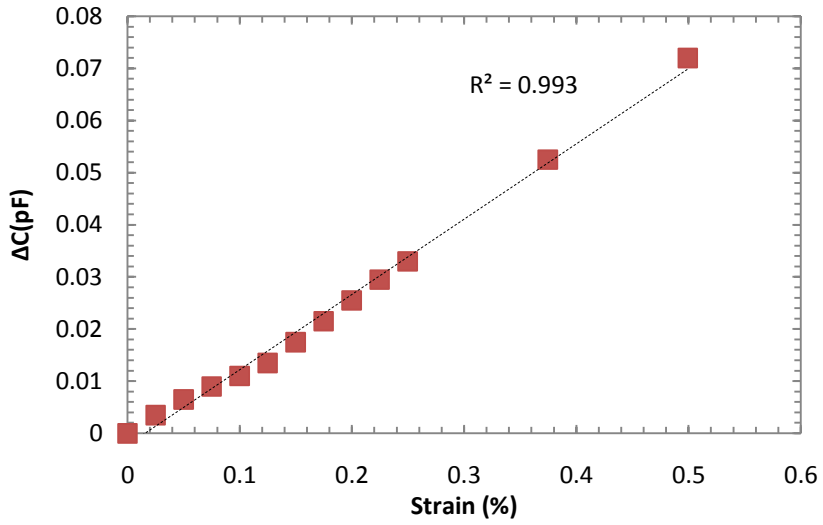

(a)

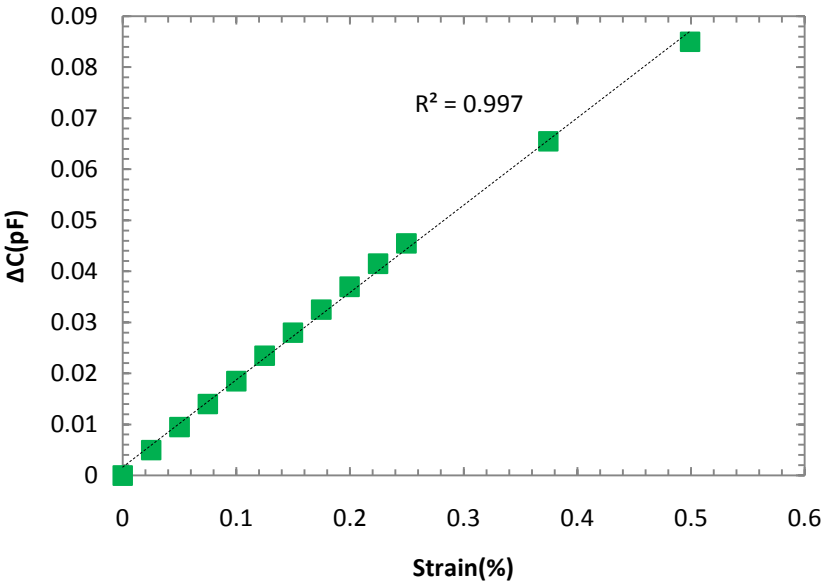

(b)

Figure 7.2: Performance of the generation III strain sensors for initial 1 pound loads followed by two 5 pound loads for a sensor (a) placed at 0.5 inches from the fixed end and (b) 3 inches from the fixed end on the cantilever.

APPENDIX A

LASER MICROMACHINING PARAMETERIZATION PROCEDURE, *G-CODE* PROGRAM FOR THE SELECTED DESIGN AND IMAGES OF THE LASER SETUP

Material-Laser Parameterization Procedure

1) Focal Length

a) Objective: To collect material-specific laser settings and optimize material parameterization effort.

b) Overview: This procedure takes the user through a set of steps that establish a reliable process for collecting parameterization data for specific materials and thicknesses.

c) Prerequisites from laser material database:

i) Laser settings (**watts, frequency, amperage, %attenuator)** starting parameters:

(1) Find these starting points in the spreadsheet or database located on the desktop.

(2) These have been developed using design of experiments and have been recorded for your use.

(3) Find a close match for your use.

(4) Also remember to record the work you do and add it to the database.

d) **Method**

i) Determine material thickness using calipers:

(1) The thickness of the material is very important information needed to determine the starting z-height so the surface of the material can be efficiently cut.

(2) When using calipers, remember to move them to zero and then press the "zero" key to calibrate the tool.

(3) Try to get the most exact measurement and make sure to measure at least 5 times around the object. Take an average if they are all different but close. This will be your "thickness of material" measurement needed for the next step.

ii) Prepare the material

(1) Place the object inside the 50mm square cut out on the jig

(2) secure the piece with screws

(3) Close the shed door

iii) "Dial in" your parameters (such as frequency, attenuator, etc.)

iv) Measure the wattage of your combined power parameters

(a) Select "zero" from the laser power area

(b) Select "measure"

(c) You will be prompted to enter in a %attenuator value. This should be the same value you plan to run for your laser focus test. This is usually 100%.

(d) Observe and record the highest stable value that appears. This is your wattage level the surface of your medium will experience.

v) Prepare to place a starting burn

(1) set the x axis at 273mm

(2) set the y axis at 127mm

(3) the laser is now aimed in the lower left hand corner of the 50mm square

(4) set the z axis at the starting z-focal length:

(a) Formula: starting *Z-focal length = 83.39mm - (thickness of material in mm)*

vi) Place a starting burn mark:

(1) *Open* the main shutter (white button)

(2) *Open* diode/software shutter

(3) Turn *On* Laser Diode

(4) *Set* the attenuator to 100%, click *operate*

(5) *Set* Frequency to 20 kHz

(6) *Set* Amperage to 48 A

(7) Turn *Off* the External Gate to braze the surface of the material and let it run for a few seconds

(8) Turn *On* the External Gate. You should have something that looks like Figure 1.

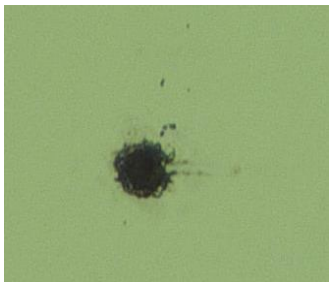

Figure A.1: a starting burn mark

vii) This will be used as a starting point for the next step: A good starting mark is large enough to be seen on the screen and differentiable from dist, grit, and oils that may be present on the surface of the material when placed under the microscope.

2) Fine Focal Length (with Program_1)

a) Objective: Identify parameters for the final focal length

b) Overview:

i) Program_1 cuts lines in a serpentine pattern. See figure 2.

ii) The z-axis is will advance towards the material

c) Prerequisites:

i) Starting origin (coordinates from previous steps)

ii) Mark starting point on material with laser as a reference point for microscopic counting.

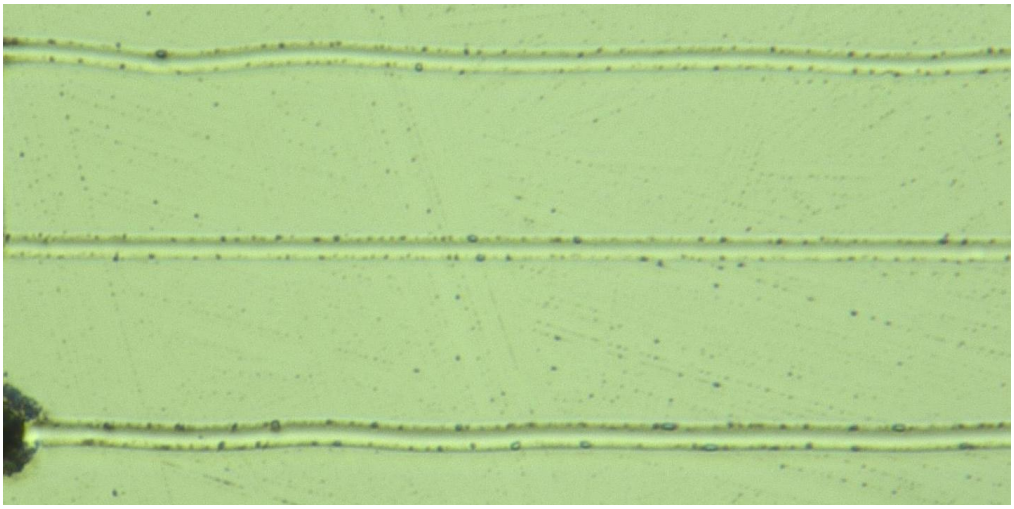

Figure A.2: channels in silicon

d) **Method**

i) Select the program tab (left side of screen) and select *load*

ii) Double click the Program_1 on the desktop

iii) Uncheck the box marked *edit mode*

iv) You will be prompted for with questions regarding your process. Each entry must be recorded in your job entry in the database spreadsheet.

v) Wait for the process to finish and record the length of time endured

vi) Take material to microscope

vii) Count the number of lines from the starting point until you find the quality you are looking for in your features.

viii) Take this number and multiply it by your Z-advance setting. _____ (um)

3) Number of Passes/Channels (with Program_1)

a) Objective: Identify how many radial passes required to pass through a material
   i) Overview: Program_3 cuts linear channels into the surface of the material at the specified settings (watts, frequency, amperage, %attenuator) in accordance with your specifications found in the database regarding your material.

b) Prerequisites:
   i) Fine focus height (Step 2) as well as the beginning location of the mill
   ii) Amperage
   iii) Frequency
   iv) Attenuator setting
   v) Wattage
      (1) After you have set the amperage, attenuator, and frequency
      (2) To find the wattages, click *zero* on the power level area and then click *measure*
      (3) Record the highest stable value that appears in the area in the database

c) The suggested starting set is:
   i) Length of channel: 10mm
   ii) Z change: 0mm – *no change*
   iii) Distance between channels:0.5mm
   iv) Speed: 1mm/s
   v) Beginning number of passes: 5
   vi) Addition advance of passes: 5
   vii) Number of channels: 50 for 1W+, 100 or more for less than 1W laser power

d) **Method**
   i) Load the program in the same way you did so in step 2, however you will now **change the default values**.
   ii) Open Program_2 from the program folder
   iii) Answer the given questions *(suggested above)*
   iv) Wait for the process to finish
   v) Inspect the results under the microscope and record ratings in datasheet.

4) Number of Rotations (with Program_2)

a) Objective: Identify how many radial passes required to pass through a material
   i) Overview: Program_2 cuts circles at the specified settings (watts, frequency, amperage, %attenuator) in accordance with your specifications found in the database regarding your material.

b) Prerequisites:
   i) Fine focus height (Step 2) as well as the beginning location of the mill
   ii) Amperage
   iii) Frequency
   iv) Attenuator setting
   v) Wattage
      (1) After you have set the amperage, attenuator, and frequency
      (2) To find the wattages, click *zero* on the power level area and then click *measure*
      (3) Record the highest stable value that appears in the area in the database

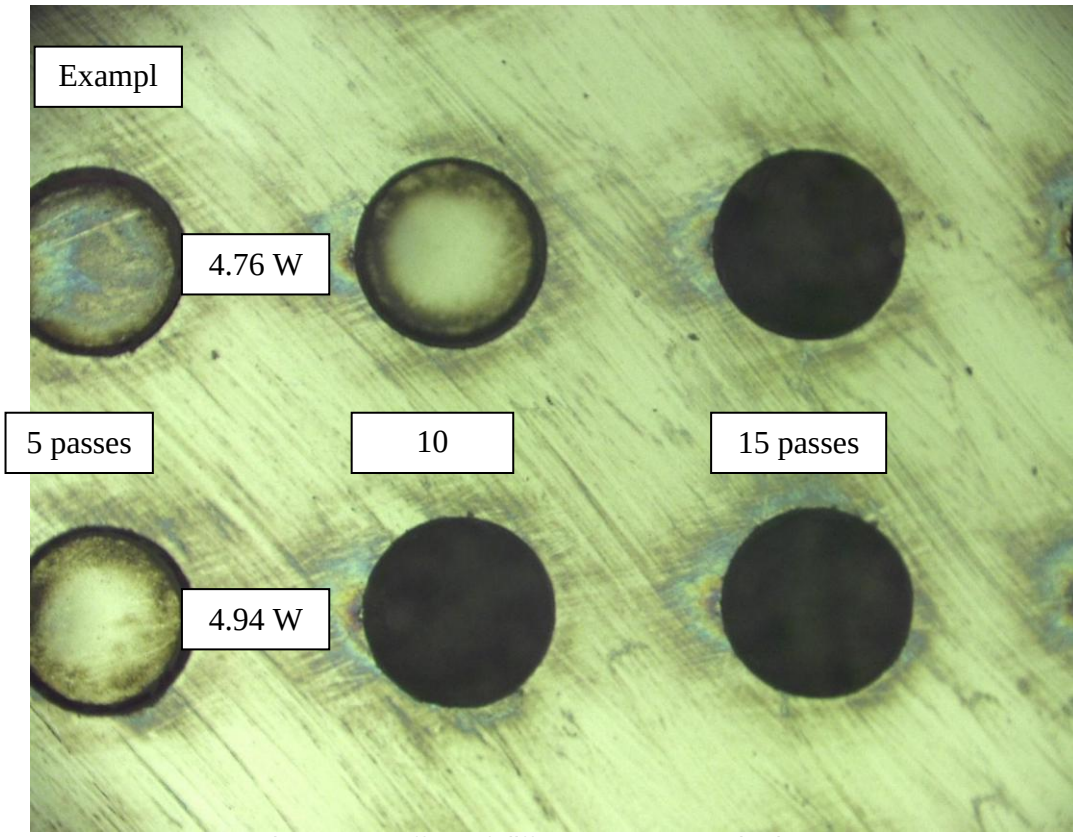

Figure A.3: Effect of different passes on the laser

c) **Method**
   i) Open Program_2 from the program folder
   ii) Answer the given questions
   iii) Wait for the process to finish
   iv) Take material to microscope if necessary (if you cannot see the results yourself).
   v) Count how many circles were etched into the material as well as the first completely open hole. Make sure to not shake the material or touch the featured areas as this may disturb/flex the material and cause pieces to break off rather than free fall.
   vi) Take the passes number and multiply it by your "number of passes per location"

   _____*_____=_____

d) This program is set by default to make 1 pass, cumulative, per every micron of material thickness (a user input).
e) Keep in mind that the wattage changes as the LED ages, so measuring the power (W) after each run and recording it is required information
   Count and record the number of circles made that **did not** fall out per each run. This number plus one will be the number needed to be recorded in to your datasheets as a *fall through* point for the material and its respective settings (watts, frequency, amperage, %attenuator).

But wait, there's more:
Both aforementioned programs are completely customizable through user input-prompt, with no additional code writing whatsoever.

Program for designed IDC

Given below is the program for cutting IDCs of 500 µm finger length, 30 finger pairs with 5 µm finger gaps.

```
DVAR $PASSES
DVAR $TIME
DVAR $FASTMOVE
DVAR $USERSPEED


MSGDISPLAY 1, "Program started"
MSGDISPLAY 1, "{#F3 #F}" "Time is #TM"

;D=500UM 5UM - 20 30 40 FINGERS
$DO0.X=0
G90   ;Absolute coordinate mode
G71   ;All units are in mm. Velocity is in mm/s
G301  ;ENABLE MULTI-BLOCK LOOK-AHEAD
G108  ;VELOCITY BLENDING ON
G92 X0 Y0

$USERSPEED=5
$PASSES=1
$FASTMOVE=5


$PASSES=MSGINPUT DF_MSGBOX_OKONLY "No. of passes per feature ;Enter the number of passes for each feature;"$PASSES

$FASTMOVE=MSGINPUT DF_MSGBOX_OKONLY "Translation speed between features ;Enter translation speed between features (mm/s);"$FASTMOVE

$USERSPEED=MSGINPUT DF_MSGBOX_OKONLY "Speed;Enter the speed (mm/s);"$USERSPEED



REPEAT $PASSES
G1 X-1.21630 Y0.70000 F $FASTMOVE
$DO0.X=1
G1 X-0.35630 Y0.70000 F $USERSPEED
G1 X-0.35630 Y0.20000 F $USERSPEED
G1 X-1.19630 Y0.20000 F $USERSPEED
G1 X-1.19630 Y0.70000 F $USERSPEED
G1 X-1.24630 Y0.70000 F $USERSPEED
G1 X-1.24630 Y0.20000 F $USERSPEED
G1 X-1.29630 Y0.20000 F $USERSPEED
G1 X-1.29630 Y0.70000 F $USERSPEED
```

G1 X-1.34630 Y0.70000 F $USERSPEED
G1 X-1.34630 Y0.20000 F $USERSPEED
G1 X-1.39630 Y0.20000 F $USERSPEED
G1 X-1.39630 Y0.70000 F $USERSPEED
G1 X-1.44630 Y0.70000 F $USERSPEED
G1 X-1.44630 Y0.20000 F $USERSPEED
G1 X-1.49630 Y0.20000 F $USERSPEED
G1 X-1.49630 Y0.70000 F $USERSPEED
G1 X-1.54630 Y0.70000 F $USERSPEED
G1 X-1.54630 Y0.20000 F $USERSPEED
G1 X-1.59630 Y0.20000 F $USERSPEED
G1 X-1.59630 Y0.70000 F $USERSPEED
G1 X-1.64630 Y0.70000 F $USERSPEED
G1 X-1.64630 Y0.20000 F $USERSPEED
G1 X-1.69630 Y0.20000 F $USERSPEED
G1 X-1.69630 Y0.70000 F $USERSPEED
G1 X-1.74630 Y0.70000 F $USERSPEED
G1 X-1.74630 Y0.20000 F $USERSPEED
G1 X-1.79630 Y0.20000 F $USERSPEED
G1 X-1.79630 Y0.70000 F $USERSPEED
G1 X-1.84630 Y0.70000 F $USERSPEED
G1 X-1.84630 Y0.20000 F $USERSPEED
G1 X-1.89630 Y0.20000 F $USERSPEED
G1 X-1.89630 Y0.70000 F $USERSPEED
G1 X-1.94630 Y0.70000 F $USERSPEED
G1 X-1.94630 Y0.20000 F $USERSPEED
G1 X-1.99630 Y0.20000 F $USERSPEED
G1 X-1.99630 Y0.70000 F $USERSPEED
G1 X-2.04630 Y0.70000 F $USERSPEED
G1 X-2.04630 Y0.20000 F $USERSPEED
G1 X-2.09630 Y0.20000 F $USERSPEED
G1 X-2.09630 Y0.70000 F $USERSPEED
G1 X-2.14630 Y0.70000 F $USERSPEED
G1 X-2.14630 Y0.20000 F $USERSPEED
G1 X-2.19630 Y0.20000 F $USERSPEED
G1 X-2.19630 Y0.70000 F $USERSPEED
G1 X-2.24630 Y0.70000 F $USERSPEED
G1 X-2.24630 Y0.20000 F $USERSPEED
G1 X-2.29630 Y0.20000 F $USERSPEED
G1 X-2.29630 Y0.70000 F $USERSPEED
G1 X-2.34630 Y0.70000 F $USERSPEED
G1 X-2.34630 Y0.20000 F $USERSPEED
G1 X-2.39630 Y0.20000 F $USERSPEED
G1 X-2.39630 Y0.70000 F $USERSPEED
G1 X-2.44630 Y0.70000 F $USERSPEED
G1 X-2.44630 Y0.20000 F $USERSPEED
G1 X-2.49630 Y0.20000 F $USERSPEED
G1 X-2.49630 Y0.70000 F $USERSPEED
G1 X-2.54630 Y0.70000 F $USERSPEED
G1 X-2.54630 Y0.20000 F $USERSPEED
G1 X-2.59630 Y0.20000 F $USERSPEED
G1 X-2.59630 Y0.70000 F $USERSPEED

G1 X-2.64630 Y0.70000 F $USERSPEED
G1 X-2.64630 Y0.20000 F $USERSPEED
G1 X-2.69630 Y0.20000 F $USERSPEED
G1 X-2.69630 Y0.70000 F $USERSPEED
G1 X-2.74630 Y0.70000 F $USERSPEED
G1 X-2.74630 Y0.20000 F $USERSPEED
G1 X-2.79630 Y0.20000 F $USERSPEED
G1 X-2.79630 Y0.70000 F $USERSPEED
G1 X-2.84630 Y0.70000 F $USERSPEED
G1 X-2.84630 Y0.20000 F $USERSPEED
G1 X-2.89630 Y0.20000 F $USERSPEED
G1 X-2.89630 Y0.70000 F $USERSPEED
G1 X-2.94630 Y0.70000 F $USERSPEED
G1 X-2.94630 Y0.20000 F $USERSPEED
G1 X-2.99630 Y0.20000 F $USERSPEED
G1 X-2.99630 Y0.70000 F $USERSPEED
G1 X-3.04630 Y0.70000 F $USERSPEED
G1 X-3.04630 Y0.20000 F $USERSPEED
G1 X-3.09630 Y0.20000 F $USERSPEED
G1 X-3.09630 Y0.70000 F $USERSPEED
G1 X-3.14630 Y0.70000 F $USERSPEED
G1 X-3.14630 Y0.20000 F $USERSPEED
G1 X-3.19630 Y0.20000 F $USERSPEED
G1 X-3.19630 Y0.70000 F $USERSPEED
G1 X-3.24630 Y0.70000 F $USERSPEED
G1 X-3.24630 Y0.20000 F $USERSPEED
G1 X-3.29630 Y0.20000 F $USERSPEED
G1 X-3.29630 Y0.70000 F $USERSPEED
G1 X-3.34630 Y0.70000 F $USERSPEED
G1 X-3.34630 Y0.20000 F $USERSPEED
G1 X-3.39630 Y0.20000 F $USERSPEED
G1 X-3.39630 Y0.70000 F $USERSPEED
G1 X-3.44630 Y0.70000 F $USERSPEED
G1 X-3.44630 Y0.20000 F $USERSPEED
G1 X-3.49630 Y0.20000 F $USERSPEED
G1 X-3.49630 Y0.70000 F $USERSPEED
G1 X-3.54630 Y0.70000 F $USERSPEED
G1 X-3.54630 Y0.20000 F $USERSPEED
G1 X-3.59630 Y0.20000 F $USERSPEED
G1 X-3.59630 Y0.70000 F $USERSPEED
G1 X-3.64630 Y0.70000 F $USERSPEED
G1 X-3.64630 Y0.20000 F $USERSPEED
G1 X-3.69630 Y0.20000 F $USERSPEED
G1 X-3.69630 Y0.70000 F $USERSPEED
G1 X-3.74630 Y0.70000 F $USERSPEED
G1 X-3.74630 Y0.20000 F $USERSPEED
G1 X-3.79630 Y0.20000 F $USERSPEED
G1 X-3.79630 Y0.70000 F $USERSPEED
G1 X-3.84630 Y0.70000 F $USERSPEED
G1 X-3.84630 Y0.20000 F $USERSPEED
G1 X-3.89630 Y0.20000 F $USERSPEED
G1 X-3.89630 Y0.70000 F $USERSPEED

```
G1 X-3.94630 Y0.70000 F $USERSPEED
G1 X-3.94630 Y0.20000 F $USERSPEED
G1 X-3.99630 Y0.20000 F $USERSPEED
G1 X-3.99630 Y0.70000 F $USERSPEED
G1 X-4.04630 Y0.70000 F $USERSPEED
G1 X-4.04630 Y0.20000 F $USERSPEED
G1 X-4.09630 Y0.20000 F $USERSPEED
G1 X-4.09630 Y0.70000 F $USERSPEED
G1 X-4.98630 Y0.70000 F $USERSPEED
G1 X-4.98630 Y0.20000 F $USERSPEED
G1 X-4.14630 Y0.20000 F $USERSPEED
G1 X-4.14630 Y0.70000 F $USERSPEED
$DO0.X=0
ENDREPEAT


REPEAT $PASSES
G1 X-5.33658 Y4.80194 F $FASTMOVE
$DO0.X=1
G1 X-5.33658 Y4.30194 F $USERSPEED
G1 X-5.83658 Y4.30194 F $USERSPEED
G1 X-5.83661 Y4.80195 F $USERSPEED
G1 X-5.33658 Y4.80194 F $USERSPEED
$DO0.X=0
ENDREPEAT

REPEAT $PASSES
G1 X-1.91598 Y-0.40005 F $FASTMOVE
$DO0.X=1
G1 X-1.19630 Y-0.40005 F $USERSPEED
G1 X-1.19630 Y-0.00000 F $USERSPEED
G1 X-0.00000 Y-0.00000 F $USERSPEED
G1 X-0.00000 Y0.90000 F $USERSPEED
G1 X-1.19630 Y0.90000 F $USERSPEED
G1 X-1.19630 Y1.30005 F $USERSPEED
G1 X-1.91598 Y1.30005 F $USERSPEED
G1 X-1.91590 Y4.95860 F $USERSPEED
G1 X-3.51599 Y4.95860 F $USERSPEED
G1 X-3.51603 Y2.95865 F $USERSPEED
G1 X-3.51603 Y1.30007 F $USERSPEED
G1 X-4.14630 Y1.30006 F $USERSPEED
G1 X-4.14630 Y0.90000 F $USERSPEED
G1 X-5.28600 Y0.90000 F $USERSPEED
G1 X-5.28600 Y-0.00000 F $USERSPEED
G1 X-4.14630 Y-0.00000 F $USERSPEED
G1 X-4.14630 Y-0.40006 F $USERSPEED
G1 X-3.51603 Y-0.40007 F $USERSPEED
G1 X-3.51603 Y-2.05865 F $USERSPEED
G1 X-3.51599 Y-4.05860 F $USERSPEED
G1 X-1.91590 Y-4.05860 F $USERSPEED
G1 X-1.91598 Y-0.40005 F $USERSPEED
$DO0.X=0
```

```
ENDREPEAT
G91   ;Incremental coordinate mode
G109  ; VELOCITY BLENDING OFF
MSGDISPLAY 1, "Program finished"
MSGDISPLAY 1, "{#F3 #F}" "Time is #TM"

M2    ;End of program
```

Laser images

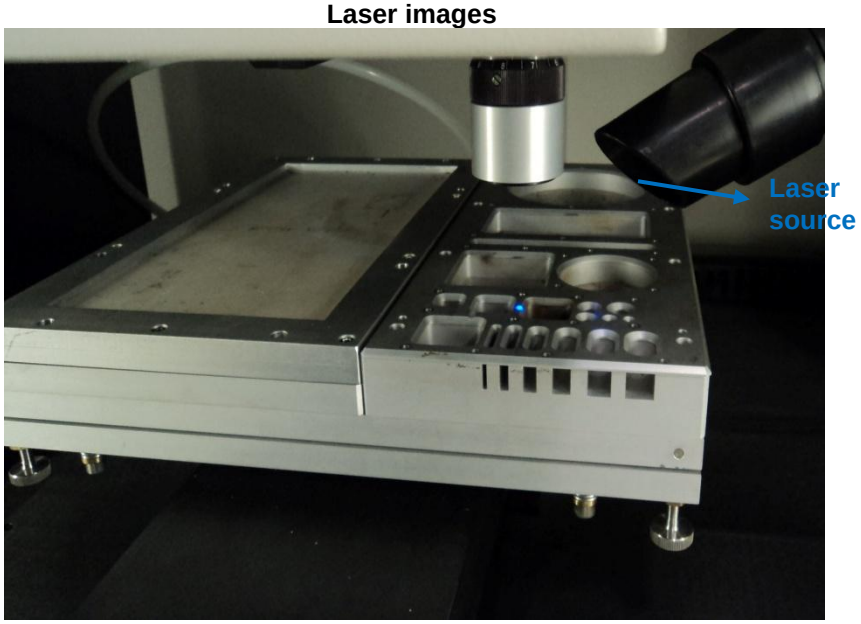

Figure A.4: The jig platform with laser source

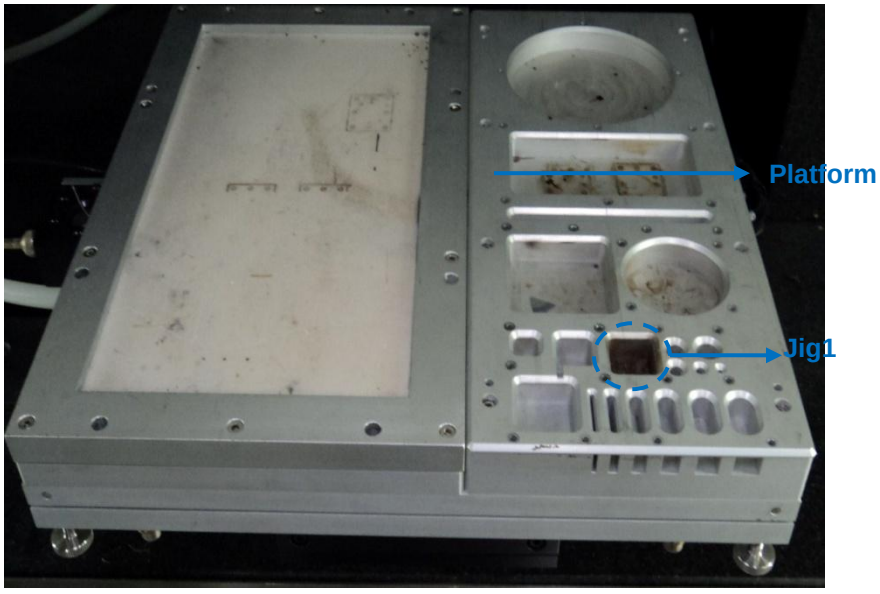

Figure A.5: The various jig positions on the platform

Figure A.6: Screen shot of the interfacing computer on the laser

REFERENCES

[1] Window A.L, “Strain Gauge Technology,” Springer Publications, Second Edition, 1992.

[2] Ewing J.A, “The Strength of Materials,” Cambridge University Press, Second Edition, 1899.

[3] Lynch J.P, Loh K.J, “A Summary Review of Wireless Sensors and Sensor Networks for Structural Health Monitoring,” *The Shock and Vibration Digest*, Vol. 38, No 2, pp 91-128, 2006.

[4] Leng J.S, Winter D,Barnes R.A, Mays G.C, and Fernando G.F, “Structural health monitoring of concrete cylinders using protected fibre optic sensors,” *Smart Materials and Structures*, Vol.15, pp 302-308, 2006.

[5] Sohn H, Farrar C.R, Hunter N.F, Worden K, “Structural health monitoring using statistical pattern recognition techniques,” *Journal of Dynamic Systems, Measurement and Control*, Vol. 123, pp 706-711, 2001.

[6] E. Sazonov, K. Janoyan, R. Jha, “Wireless intelligent sensor network for autonomous structural health monitoring,” *Proceedings of SPIE*, Vol 5384, pp 305-315, 2004.

[7] V. Giurgiutiu, C.A. Rojers, “Recent advancements in the electro-mechanical (E/M) impedance method for structural health monitoring and NDE,” *SPIE’s 5th Annual International Symposium on Smart Structures and Materials*, San Diego, CA, USA, March 1-5, 1998.

[8] Y. Jia, K. Sun, F. J. Agosto, M. T. Qui ˜nones, “Design and characterization of a passive wireless strain sensor,” *Measurement Science and Technology*, Vol. 17, pp. 2869-2876, 2006.

[9] D. A. Smith, “Urinary Incontinence: Epidemiology, Demographics, and Costs,” *Incontinence*, Vol. 11, 2003.

[10] S. Rajagopalan, M. Sawan, E. Ghafar-Zadeh, O. Savadogo, and V. P. Chodavarapu, “A Polypyrrole-based Strain Sensor Dedicated to Measure Bladder Volume in Patients with Urinary Dysfunction,” *Sensors*, Vol. 8, pp. 5081-5095, 2008.

[11] Philippe Jourand P, Puers R, “An Autonomous, Capacitive Sensor Based and Battery Powered Internal Bladder Pressure Monitoring System, ” *Procedia Chemistry,* Vol. 1, pp. 1263–1266, 2009.

[12] Blake C, Abrams P, “Noninvasive Techniques For The Measurement of Isovolumetric Bladder Pressure,” *J Urol,* Vol. 171, pp. 9-12, 2004.

[13] Harding C.K, Robson W, Drinnan M.J, Ramsden P.D, Griffiths C, Pickard R.S, “Variation in Invasive and Noninvasive Measurements of Isovolumetric Bladder Pressure and Categorization of Obstruction According to Bladder Volume,” *Journal of Urology,* Vol. 176, pp. 172–176, 2006.

[14] Coosemans J. “Wireless and Battery-less Medical Monitoring Devices” *PhD* 2008, Katholieke Universiteit Leuven.

[15] Tan R, McClure T, Lin C.K, Jea D, Dabiri F, Massey T, et al. “Development of a Fully Implantable Wireless Pressure Monitoring System,” *Biomed Microdevices,* Vol. 11, pp. 259–264, 2009.

[16] Sawhney A.K, “Electrical and Electronics Measurement and Instrumentation,” Dhanpat Rai and Co, Tenth Edition, 1992.

[17] Guo J, Kuo H.I, Young D.J, Ko W.H, “Buckled beam linear output capacitive strain sensor,” *Solid State Sensor, Actuator, and Microsyst. Workshop*, Jun. 2004, pp. 344–347.

[18] Joshi H, Burlacu B, Prabhu M, Yoon S, Sichitiu M, Dutta R, and Rizkalla S, “Wireless structural health monitoring system design, implementation and validation,” Research Report RD-06-02, submitted to the National Science Foundation (NSF), North Carolina State University (NCSU), Constructed Facilities Lab (CFL), Raleigh, North Carolina, January 2006.

[19] Chiang C.C, Chou-Ching, Lin K, Ju M.S, “An implantable capacitive pressure sensor for biomedical applications,” *Sensors and Actuators A,* Vol. 134, pp. 382–388, 2007.

[20] Han B, Ou J, “Embedded piezoresistive cement-based stress/strain sensor,” *Sensors and Actuators A,* Vol.138, pp. 294–298, 2007.

[21] Gutierrez C. A, Cho A, Geathers J, Yu L, Abram T, and Meng E, **“**An Implantable Low-Cost Multilayer Screen-Printed Carbon Thick-Film Strain Sensor,” *Proceedings of 2009 International Conference on Microtechnologies in Medicine and Biology*, Québec City, Canada, April 1-3, 2009.

[22] Li J, Longtin J.P, Tankiewicz S, Gouldstone A, Sampath S, “Interdigital capacitive strain gauges fabricated by direct-write thermal spray and ultrafast laser micromachining,” *Sensors and Actuators A,* Vol. 133, pp. 1–8, 2007.

[23] Andeen C, Fontanel J, Schuele D, “Capacitive gauge for accurate measurement of high pressures,” *Rev. Sci. Instrum*., Vol. 42, pp. 495–502, 1971.

[24] Nath J, Ghosh D, Maria J.P, Michael B. Steer', Kingon A, and Staur G.T, “Microwave Properties of BST Thin Film Interdigital Capacitors on Low Cost Alumina Substrates,” *34 European Microwave Conference,* Amsterdam, pp. 1497-1500, 2004.

[25] Igreja R, Dias C.J, “Analytical evaluation of the interdigital electrodes capacitance for a multi-layered structure,” *Sensors and Actuators A,* Vol. 112, pp. 291–301, 2004.

[26] Feng Y, H°allstedt J,Qiang Chen and Zheng L-R, Huang Y, “Development and experimental verification of analytical models for printable interdigital capacitor

sensors on paperboard,” *IEEE SENSORS Conference*, Christchurch, October 25-28, 2009.

[27] Villalobos J.G, Zhen X, Yi J, "IDC based battery-free wireless pressure sensor*,"2010 IEEE/ASME International Conference on Embedded Systems and Applications (MESA)*, Qingdao, ShanDong July 15-17, 2010.

[28] Matsuzaki R, Todoroki A, "Wireless flexible capacitive sensor based on ultra-flexible epoxy resin for strain measurement of automobile tires," *Sensors and Actuators A,* Vol.140, pp. 32–42, 2007.

[29] Matsuzaki R, Keating T, Todoroki A, Hiraoka N, "Rubber-based strain sensor fabricated using photolithography for intelligent tires," *Sensors and Actuators A*, Vol. 148, pp. 1–9, 2008.

[30] Alley G.D, "Interdigital Capacitors and Their Application to Lumped-Element Microwave Integrated Circuits," *IEEE Transacttons On Microwave Theory And Techniques*, Vol. Mtt-18, No. 12,1970.

[31] Gadre A, Kastantin M, Li S, and Ghodssi R, "An integrated bioMEMS fabrication technology," *Int. Semiconductor Device Research Symposium (ISDRS)*, Washington, D.C., 2001.

[32] Adrega T, and Lacour S.P, "Stretchable gold conductors embedded in PDMS and patterned by photolithography: fabrication and electromechanical characterization," *Journal of Micromechanics and Microengineering*, Vol. 20, pp. 1-9, 2010.

[33] Morent R, De Geyter N, Axisa F, De Smet N, Gengembre L, De Leersnyder E, Leys C, Vanfleteren J, Rymarczyk-Machal M, Schacht E and Payen E, "Adhesion enhancement by a dielectric barrier discharge of PDMS used for flexible and stretchable electronics," *Journal of Physics D: Applied Physics*, Vol. 40, pp. 7392–7401, 2007

[34] Galliano A, Bistac S, and Schultz J, "Adhesion and friction of PDMS networks: molecular weight effects," *Journal of Colloid and Interface Science*, Vol. 265, pp. 372–379, 2003.

[35] Tata U, Deshmukh S, Chiao J C, Carter R and Huang H, "Bio-inspired sensor skins for structural health monitoring," *Smart Material and Structures,* Vol. 18, pp. 1-9, 2009.

[36] Denis Y, Yu W, and Spaepen F, "The yield strength of thin copper films on Kapton," *Journal Of Applied Physics*, Vol. 95, No. 6, 2004.

[37] Fuard D, Tzvetkova-Chevolleau T, Decossas S, Tracqui P, Schiavone P, "Optimization of poly-di-methyl-siloxane (PDMS) substrates for studying cellular adhesion and motility," *Microelectronic Engineering,* Vol. 85, pp. 1289–1293, 2008.

[38] Beer F.P and Johnston E.R, Jr., "Mechanics of Materials," McGraw Hill, Third Edition, 2002.

[39] Cockbain A.G, and Harrop P.J, "The temperature coefficient of capacitance," *British Journal of Applied Physics D: Applied Physics*, Vol. 1, pp. 1109-1115, 1968.

[40] Vita G. and Iannaccone G, "Design criteria for the RF section of UHF and microwave passive RFID transponders," *IEEE T. Microwave Theory*, Vol. 53, pp. 2978-2990, 2005.

[41] K. Wise, D. Anderson, J. Hetke, D. Kipke, K. Najafi, “Wireless implantable microsystems: high-density electronic interfaces to the nervous system,” *Proceedings of IEEE*, Vol. 92, pp.76-97, 2004.

BIOGRAPHICAL INFORMATION

Shreyas Kiran Thakar received his Bachelor's of Engineering in Electrical Engineering from University of Pune, India in 2009. He is pursuing his Master's of Science in Electrical Engineering from the University of Texas at Arlington. His research interests include MEMS based micro-sensors, microcontrollers and electronics for bio-medical applications. He has published several conference papers and posters during his work in the iMEMS laboratory.